

DISSERTATION

Charge Transport in Organic Semiconductor Materials and Devices

ausgeführt zum Zwecke der Erlangung des akademischen Grades
eines Doktors der technischen Wissenschaften

eingereicht an der Technischen Universität Wien
Fakultät für Elektrotechnik und Informationstechnik

von

Ling Li

Wien, im November 2007

Abstract

Organic semiconductors in general are a family of electronic materials that are based on π -conjugated carbon atoms. In the last three decades electronic devices based on this family of materials, such as field-effect transistors and light emitting diodes, have attracted much attention as possible inexpensive and flexible alternatives to inorganic devices. Although we witnessed considerable progress in the introduction of new commercial applications that are based on these materials, the nature of charge transport in these organic materials and devices has not been understood very well. The main goal of this thesis is to theoretically investigate the charge transport properties of organic semiconductor materials and devices.

Charge transport properties presented here are investigated in the framework of variable range hopping theory. In a previously published paper by Vissenberg, a percolation model has been developed in order to explain the temperature dependence of hopping mobility in organic semiconductors. One of our main theoretical goals is to develop different models that can explain the dependence of the mobility in organic semiconductors on electric field, temperature, carrier concentration, and doping and trap concentration. A both temperature and electric field dependent mobility model is developed based on a modified Miller-Abrahams rate equation. The carrier concentration dependent mobility is formulated assuming a Gaussian density of states. A unified mobility model is presented which can explain the temperature, electric field and carrier concentration dependence. The doping and trap dependent mobility model is obtained by assuming a superposition of two exponential density of states functions.

The charge injection process between metal and organic semiconductor is examined for organic light-emitting diodes. For this goal we develop both a diffusion-controlled and a master equation based injection model. These two models can explain the dependence of the injection current on the temperature, electric field and barrier height. Good agreement between calculation and experimental data is found.

We examine closely the space charge limited current (SCLC) and the effect of the Fermi-Dirac statistics on the transport energy. It is found that the SCLC due to a Gaussian density of states is similar to SCLC controlled by shallow traps in regular semiconductors.

The Fermi-Dirac statistics plays an important role for transport energy, even at low temperature.

Finally, analytical models applicable to organic thin film transistors and to unipolar organic light-emitting diodes are presented.

Kurzfassung

Organische Halbleiter gehören zu einer speziellen Klasse von Kunststoffen, die sich durch ein konjugiertes Bindungssystem auszeichnen. In den vergangenen drei Jahrzehnten wurde der Entwicklung von Kunststoff-basierten, mikroelektronischen Bauelementen stets wachsende Aufmerksamkeit gewidmet. Insbesondere Anwendungen wie organische Dünnschichttransistoren und organische Leuchtdioden versprechen vielfältige und vor allem kostengünstige Alternativen zu Silizium-basierten Bauelementen. Trotz zahlreicher wissenschaftlicher Bemühungen und Fortschritten in der Einführung neuer kommerzieller Anwendungen wirft der Ladungstransport in polymeren Halbleiterbauelementen sowohl in der Praxis als auch in theoretischer Hinsicht immer noch zahlreiche offene Fragen auf. Das Ziel dieser Arbeit ist die theoretische Untersuchung des Ladungsträger-Transports in organischen Halbleitern und Halbleiterbauelementen.

Das in der Arbeit verwendete theoretische Modell des *variable range hopping* basiert auf Vissensbergs Perkolationsmodell, welches zur Erklärung der Temperaturabhängigkeit der Beweglichkeit in organischen Halbleitern entwickelt wurde. Es werden verschiedene Modelle entwickelt, die den funktionalen Abhängigkeiten der Beweglichkeit vom elektrischen Feld, der Temperatur, sowie der Konzentration von Ladungsträgern, Dopanten und Haftstellen Rechnung tragen. Anhand des klassischen Ratenausdruckes von Miller und Abrahams wurde ein Modell für die Beweglichkeit entwickelt, welches simultan den Einfluss der Temperatur und der elektrischen Feldstärke berücksichtigt.

Der Zusammenhang zwischen Beweglichkeit und Trägerkonzentration wurde im Rahmen des Gaussischen Unordnungsmodells untersucht und mündete in ein Modell, welches den Einfluss der Temperatur, der Trägerkonzentration und des elektrischen Feldes auf die Beweglichkeit in einer Formel vereint. Der Einfluss von Haftstellen und Dopanten auf die elektrische Leitfähigkeit eines organischen Halbleiters konnte mittels einer Überlagerung zweier exponentieller Zustandsdichten modelliert werden.

Die Injektion von Ladungsträgern mittels Metallkontakten wurde für den Fall organischer Leuchtdioden untersucht. Zu diesem Zweck wurden sowohl ein diffusionsbegrenztes Modell als auch ein Modell basierend auf einer Mastergleichung hergeleitet. Diese Modelle beschreiben die Abhängigkeit des Injektionsstromes von der Temperatur,

dem elektrischen Feld und der Barrierenhöhe an der Grenzfläche zwischen Halbleiter und Kontakt. Die Übereinstimmung zwischen Theorie und Experiment kann als durchaus zufriedenstellend bezeichnet werden.

Des Weiteren wurden raumladungsbegrenzte Ströme sowie der Einfluss der Fermi-Dirac Verteilung auf die Transportenergie einer eingehenden Betrachtung unterzogen. Wie sich dabei herausstellte, verhalten sich raumladungsbegrenzte elektrische Ströme in normalverteilten Zustandsdichten ähnlich wie Ströme in klassischen Halbleitern in Gegenwart seichter Haftstellen. Der Einfluss der Fermi-Dirac Verteilung auf die Transportenergie ist vor allem bei niedriger Temperatur sehr stark ausgeprägt.

Schließlich werden in dieser Arbeit Kompaktmodelle für Dünnschichttransistoren und organische Leuchtdioden präsentiert.

Acknowledgment

First and foremost, I would like to thank my advisor, Prof. Hans Kosina for his support, understanding and patience during the past three years over this project. Without his guidance as a great mentor, this work would not have been possible, and I certainly would not be here. I would also like to thank Prof. Siegfried Selberherr and Prof. Tibor Grasser for valuable time and providing great guidance for this work.

Secondly, my special gratitude goes to my fellow lab mates, Dr. Alireza Sheikholeslami and Dr. Christian Hollauer for their friendship and help in the working and living. Special thanks to M.Sc. Gregor Meller for his friendship and many detailed and enlightening discussions in pursuing deeper understanding of organic semiconductors. I also thank Dipl.-Ing. Rene Heinzl and Dipl.-Ing. Philipp Schwaha, who introduced me to the Linux system. Finally, my deep gratitude goes to Dipl.-Ing. Thomas Windbacher, Dipl.-Ing. Otmar Ertl, Dipl.-Ing. Alexander Nentshev and others who in one way or another further made by my time at TU-Wien worthwhile.

Without the love and support of my family, this would have been a very hard journey. I thank my father for teaching me good values such as hard work and appreciation for the gift of life and my mother without whom I would not be the person that I am today. My love for them is eternal.

Finally, I am grateful to the financial support from the Austrian Science Fund (FWF) through contract P16862-N02.

Contents

List of Abbreviations and Acronyms	ix
List of Symbols	xii
Constants	xiv
1 Introduction	1
1.1 Organic Semiconductors: History and Applications	1
1.2 Organic Semiconductor Physics	1
1.3 Theoretical Concepts	4
1.3.1 Gaussian Disorder Model (GDM)	5
1.3.2 Percolation Theory	6
1.3.3 Transport Energy	7
1.3.4 Multiple Trapping Theory	9
1.4 Organic Light-Emitting Diodes (OLED)	10
1.5 Thin Film Organic Field-Effect Transistors (OTFT)	11
1.6 Solar Cells	12
1.7 Organic Lasers	12
1.8 Organic Memory	13
1.9 Scope and Outline of this Thesis	13
2 Mobility Models for Organic Semiconductors	14
2.1 Introduction	14
2.2 Carrier Concentration Dependence of Mobility	15

2.2.1	Theory	15
2.2.2	Results and Discussion	17
2.3	Temperature and Electric Field Dependence of the Mobility	22
2.3.1	Theory	22
2.3.2	Low Electric Field Regime	22
2.3.3	High Electric Field Regime	26
2.4	Unified Mobility Model	29
2.4.1	Theory	29
2.4.2	Results and Discussion	31
3	The Effect of Fermi-Dirac Statistics on the Transport Energy	38
3.1	Introduction	38
3.2	Theory	39
3.3	Results and Discussion	40
4	Doping and Trapping Model for Organic Semiconductors	46
4.1	Introduction	46
4.2	Theory	47
4.3	Doping Characteristics	49
4.4	Trapping Characteristics	55
5	Charge Injection Models for Organic Light-emitting Diodes	60
5.1	Introduction	60
5.2	Diffusion Controlled Injection Model for OLEDs	61
5.2.1	Theory	62
5.2.2	Results and Discussion	63
5.3	Charge Injection Model for OLED Based on Master Equation	65
5.3.1	Theory	66
5.3.2	Results and Discussion	68
6	Space Charge Limited Current in Organic Light-emitting Diodes	71

6.1	Introduction	71
6.2	Theory	71
6.3	Results and Discussion	73
7	Organic Semiconductor Device Models	79
7.1	Introduction	79
7.2	Analytical Model for Organic Thin Film Transistors	80
7.2.1	Variable Range Hopping Transport in Organic Semiconductors	80
7.2.2	Sheet Conductance of the OTFT	81
7.2.3	Drain Current	85
7.2.4	Results and Discussion	85
7.3	Device Model for Unipolar OLEDs	88
7.3.1	Theory	88
7.3.2	Results and Discussion	88
8	Conclusion	91
8.1	Current Progress	91
8.2	Future Work	92
	Curriculum Vitae	113

List of Abbreviations and Acronyms

CTRW	...	Continuous Time Random Walk
DASMB	...	Diphenylaminostyrylbenzene
DAT	...	Polydiazotized-3-amino-L-tyrosine
DOS	...	Density of States
FN	...	Fowler Nordheim
F4-TCNQ	...	Tetrafluoro-tetracyanoquinodimethane
GDM	...	Gaussian Disorder Model
HOMO	...	Highest Occupied Molecular Orbital
ITO	...	Indium Tin Oxide
LUMO	...	Lowest Unoccupied Molecular Orbital
NNH	...	Nearest Neighbor Hopping
NPB	...	4,4'-bis[N-1-naphthyl-N-phenyl-amino]biphenyl
OFET	...	Organic Field Effect Transistor
OLED	...	Organic Light-Emitting Diode
OTFT	...	Organic Thin-Film Transistor
PPV	...	Poly Phenylenevinylene
PTF	...	Polymer Thick Film Technology
RS	...	Richardson Schottky
SCLC	...	Space Charge Limited Current
SCL	...	Space Charge Limited
TCL	...	Trapped Charge Limited
TCNQ	...	7,7,8,8-tetracyanoquinodimethane
TSL	...	Thermally Stimulated Luminescence

TTA	...	Tolyltriazole
TOF	...	Time of Flight
VRH	...	Variable Range Hopping
ZnPc	...	Zinc Phthalocyanine

List of Symbols

Physical Quantities

Symbol	Unit	Description
ω_{ij}	ms^{-1}	Hopping rate between two sites
α	cm^{-1}	Inverse localization length
ν_0	s^{-1}	Attempt to escape frequency
E_i	eV	Energy at site i
E_j	eV	Energy at site j
R_{ij}	cm	Distance between site i and j
f_i	1	Occupation probability of site i
f_j	1	Occupation probability of site j
t	s	Time
μ_i	eV	Chemical potential at site i
μ_j	eV	Chemical potential at site j
σ_{ij}	S/cm	Conductivity between sites i and j
$\Delta\mu$	eV	Voltage drop over a single hopping distance
k_B	J/K	Boltzmann constant
T	K	Temperature
ΔE	eV	Energy drop over a single hopping distance
G	S/cm	Hopping conductivity
R_{max}	cm	Maximum hopping distance between two sites
E_{max}	eV	Maximum hopping energy of ininitial or finial site
N_s	cm^{-3}	Sites density in percolation theory
N_b	cm^{-3}	Bonds density in percolation theory
$g(E)$	$\text{cm}^{-3}\text{eV}^{-1}$	Density of states
θ	1	Unit step function

Symbol	Unit	Description
E_{tr}	eV	Transport energy
p	cm^{-3}	Total hole concentration
p_c	cm^{-3}	Mobile hole concentration
n	cm^{-3}	Electron concentration
Φ	V	Potential
δ	1	Fraction of occupied states
N_t	cm^{-3}	Concentration of trap states
Z_c	S/cm	Critical conductivity in percolation theory
E_F	eV	Fermi energy
T_0	K	Width of exponential DOS
T_σ	eV	Width of Gaussian DOS
\mathbf{R}_{ij}	1	Distance vector between sites i and j
F	V/m	Electric field
X_f	m	Average hopping distance along the electric field
R_{nn}	m	Nearest hopping range
σ	eV	Variance of Gaussian DOS
σ_0	S/cm	Conductivity prefactor in percolation theory
E_∞	eV	Thermal equilibrium energy of hopping carriers
E_A	eV	Activation energy
N_d	cm^{-3}	Total concentration of dopant states
T_1	K	Width of exponential DOS for dopants
j	A/cm^{-2}	Current density
Δ	eV	Barrier height between metal and organic semiconductor
m_{eff}	kg	Effective mass
x_d	m	Critical distance
ϵ_r	Fm^{-1}	Relative dielectric constant
G_s	S/cm	Sheet conductance
I_d	A/cm^{-2}	Drain current density
V_G	V	Gate voltage
τ_{rel}	s	Relaxation time for hopping transport

Constants

k_B	...	Boltzmann's constant	$1.380662 \times 10^{-23} \text{ JK}^{-1}$
q	...	Elementary charge	$1.602 \times 10^{-19} \text{ C}$
\hbar	...	Planck constant	$1.054 \times 10^{-34} \text{ Js}$
m_0	...	Electron mass	$9.108 \times 10^{-31} \text{ kg}$

Chapter 1

Introduction

1.1 Organic Semiconductors: History and Applications

For the past fifty years, inorganic semiconductors such as silicon and gallium arsenide silicon dioxide insulators, and metals such as aluminum and copper have been the backbone of the semiconductor industry. However, in 1977 the first highly conducting polymer, chemically doped polyacetylene [1] was discovered, which demonstrated that polymers could be used as electrically active materials as well. This discovery resulted in a huge research effort on conjugated organic materials. In the earlier time, the performance and stability of organic semiconductors were very poor. However, with drastic improvements in synthesis and processing of new classes of molecular materials such as conjugated polythiophenes in the past two decades [2], the prospects of commercially using organic semiconductors in applications such as organic light-emitting diodes (OLEDs), field-effect transistors (OFETs) and solar cells are now greater than ever [3, 4, 5]. In fact, in 2002 Philips introduced the Sensotec Philishave [6] as the first product in the market featuring a display panel based on OLED technology, and following that, Kodak has introduced [6] the Kodak EasyShare LS633 digital zoom camera with an award-winning OLED display technology. Sony produced 27-inch prototype OLED TV with a contrast ratio of greater than 10^6 and NTSC color reproduction ≥ 100 (Fig 1.1). Simplicity in manufacturing and lower costs of organic devices have been the primary reasons driving these devices towards commercialization.

1.2 Organic Semiconductor Physics

In inorganic semiconductor crystals such as silicon or germanium, the strong coupling between the constituting atoms and the long-range order lead to the delocalization of the



Figure 1.1: Two examples of use of OLEDs in commercial products. The image on the left shows a new Philips shaver introduced to the market in 2002. The image on the right shows the OLED TV produced by Sony recently. Images were taken from [6].

electronic states and the formation of allowed valence and conduction bands, separated by a forbidden gap. By thermal activation or photo-excitation, free carriers are generated in the conduction band, leaving behind positively charged holes in the valence band. The transport of these free carriers is described in quantum mechanical terms by Bloch functions, wave vector-space and dispersion relations.

However, because of structural or chemical defects in organic semiconductors, the motion of carriers is typically described by hopping transport, which is a phonon-assisted tunneling mechanism from site to site (Fig 1.2). Many hopping models are based on the Miller-Abrahams equation [7]. In this model hopping from a localized state i to a state j takes place at frequency ν_0 , corrected for a tunneling probability and the probability to absorb a phonon for hops upwards in energy:

$$\omega_{ij} = \nu_0 \begin{cases} \exp\left(-2\alpha R_{ij} - \frac{E_j - E_i}{k_B T}\right) & : E_j - E_i \geq 0 \\ \exp(-2\alpha R_{ij}) & : E_j - E_i \leq 0 \end{cases} \quad (1.1)$$

Here α is the inverse localization length, R_{ij} the distance between the localized states, E_i the energy at the state i , and ν_0 the attempt-to-escape frequency.

Since the hopping probability depends on both the spatial and energetic difference between the hopping sites, it is natural to describe the hopping processes in a four-dimensional hopping space, which is spanned by three spacial and one energy coordinate.

In organic solids, interactions are mainly covalent, but intermolecular interactions are due to much weaker van der Waals and London forces. These organic semiconductors typically have narrow energy bands, the highest occupied molecular orbital (HOMO) and the lowest unoccupied molecular orbital (LUMO), which can be easily disrupted

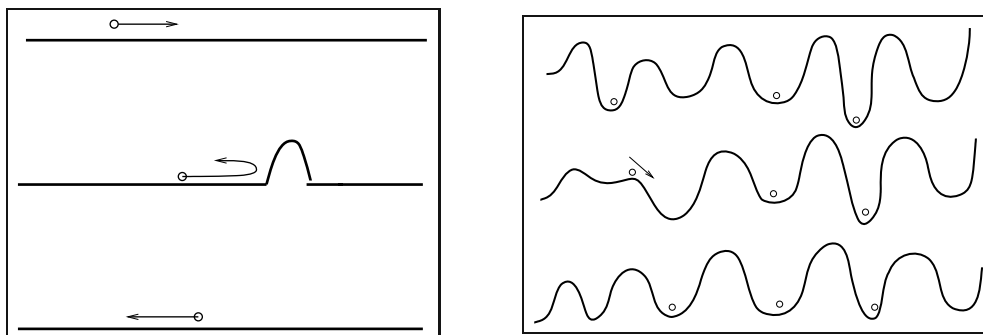


Figure 1.2: Charge transport mechanism in solids. The left image describes the band transport. In a perfect crystal, depicted as a straight line, free carriers are delocalized. There are always lattice vibrations that disrupt the crystal symmetry. Carriers are scattered at these phonons, which limit the carriers mobility. The image on the right describes hopping transport. If a carrier is localized due to defects, disorder or selflocalization, the lattice vibrations are essential for a carrier to move from one site to another. The figure is from [8].

by disorder. Thus, even in molecule crystals, the concepts of allowed energy band is of limited validity and excitations and interactions localized on individual molecules play a predominant role. The charge transport sites have a Gaussian distribution of energies and are localized [8]. The shape of the density of states (DOS) is suggested to be Gaussian based on the observed Gaussian shape of the optical spectra [9].

Transport energy [10] is a useful concept for the analysis of hopping transport in organic semiconductors. Importance of the transport energy stems from the fact that this is the energy that maximizes the probability for a carrier to hop upward in energy. It does not depend on the carrier initial energy, thus serving as an analog to the mobility edge.

For polycrystalline organic semiconductor layers, the temperature dependent transport data is often interpreted in terms of a multiple trapping and release model [11, 12]. In this model the organic semiconductor film consists of crystallites which are separated from each other by amorphous grain boundaries. In the crystallites the carriers are delocalized, while the carriers in the grain boundaries become trapped in localized states. The transport description in terms of trapped carriers that can be thermally activated to transport level, is very similar to hopping transport as discussed above.

1.3 Theoretical Concepts

The incoherent dynamics of carriers as well as excitons can be described by a master equation,

$$\frac{df_i(t)}{dt} = f_i(t)(1 - f_j(t))\omega_{ij} - f_j(t)(1 - f_i(t))\omega_{ji} + \lambda_i f_i(t). \quad (1.2)$$

with f_i denoting the occupation probability of state i and ω_{ij} the electron or hole transition rate of the hopping process between the occupied state i to empty state j . Defining μ_i as the chemical potential at the position of state i and E_i as the energy of state i , the occupation probability is given by the Fermi-Dirac distribution function

$$f_i = \frac{1}{1 + \exp\left(\frac{E_i - \mu_i}{k_B T}\right)}. \quad (1.3)$$

Assuming no correlations between the occupation probability of different localized states, the steady-state current between these two sites is given by

$$I_{ij} = q [f_i(t)(1 - f_j(t))\omega_{ij} - f_j(t)(1 - f_i(t))\omega_{ji}]. \quad (1.4)$$

Substituting the Miller-Abrahams rate (1.1) in (1.4) the current becomes

$$I_{ij} = \frac{q\nu_0 \exp\left(-2\alpha R_{ij} - \frac{|E_i - E_j|}{2k_B T}\right) \sinh\left[\frac{\mu_i - \mu_j}{2k_B T}\right]}{\cosh\left[\frac{E_i - \mu_i}{2k_B T}\right] \cosh\left[\frac{E_j - \mu_j}{2k_B T}\right]}. \quad (1.5)$$

In the case of low electric field, resulting in a small voltage drop over a single hopping distance ($\Delta\mu = \mu_j - \mu_i \ll k_B T$), the following conductance is obtained

$$\sigma_{ij} = \frac{I_{ij}}{\Delta\mu} \propto \exp\left[-2\alpha |R_{ij}| - \frac{|E_i - \mu| + |E_j - \mu| + |E_i - E_j|}{2k_B T}\right]. \quad (1.6)$$

Here $\mu_i \approx \mu_j \approx \mu$. This expression was introduced in 1960 by Miller and Abrahams [7] and is often referred as the Miller-Abrahams conductance. Equation (1.6) has an important implication. Even if the energies are moderately distributed, the exponential dependence of σ_{ij} on these energies makes them enormously broadly distributed. This can be used to reduce the computations of the effective properties of the network, since the broadness of the distribution of σ_{ij} implies that there are many small conductances that can be removed from the network. This resulting network is called the reduced network [13].

Miller and Abrahams [7] were the first to calculate the hopping conductivity G of semiconductors using reduced networks. They assumed that the statistical distribution of the resistances depends only on R_{ij} and not on the site energies. This was justified because the experimental data for some semiconductors indicated that the impurity

conduction exhibits a well-defined activation energy. But Mott [16] pointed out that the exponential dependence of the resistances on the site energies can not be ignored in most cases. When a carrier close to the Fermi energy hops away over a distance R with an energy ΔE , it has $\frac{4}{3}\pi R^3 \rho \Delta E$ sites to choose from, where ρ is the site density function. In general, the carrier will jump to a site for which ΔE is as small as possible. The constraint to find a site within a range $(R, \Delta E)$ is given by $\frac{4}{3}\pi R^3 \rho \Delta E \approx 1$. Substituting this relation into (1.6) yields

$$G \propto \exp \left[-2\alpha R - \frac{1}{k_B T (4/3) \pi R^3 \rho} \right]. \quad (1.7)$$

The optimum conductance is obtained by maximizing G with respect to the hopping distance R as

$$G \propto \exp \left[- \left(\frac{T_1}{T} \right)^{1/4} \right], \quad (1.8)$$

with $k_B T_1 \propto \gamma^3 / \rho$.

1.3.1 Gaussian Disorder Model (GDM)

Much theoretical work has been done by investigating the mobilities of organic semiconductors within the framework of GDM [9]. Non-crystalline organic solids, such as molecularly doped crystals, molecular glasses, and conjugated polymers, are characterized by small mean free paths for the carriers, as a result of the high degree of disorder present in the organic system. Therefore, the elementary transport step is the charge transfer between adjacent elements, which can either be molecules participating in transport or segments of a polymer separated by topological defects. These charge transporting elements are identified as sites whose energy are subjected to a Gaussian distribution

$$g(E) = \frac{N_t}{\sqrt{2\pi}\sigma} \exp \left(-\frac{E^2}{2\sigma^2} \right),$$

where E is the energy measured relative to the center of the density of states and σ is the standard deviation of the Gaussian distribution. Within this distribution, all the states are localized. The choice of such distribution was based on the Gaussian profile of the excitonic absorption band, as well as on the recognition that the polarization energy is determined by a large number of internal coordinates, which vary randomly by a small amount, so the central limit theorem of statistics holds.

The Gaussian disorder model has been treated by the Monte Carlo simulation technique based on the Miller Abraham equation [9]. In this simulation charge transport is described as an incoherent random walk. The carriers start their motion from randomly chosen sites at one of the boundaries of the system sample. Their trajectories are specified from the constraint that the probability for a carrier to jump between two transport

sites is

$$p_{ij} = \frac{\omega_{ij}}{\sum_{i \neq j} \omega_{ij}}.$$

With this technique, TOF measurements can be simulated [9], in which mobility is derived from the mean arrival time of the carrier at the end of the sample and from their mean displacement. The predictions made concern the temperature and electric field dependence of the mobility.

In the Gaussian disorder model, the strength of electronic coupling among sites is split into separate contributions from the relevant sites, each obtained from a Gaussian probability density. However, the choice for the off-diagonal disorder of a Gaussian distribution is not theoretically sustained unlike in the case of energy disorder, and a more realistic way of representing geometric disorder has been pursued. One of such attempt is described in [14], in which an alternative approach comprising positional and orientation disorder is introduced via fluctuations in the bonds adjoining the various transport sites rather than site fluctuations. This model gets rid of the unnecessary corrections between hops and results in overestimating the contribution of the log hops.

In particular, Gartstein and Conwell's [14] Monte Carlo simulations of hopping with the elementary jump rate described by 1.1, but in which

$$\omega_{ij} = \exp(\varsigma_{ij}) \exp(-2\alpha R_{ij}),$$

where ς_{ij} is a uniformly distributed random variable. In this way, the different bonds of a given site with its neighbors are uncorrelated.

Another approach for the description of positional disorder was presented by Hartenstein [15], and was also based on Monte Carlo simulations of transport in a dilute lattice. This treatment employs the GDM, but without the need for defining a distribution function for the electronic coupling between different sites. In this case the hopping sites having the nearest neighbors were grouped in clusters whose size depends on the random intercluster distances, but ignores any contribution from the random orientation of the transporting elements. Nevertheless, the model is adequate for low dopant concentrations for which there are large fluctuations in the intersite distances.

1.3.2 Percolation Theory

Ambegaokar and coworkers argued that an accurate estimate of G is the critical percolation conductance G_c [17], which is the largest value of the conductance such that the subnet of the network with $G_{ij} \geq G_c$ still contains a conducting sample-spanning cluster. They divided the network into three parts. First, a set of isolated clusters of high conductivity where each cluster consists of a group of sites connected together by conductances $G_{ij} \gg G_c$; Second, a small number of resistors with G_{ij} of order G_c , which

connect together a subset of high conductance clusters to form the sample-spanning cluster, called the critical subnetwork, essentially the same as the static limit of the reduced network discussed above; and third, the remaining resistors with $G_{ij} \ll G_c$. The resistors in the second part dominate the overall conductance of the network. The critical conductance G_c is calculated as follows.

The percolation subnetwork consists of conductances with $G_{ij} \geq G_c$. Using (1.6), this condition can be written as

$$\frac{R_{ij}}{R_{max}} + \frac{|E_i - \mu| + |E_j - \mu| + |E_i - E_j|}{2E_{max}} \leq 1, \quad (1.9)$$

with

$$R_{max} = \frac{1}{2\alpha} \ln \left(\frac{G_c k_B T}{e\nu_0} \right), \quad (1.10)$$

$$E_{max} = k_B T \ln \left(\frac{G_c k_B T}{e\nu_0} \right). \quad (1.11)$$

R_{max} is the maximum distance between any two sites between which a hop can occur, and E_{max} is the maximum energy that any initial or final state can have. Thus the density of states that can be part of the percolating subnetwork is given by

$$N_s = 2\rho E_{max}. \quad (1.12)$$

Since the sites in the subnetwork are linked only to sites within a range R_{max} , this criterion has the form

$$N_s R_{max}^3 = \nu_c, \quad (1.13)$$

with ν_c being a dimensionless constant. A combination of (1.9) to (1.11) yields Mott's law (1.8), with $k_B T_1 = 4\nu_c \gamma^3 / \rho$.

1.3.3 Transport Energy

According to the Miller Abraham equation (1.1) we can roughly calculate the nearest-neighbor distance for an upward hop from an initial site with energy E_i to a final site with energy $E_f \geq E_i$ from the equations below [10]

$$\frac{4\pi}{3} R^3(E_f) \int_{-\infty}^{E_f} g(E) dE \approx 1. \quad (1.14)$$

Here $g(E)$ is the DOS function. The hopping distance can be calculated as

$$R(E_f) = \left[\frac{4\pi}{3} \int_{-\infty}^{E_f} g(E) dE \right]^{-1/3}. \quad (1.15)$$

So the corresponding hopping rate is

$$\nu = \nu_0 \exp \left(-2\alpha R(E_f) - \frac{E_f - E_i}{k_B T} \right). \quad (1.16)$$

Maximization of (1.16) over energy E_f gives the equation

$$g(E_f) \left[\int_{\infty}^{E_f} g(E) dE \right]^{-4/3} = \frac{1}{\gamma k_B T} \left(\frac{9\pi}{2} \right)^{1/3}. \quad (1.17)$$

The final energy E_f that maximizes the hopping probability does not depend on the initial energy E_i . This particular energy is called transport energy E_{tr} [10].

Arkhipov extended this theory to the effective transport energy [18]. In this theory, the Miller Abrahams equation is rewritten as

$$\nu = \nu_0 \exp(-\mu(R_{ij}, E_i, E_j)) = \nu_0 \exp \left[-2\alpha R_{ij} - \frac{\theta(E_j - E_i)}{k_B T} \right], \quad (1.18)$$

with the hopping parameter μ and the unity step function θ . The average number $n(E_i)$ of target sites for a starting site with energy E_i , whose hopping parameters are not larger than μ can be calculated as

$$n(E_i, \mu) = 4\pi \int_0^{\mu/2\alpha} R_{ij}^2 dR_{ij} \int_{-\infty}^{E_i + k_B T(\mu - 2\gamma R_{ij})} g(E_t) dE_t. \quad (1.19)$$

Neglecting the downward jumps and defining

$$E_{tr} = E_i + k_B T \mu \quad (1.20)$$

transform (1.19) into

$$n(E_i, \mu) = \frac{\pi}{6} (\alpha k_B T)^{-3} \int_{E_i}^{E_{tr}} g(E_t) (E_{tr} - E_t)^3 dE_t. \quad (1.21)$$

According to variable range hopping theory [19], a hop is possible if there is at least one such hopping neighbor, i.e. $n = 1$. This leads to the following equation

$$\int_{E_i}^{E_{tr}} g(E_t) (E_{tr} - E_t)^3 dE_t = \frac{6}{\pi} (\alpha k_B T)^3. \quad (1.22)$$

If the DOS distribution decreases with energy faster than E^{-4} then the integral on the left-hand side of (1.22) depends weakly upon the lower bound of integration for sufficiently deep starting sites, and (1.22) is reduced to

$$\int_{-\infty}^{E_{tr}} g(E_t) (E_{tr} - E_t)^3 dE_t = \frac{6}{\pi} (\alpha k_B T)^3, \quad (1.23)$$

where E_{tr} is the effective transport energy.

1.3.4 Multiple Trapping Theory

To investigate charge transport and charge buildup in SiO_2 films, an analysis of hole transport has been presented which is predicated on a model involving stochastic hopping transport. This description, based on the work of Scher and Montroll [20], accounts for many of the features of hole conduction in SiO_2 and has been termed the continuous-time random walk (CTRW) model. A wide range of experimental observation can be understood on this basis [20, 21, 22]. However, there has been some reticence to accept the CTRW model completely because of observations that the apparent activation energy for the charge collection process depends on the fraction of charge collected [23]. This observation is at odds with the CTRW model as it has been presented, since that model predicts universality, i.e., charge transport curves obtained at different temperature should superimpose with a simple shift in the time axis [24]. Although charge collection curves obtained at different temperature do superimpose approximately, there is some deviation, and this deviation is in the direction predicted by the multiple-trapping model.

The multiple-trapping model for unipolar conduction is defined by the following equations [12]

$$\frac{\partial \rho(\mathbf{x}, t)}{\partial t} = g(\mathbf{x}, t) - \nabla \cdot f(\mathbf{x}, t), \quad (1.24)$$

where

$$\rho(\mathbf{x}, t) = p(\mathbf{x}, t) + \sum_i p_i(\mathbf{x}, t) \quad (1.25)$$

and

$$\frac{\partial p_i(\mathbf{x}, t)}{\partial t} = p(\mathbf{x}, t) \omega_i - p_i(\mathbf{x}, t) \gamma_i \quad (1.26)$$

Here $g(\mathbf{x}, t)$ is the local photogeneration rate, f is the flux of mobile charge carriers, the total carrier concentration is $\rho(\mathbf{x}, t)$, $p(\mathbf{x}, t)$ is concentration of mobile carriers, $p_i(\mathbf{x}, t)$ is the carrier concentration temporarily immobilized in the i th trap, ω_i is the capture rate by the i th trap and γ_i is the release rate.

Later multiple trapping theory was extended for disordered organic semiconductors as:

$$p = p_c + \int \rho(E) dE. \quad (1.27)$$

Here p is the total hole concentration, p_c is the hole concentration in extended states and $\rho(E)$ is the energy distribution of localized (immobile) holes. Since carrier trapping does not change the total carrier concentration p , the continuity equation can be written as

$$\frac{\partial p}{\partial t} + \mu_c F \frac{\partial p_c}{\partial x} - D_c \frac{\partial^2 p_c}{\partial x^2} = 0, \quad (1.28)$$

with the mobility μ_c and the diffusion coefficient D_c . This equation assumes two simplifications: no carrier recombination and constant electric field (no space charge). Substituting the trapping rate

$$\frac{p_c g(E)}{\tau_0 N_t} \quad (1.29)$$

and release rate

$$\nu_0 \exp\left(-\frac{E}{k_B T}\right) \rho(E) \quad (1.30)$$

gives the following equation

$$\frac{\partial \rho(E)}{\partial t} = \frac{1}{\tau_0 N_t} g(E) - \nu_0 \exp\left(-\frac{E}{k_B T}\right) \rho(E) \quad (1.31)$$

In equilibrium the energy distribution of localized carriers is established, and the function $\rho(E)$ does not depend upon time

$$\frac{\partial \rho(E)}{\partial t} = 0. \quad (1.32)$$

1.4 Organic Light-Emitting Diodes (OLED)

A major breakthrough in the field of organic semiconductors was the discovery of light emission from an electrically active polymer [25]. The ease of processing, combined by pure colors make it an ideal candidate for lighting applications [26, 27]. Especially the display industry is highly interested in organic semiconductors, as these have advantages over liquid crystal displays such as high switching speed, wide viewing angle, pure color, and also over cathode ray tubes such as low energy consumption, flat screen, and light weight. These properties stimulated the research on organic semiconductors strongly. Basically, a OLED consists of a thin layer of a polymer sandwiched between two electrodes on top of glass substrate (see Fig 1.3). On top of this bottom contact, a thin organic semiconductor layer is deposited. Layer thicknesses of this active layer are typically only of the order of 100nm, because of the low carrier mobility. Under forward bias electrons and holes are injected into the organic semiconductor from the cathode and the anode, respectively. Driven by the applied electric field, the carriers move through the organic semiconductors in opposite direction until recombination takes place. The device operation of an OLED is thus determined by four processes: charge injection, transport, recombination and phonon emission.

The transport and injection properties of holes can be investigated by choosing a special contact material. In these hole-only devices, the workfunction of both electrodes are very close to the HOMOs of the organic semiconductor, preventing electron injection from the cathod.

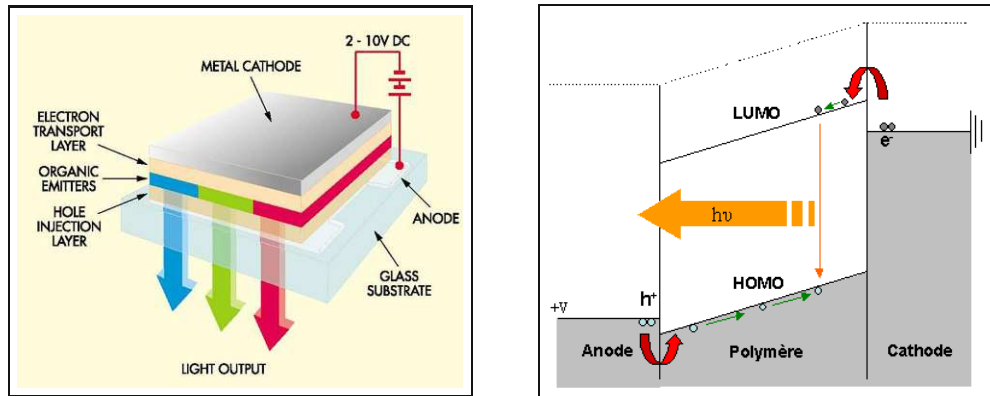


Figure 1.3: Left: device layout of a typical organic light-emitting diode (OLED). It consists of a glass substrate with an indium-tin-oxide (ITO) coating functioning as anode, a spin-coated layer of an organic semiconductor as the active layer, and an evaporated metal cathode. Right: working principle of an OLED. Four important processes are shown: (1) Charge injection (2) Transport (3) Exciton formation (4) Photon emission. The last two steps form the recombination process.

1.5 Thin Film Organic Field-Effect Transistors (OTFT)

A field-effect transistor is a three-terminal device configured like a parallel plate capacitor, where one conduction electrode, the gate electrode, is electrically insulated from the organic semiconductor layer (see Fig 1.4) [28, 29]. Two electrodes, the source and the drain, are connected to the organic semiconductor layer. By controlling the voltage on the gate, a charge can be induced. These charges are injected from the source electrode and cross the conducting channel towards the drain by applying voltage between the two electrodes. Silicon has been the most widely used semiconductor material in field-effect transistors, because these devices exhibit fast switching speeds and are therefore suitable for use in modern processors. However, there are many applications for field-effect devices where fast switching speed is not a requirement, such as, for example, large-area coverage, mechanically flexible and low cost integrated circuits. With the successful synthesis of the first organic transistors in 1986 [30], the prospect of replacing costly and labor-intensive inorganic devices with cheaper and more flexible organic electronic materials entered a new era.

Despite considerable improvement in the fabrication and characterization of thin-film organic field-effect transistors, the physics of charge injection and transport in these devices is not well understood.

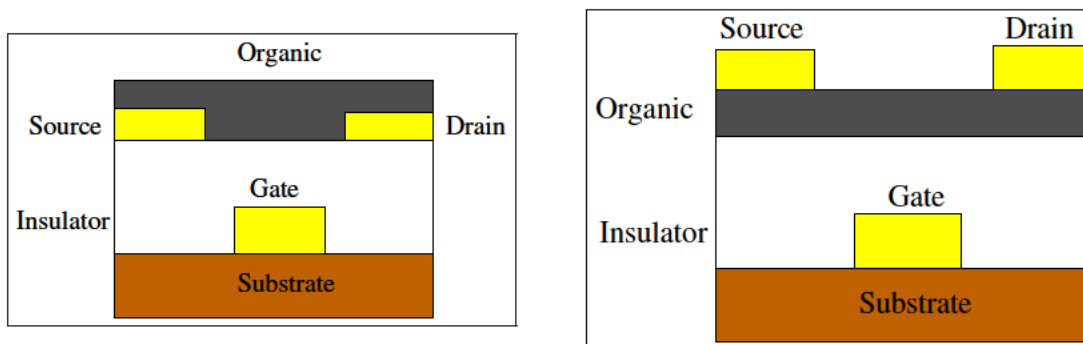


Figure 1.4: Left: A schematic view of a bottom contact OFET. The source electrode is grounded, while the drain and the gate are biased negatively. In this mode, holes are injected from the source and collected at the drain. Right: a top contact OFET with the electrodes patterned on top of the organic semiconductor.

1.6 Solar Cells

The solar cell in principle consists of a photoactive layer sandwiched between two electrodes [31]. The bandgap of the photoactive layer should be chosen to match the solar irradiance spectrum. In order to create carriers rather than excitons that would be formed in a pure material, polymer solar cells commonly use a combination of two semiconductors with complementary electronic levels. The initial step after photoexcitation is the dissociation of an exciton via charge transfer at the interface of these two materials. After the charge transfer the electrons and holes have to escape their Coulomb potential and migrate towards either electrode due to the internal field. This migration leads to an electric field opposing the external field that will be reduced up to a certain distance from the electrodes. As both carriers will recombine at the opposite electrodes a continuous current flow is created. The resulting electric field in the organic layer depends thus on the free electron and hole concentration, their drift mobility and diffusion coefficient, the generation, and the recombination rate in the bulk and at the electrodes.

1.7 Organic Lasers

Conjugated polymers in particular are good candidates for laser application for several reasons. The first is that the inherent electronic structure of most conjugated polymers is a four-level system. Materials with a four or more level system are attractive for laser application. Another advantage of conjugated polymers for laser applications is the disorder of the conjugated system, which promotes the energy transfer from one region to another in the active layer. Conjugated polymers also have high luminescence efficiencies. Some of the conjugated polymers have the additional advantage that the

emission and absorption spectra do not overlap.

1.8 Organic Memory

Electrical bistability has been demonstrated in organic materials. Bistability means that the material shows two different states of conductivity at the same applied voltage, typically a highly conductive on-state and poorly conductive off-state. These states are stable, and a transition between them can occur when a defined criterion such as a high voltage bias is met. This property is ideal for rewritable memory applications. Organic memory devices are generally realized by interposing thin layers containing organic materials between two electrodes. Such devices have the potential advantages of flexibility, easy processing, low cost, and large area fabrication by printing techniques.

1.9 Scope and Outline of this Thesis

The chapters of this thesis are related in the following manner. In Chapter 2, we study the electric field, temperature and carrier concentration dependence of the mobility. In Chapter 3, the effect of Fermi-Dirac statistics on transport energy is discussed. In Chapter 4, a doping and trap concentration dependent conductivity model is presented. In Chapter 5 and 6 we investigate the charge injection model and space charge limited current in organic light-emitting diodes. Device models are presented in Chapter 7.

Chapter 2

Mobility Models for Organic Semiconductors

2.1 Introduction

The carrier mobility of organic semiconductors has improved tremendously over the past few years. A field-effect mobility as high as $0.1\text{cm}^2/\text{Vs}$ has recently been measured in region-regular poly(thiophenes) [32, 33, 34]. Because the structure of the polymer depends on the processing conditions, it is not uncommon to find in the literature widely differing mobility values obtained for the same polymer. In particular, the dielectric surface energy prior to the deposition of the polymer [35, 36, 37, 38], the solvent evaporation rate [33], the molecular weight of the polymer [39] and thermal post-processing of the film [40] all influence the carrier mobility.

There is no general consensus on the mechanism of charge transport in these amorphous organic materials. A complete model of the electrical properties should include a description of the energy distribution of carriers and how the conduction varies as a function of carrier energy. Disorder-induced localized states are also important for the transport, and the essential problem is the relation between temperature, electric field, carrier concentration and the transport properties. Generally, charge transport in disordered materials is described either as hopping between localized states, or as trapping and release from localized states into higher energy mobile states. The degree of structural disorder may change the mechanism even within the same class of polymer.

Because the electronic structure of polymer films is not known exactly, a simplified model has to be assumed. The model was proposed by Bassler [9] assuming that the energy distribution is Gaussian due to the random disorder in the material. The standard deviation of Gaussian is around 0.1eV and increases with increasing disorder of the

material. To simplify the calculations, an electronic structure comprising an exponential tail in the bandgap is often used as well.

In this chapter, we present three different models to describe the carrier concentration dependence of the mobility, the temperature and electric field dependence, and a unified mobility model that can explain the temperature, electric field and carrier concentration characteristics together.

2.2 Carrier Concentration Dependence of Mobility

Recently it has been realized that the carrier concentration plays an important role for the mobility. Experiments show that for a hole-only diode and a FET fabricated from the same conjugated polymer, the mobility could differ up to three orders of the magnitude [41]. This difference can only be explained by taking into account the dependence of mobility on the carrier concentration. Rubel [42] analyzed this problem with the concept of a transport energy E_t , but there is no direct proof for the existence of such transport energy in organic systems. In this work we will focus on extending the percolation model based on VRH theory by Vissenberg [43] to explain the discrepancy of mobilities measured in OLEDs and OFETs.

In this section, an analytical mobility model with a Gaussian DOS function has been obtained. It can explain the relation between the mobility and carrier concentration. Results are in good agreement with experimental data.

2.2.1 Theory

To calculate the mobility of an organic semiconductor, one can use percolation theory, regarding such system as a random resistor network (network of Miller and Abrahams) [7, 44]. The current flows through the bonds connecting the sites in the network. The conductance between the states m and m' can be described as

$$Z_{mm'}^{-1} = Z_0^{-1} \exp(-2\alpha |R_m - R_{m'}|) \exp\left(-\frac{|E_m - E_F| + |E_{m'} - E_F| + |E_{m'} - E_m|}{2k_B T}\right),$$

where Z_0^{-1} is a prefactor, α^{-1} is the Bohr radius of the localized wave functions, T is the temperature, R_m and E_m denote the position and energy of site m . In theory the value of $Z_{mm'}$ is determined by the threshold or critical conductance Z_c , at which the first infinite cluster will form, given by the relation

$$\sigma = \sigma_0 Z_c^{-1}. \quad (2.1)$$

Here σ_0 is a prefactor. To describe the field-effect mobility in organic transistors, Visenberg assumed an exponential density of localized states [43].

$$g(E) = \frac{N_t}{k_B T_0} \exp\left(\frac{E}{k_B T_0}\right) \quad (E \leq 0) \quad (2.2)$$

N_t is the number of states per unit volume and T_0 specifies the width of the exponential distribution. Connecting (2.1) and (2.2), the conductivity can be described as [43]

$$\sigma(\delta, T) = \sigma_0 \left(\frac{\pi \delta N_t (T_0/T)^3}{(2\alpha)^3 B_c \Gamma(1 - T_0/T) \Gamma(1 + T_0/T)} \right)^{T_0/T}. \quad (2.3)$$

Here B_c is the critical number of bonds per site and δ is the fraction of occupied states, defined as

$$\delta \cong \exp\left(\frac{\epsilon_F}{k_B T_0}\right) \Gamma(1 - T/T_0) \Gamma(1 + T/T_0),$$

Γ is the gamma function. Then an expression for the mobility as a function of the carrier concentration n can be obtained.

$$\mu(n, T) = \frac{\sigma_0}{q} \left(\frac{(T_0/T)^4 \sin(\pi T/T_0)}{(2\alpha)^3 B_c} \right)^{T_0/T} n^{T_0/T-1}. \quad (2.4)$$

However, this expression can not account for the carrier concentration independent mobility when the carrier concentration is very low (LED regime). To overcome this problem, we derive another mobility model assuming a Gaussian DOS [9] and VRH theory. In this model, the DOS function is given as

$$g(E) = \frac{N_t}{\sqrt{\pi} k_B T_\sigma} \exp\left[-\left(\frac{E}{k_B T_\sigma}\right)^2\right]. \quad (2.5)$$

Here E is the energy measured relative to the center of the DOS and T_σ indicates the width of the DOS. The value of the Fermi energy E_F can be determined by the equation for the carrier concentration n .

$$n = \int_{-\infty}^{\infty} \frac{g(E) dE}{1 + \exp((E - E_F)/k_B T)}. \quad (2.6)$$

At low concentration, the exponential function is large compared to one (the nondegenerate case) [45], and we obtain the Fermi energy as

$$E_F = -\frac{k_B T_\sigma^2}{4T} + k_B T \ln \delta. \quad (2.7)$$

According to percolation theory [17], at the onset of percolation, the critical number B_c can be written as

$$B_c = \frac{N_b}{N_s}. \quad (2.8)$$

$B_c = 2.8$ for a three-dimensional amorphous system, N_b and N_s are, respectively, the density of bonds and density of sites in a percolation system, which can be calculated as [43, 46]

$$N_b = \int d\mathbf{R}_{ij} dE_i dE_j g(E_i) g(E_j) \theta(s_c - s_{ij})$$

and

$$N_s = \int dE g(E) \theta(s_c k_B T - |E - E_F|).$$

Here \mathbf{R}_{ij} denotes the distance vector between sites i and j , s_c is the exponent of the conductance given by the relation $\sigma = \sigma_0 e^{-s_c}$ [13] and θ is step function.

Substituting (2.5) and (2.7) into (2.8), we obtain a new percolation criterion for an organic system as

$$B_c \approx \frac{2N_t (\sqrt{2} + 1) \sqrt{\pi}}{(2\alpha T/T_\sigma)^3} \left(\frac{E_F + k_B T s_c}{k_B T_\sigma} \right)^2 \exp \left(- \left[\frac{E_F + k_B T s_c}{k_B T_\sigma} \right]^2 \right).$$

This equation has to be solved for s_c and an expression for mobility can be obtained.

$$\mu = \frac{\sigma_0}{qN_t} \exp(\eta), \quad (2.9)$$

where

$$\eta = -\frac{T_\sigma}{T} \sqrt{-W \left[-\frac{B_c (2\alpha T/T_\sigma)^3}{2\pi N_t (1 + \sqrt{2})} \right] - \frac{T_\sigma^2}{4T^2}}$$

W is the Lambert function [47]. Equation (2.9) is obtained assuming

- that the site positions are random,
- the energy barrier for the critical hop is large,
- and the charge carrier concentration is very low.

2.2.2 Results and Discussion

So far, much attention has been devoted to explain the temperature dependence of the mobility [48, 49, 50]. As shown in Fig 2.1, the model (2.9) gives a non-Arrhenius-type temperature dependence of the form $\mu \propto \exp \left(- (C\sigma/k_B T)^2 \right)$, which has also been supported by numerical simulations [51] and analytical calculations [53]. The model (2.9) shows good agreement for a value $C \approx 0.71$. This value is close to $C \approx 0.69$ given in [52] and 0.64 in [53].

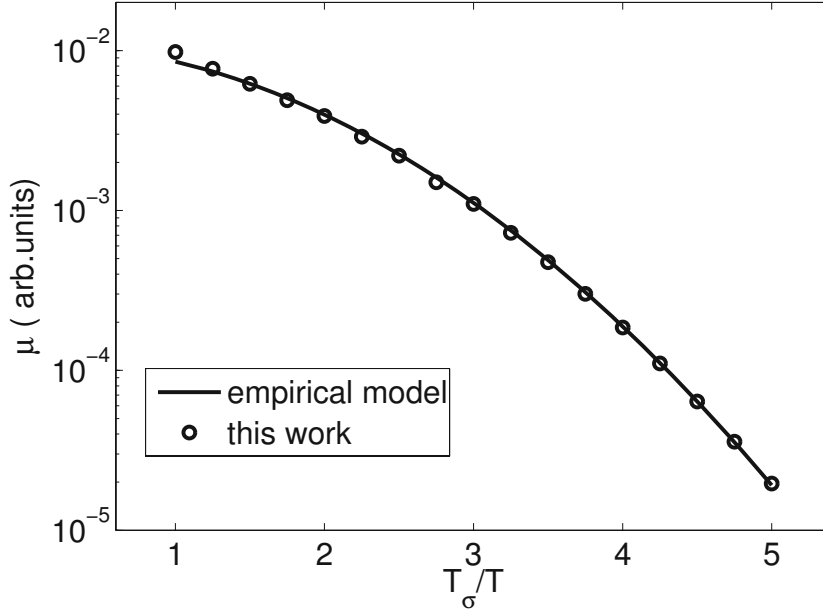


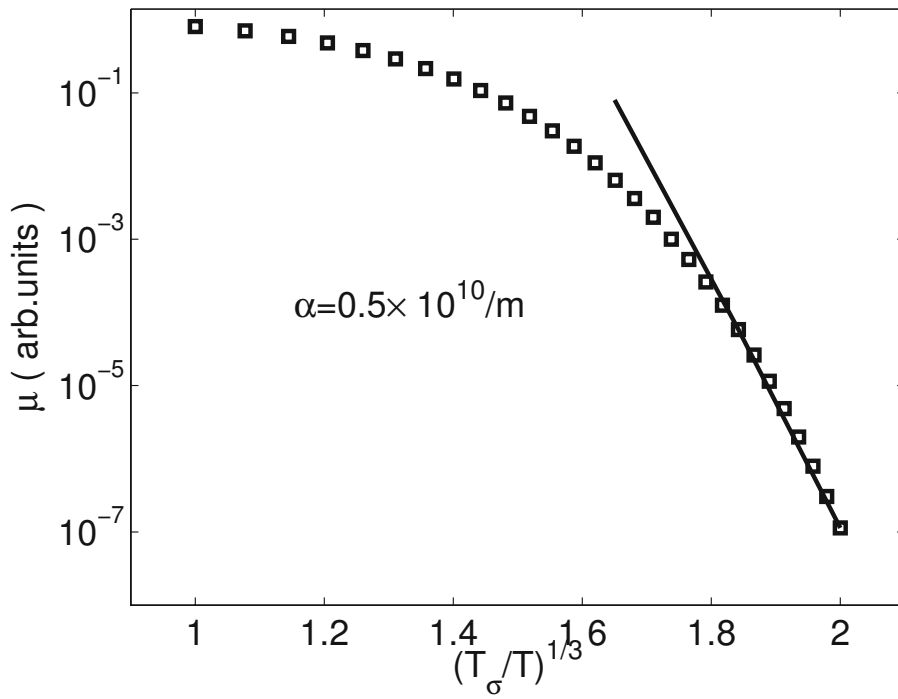
Figure 2.1: Comparison between the analytical model (2.9) and empirical model $\mu \approx \exp\left(- (C\sigma/k_B T)^2\right)$ for different temperature.

In Fig 2.2, the mobility is plotted as a function of $(T_\sigma/T)^{1/3}$. When plotted in this way, there exists the regime with a linear relation between μ and $T^{-1/3}$. This indicates that the variable-range hopping effect has to be taken into account [54, 55].

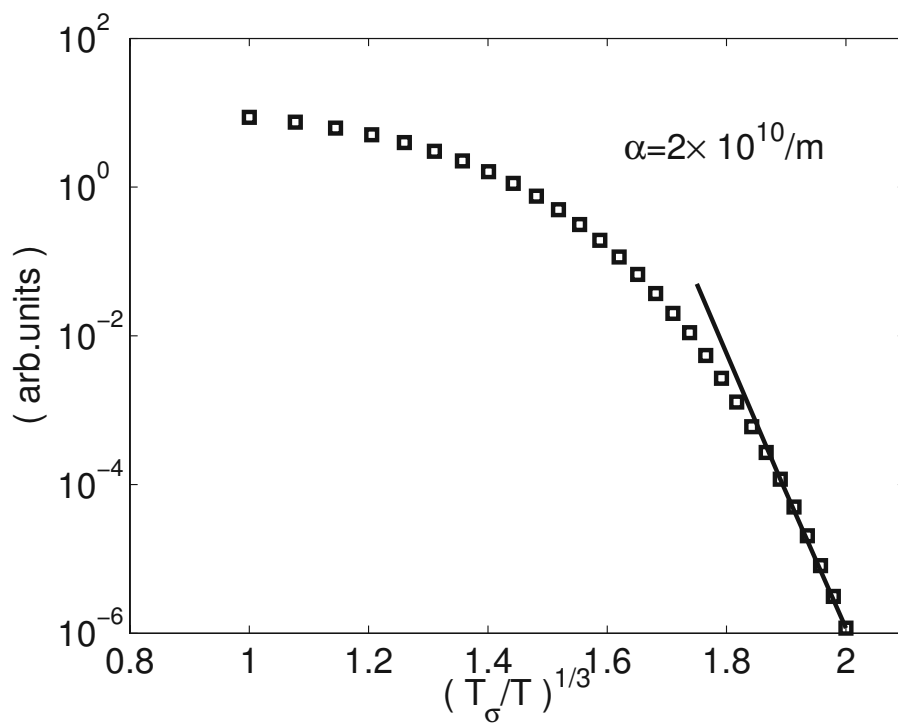
To obtain (2.7), a Boltzmann distribution function has been used. The degenerate limit of organic semiconductors has been studied in [56, 57]. In Fig 2.3 (a) we show the Fermi energy for Boltzmann and Fermi-Dirac distributions assuming some typical values of the parameter T_σ/T as 1.5, 3.5 and 6.0 [48]. Fig 2.3 (b) is a comparison especially for the higher carrier occupation regime. The analytical result (2.7) agrees well with the numerically calculated result for decreasing carrier occupation and increasing T_σ/T . Therefore, for the LED regime with low charge carrier concentration, (2.7) is a good approximation of the solution of (2.6).

The mobility as a function of the carrier concentration is presented in Fig 2.4, where T_σ/T is in the range 1.5–9.0, corresponding to some typical values for organic semiconductors. The mobility stays constant until a certain threshold value of the carrier occupation. Above this threshold, the mobility can increase about four orders of magnitude at $T_\sigma/T=9$. These effects have also been observed experimentally [41, 58].

However, (2.9) is valid only in the LED regime with very low carrier concentration. As it is difficult to get an analytical expression for the mobility at higher carrier concentration,

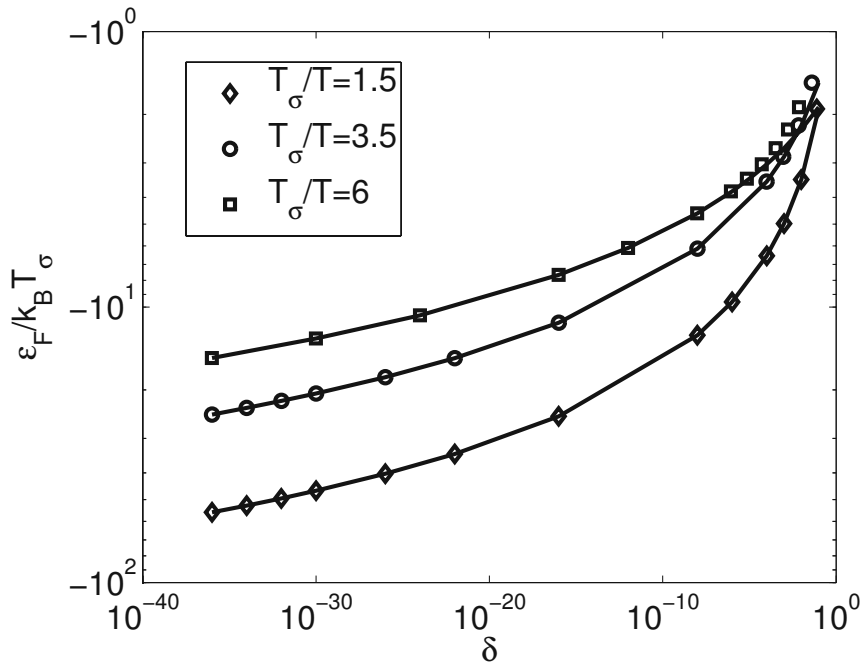


a

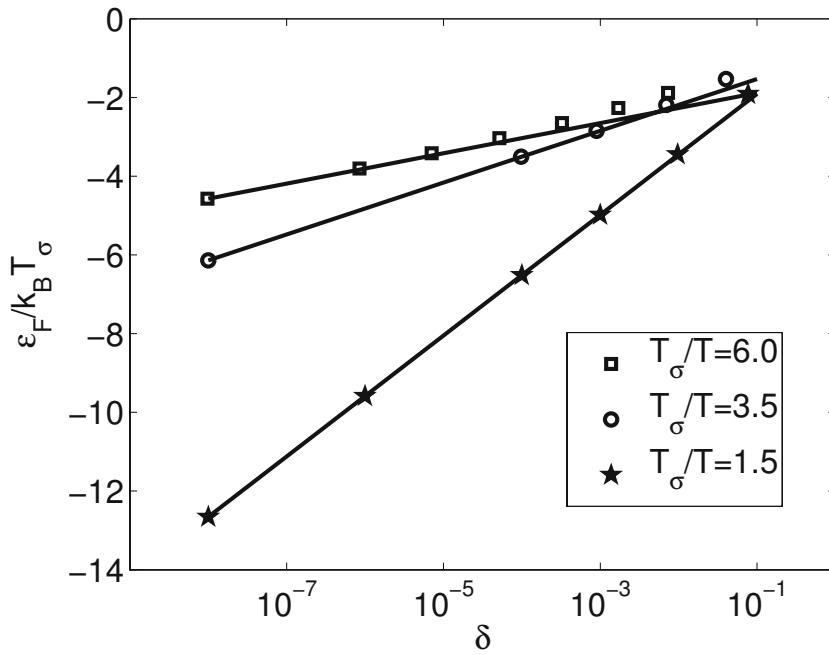


b

Figure 2.2: The mobility as a function of $(T_{\sigma}/T)^{1/3}$ for different α .



(a)



(b)

Figure 2.3: Fermi-energy as a function of the carrier occupation probability. The symbols represent Fermi-Dirac and the solid lines Boltzmann represent statistics. Panel (a) shows the case of carrier occupation between 10^{-40} and 1. Panel (b) shows the case of carrier occupation bigger than 10^{-10} .

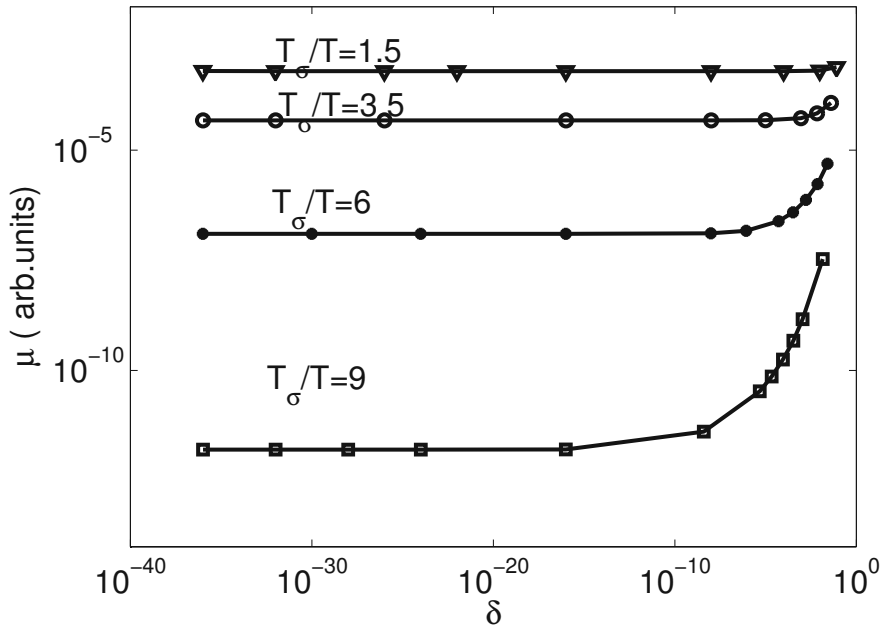


Figure 2.4: The calculated mobility versus carrier occupation at different temperature.

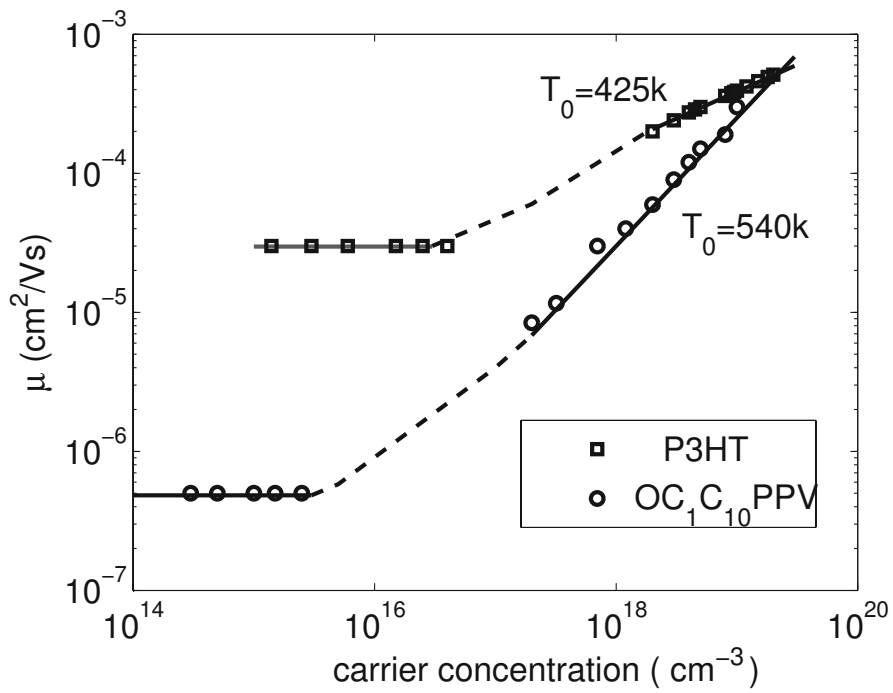


Figure 2.5: Comparison between calculation and typical experimental results [41].

we use (2.4) as the mobility model for the higher carrier concentration. The combined model can explain the experimental data in [41, 58], as shown in Fig 2.5.

2.3 Temperature and Electric Field Dependence of the Mobility

VRH theory has been applied successfully to describe the temperature dependence of conductivity in organic materials [17, 43, 59]. However, it is more difficult to obtain the experimentally observed electric field dependence. In this section, we extend the VRH theory to get a temperature and electric field dependent conductivity model.

For a disordered organic semiconductor we assumed that localized states are randomly distributed in both energy and space coordinates, and that they form a discrete array of sites. The presented theoretical calculations are applied to explain recent experiment. A good agreement between theory and experiment is observed.

2.3.1 Theory

When an electric field F exists, the transition rate of a carrier hopping from site i to site j is described as [60]

$$\omega_{ij} = \nu_0 \begin{cases} \exp \left[- \left(2\alpha + \frac{qF}{k_B T} \cos \theta \right) R_{ij} - \frac{E_j - E_i}{k_B T} \right] & : E_j - E_i \geq qF R_{ij} \cos \theta \\ \exp(-2\alpha R_{ij}) & : E_j - E_i \leq qF R_{ij} \cos \theta \end{cases} \quad (2.10)$$

where θ is the angle between E and R_{ij} . Assuming no correlation between the occupation probabilities of different localized states, the current between the two sites is given by

$$I_{ij} = \nu_0 \exp \left[-2\alpha R_{ij} - \frac{|E_j - E_i + qF \cos \theta R_{ij}|}{2k_B T} \right] \sinh \left(\frac{\mu_j - \mu_i}{2k_B T} \right) \times \left[\cosh \left(\frac{E_i - \mu_i}{2k_B T} \right) \cosh \left(\frac{E_j - \mu_j}{2k_B T} \right) \right]^{-1}, \quad (2.11)$$

where μ_i and μ_j are the chemical potentials of sites i and j , respectively [64].

2.3.2 Low Electric Field Regime

To determine the conductivity of an organic system, one can use percolation theory, regarding the system as a random resistor network [61, 62]. In the case of low electric field, the resulting voltage drop over a single hopping distance ($\Delta\mu \ll k_B T$) is small.

The conductance between sites i and j can be simplified from (2.12) to the form

$$\sigma_{ij} = \sigma_0 \exp \left(-2\alpha R_{ij} + \frac{|E_i - E_F| + |E_j - E_F| + |E_j - E_i + qF \cos \theta R_{ij}|}{2k_B T} \right). \quad (2.12)$$

Using the same derivation discussed in the previous section, we obtain as a result the percolation criterion for an organic system as

$$B_c \approx N_t \frac{\pi k_B T}{2qF} \left(\frac{T_0}{T} \right)^3 \exp \left(\frac{E_F + s_c k_B T}{k_B T_0} \right) \zeta(F, T), \quad (2.13)$$

with

$$\zeta = \left(2\alpha - \frac{qF}{k_B T} \right)^{-2} - \left(2\alpha + \frac{qF}{k_B T} \right)^{-2}$$

This yields the expression for the conductivity as

$$\sigma = \sigma_0 \left\{ \frac{\pi k_B T \delta N_t}{2qF B_c} \left(\frac{T_0}{T} \right)^3 \frac{1}{\Gamma(1 - T/T_0) \Gamma(1 + T/T_0)} \zeta(F, T) \right\}^{T_0/T}. \quad (2.14)$$

Equation (2.14) is obtained assuming

- that the site positions are random,
- the energy barrier for the critical hop is large compared to $k_B T$,
- and the charge carrier concentration is very low.

To describe the mobility, we use the mobility definition given by [63]

$$\mu = \sigma(\delta, T) \frac{T_0}{T} \frac{1}{q \delta N_t}. \quad (2.15)$$

Results and Discussion

Using expression (2.14), the conductivity has been calculated as a function of T at an electric field of 100V/cm, as shown in Fig 2.6. One can see the linear dependence of conductivity on $T^{-1/4}$ (the dashed line is a guide to the eye). We also use the presented model to calculate the temperature and electric field dependences of the conductivity and mobility of ZnPc (Zinc phthalocyanine). In Fig 2.7, the results are obtained from (2.14) using $\sigma_0 = 12.5 \times 10^5 S/m$, $T_0 = 485K$ and $\alpha^{-1} = 0.3\text{\AA}$. The experimental data is from [63].

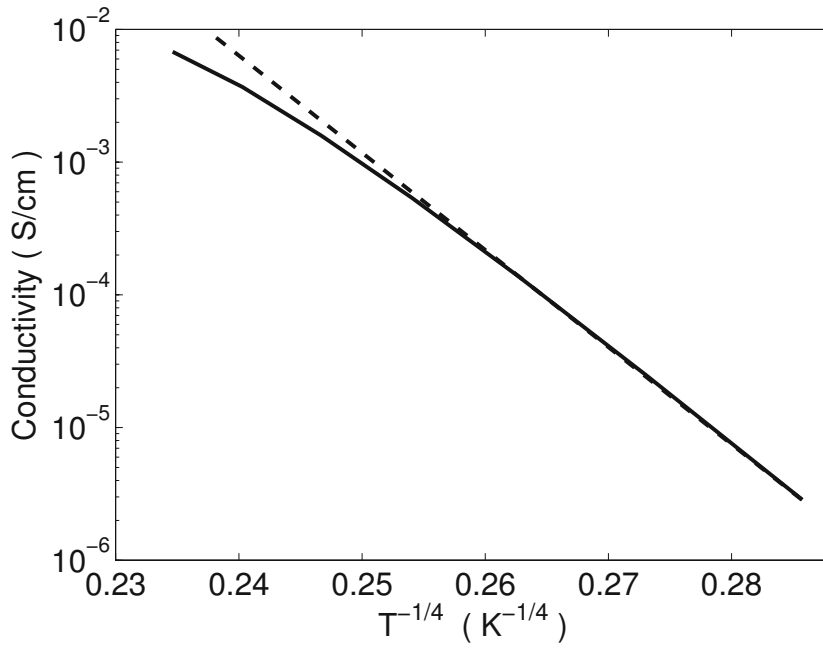


Figure 2.6: Plot of $\log \sigma$ versus $T^{-1/4}$ at the electric field $100V/cm$.

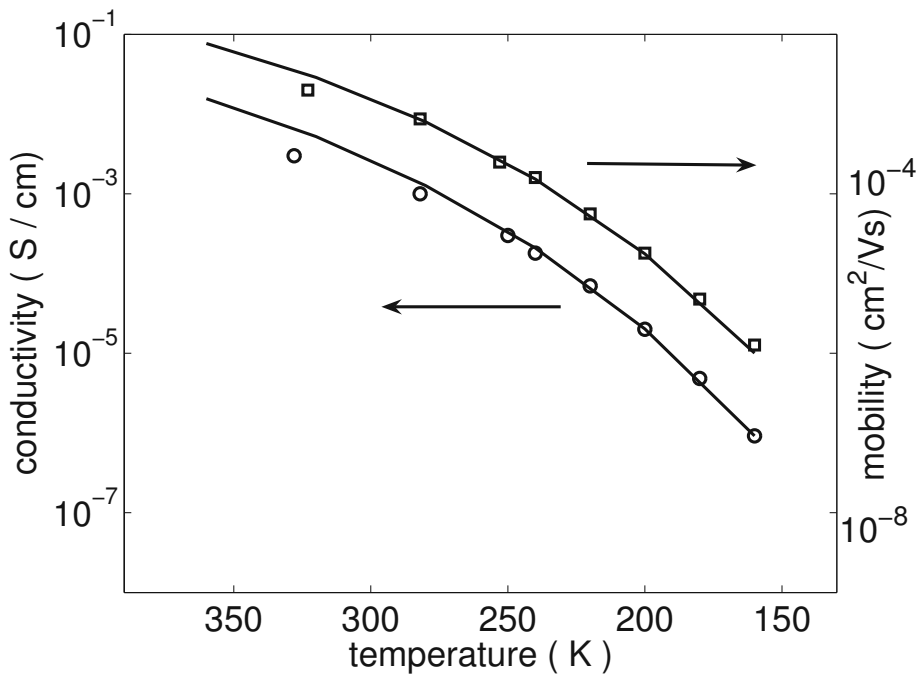


Figure 2.7: Conductivity and mobility versus temperature for ZnPc as obtained from the model (2.14) and (2.15) in comparison with experimental data (symbols).

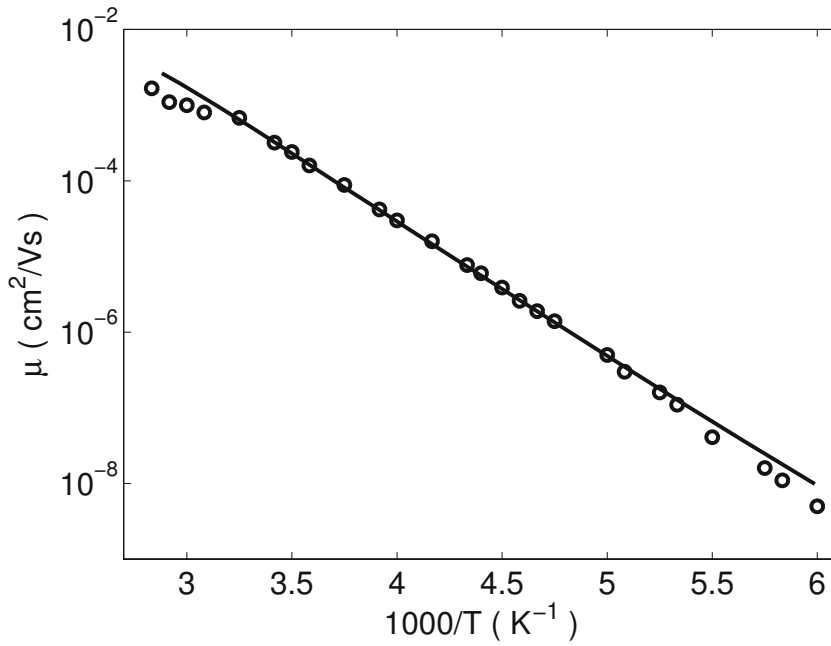


Figure 2.8: Logarithm of the mobility versus T^{-1} . The electric field is $10^5 V/cm$, $\sigma_0 = 1.1 \times 10^9 S/cm$, $T_0 = 340K$, $\alpha^{-1} = 0.5 \text{ \AA}$

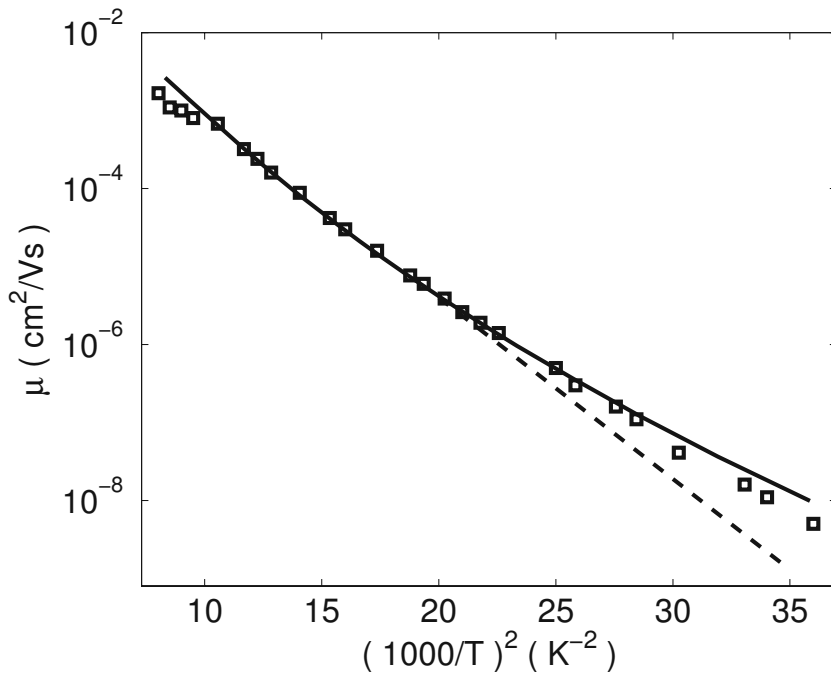


Figure 2.9: The same data as in Fig 2.8 plotted versus T^{-2} .

Fig 2.8 and Fig 2.9 show the mobility plotted semilogarithmically versus T^{-1} and T^{-2} , respectively. Symbols are TOF (time of flight) experimental data for ZnPc from [65] and the solid lines are the results of the analytical model. The dashed line is to guide the eye. In both presentations a good fit is observed. But when plotted as $\log \mu$ versus T^{-2} , the slope is reduced when temperature is lower than the transition temperature $T_c \approx 210\text{K}$. This transition has also been observed by Monte-Carlo simulation [48].

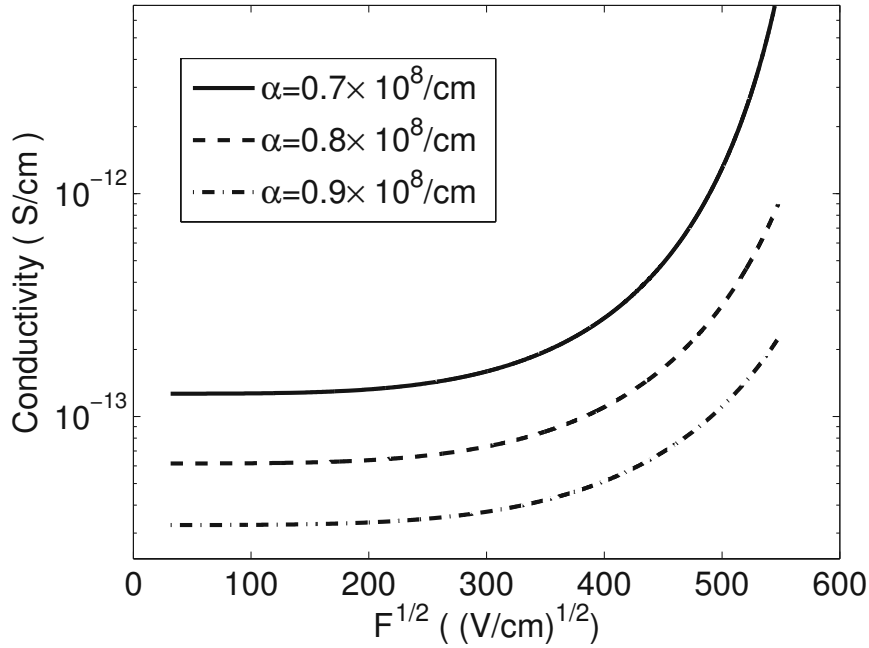


Figure 2.10: Plot of $\log \sigma$ versus $F^{1/2}$ at $T = 204$ K.

The field dependence of the conductivity is presented in Fig 2.10. The conductivity is approximately constant for very low fields, and increases as we increase the field. This is the result of the fact that the field can decrease the activation energy for forward jumps, enabling the motion of carriers. In Fig 2.11 we also compare the mobility (2.15) to the Monte-Carlo result reported in [49].

2.3.3 High Electric Field Regime

With increasing electric field, the voltage drop over a single hopping distance increases. If this voltage drop is of the order of $k_B T$ or larger, the approximate expression (2.14) for conductivity does not longer hold. The current between the two sites depends on the chemical potential of the sites, which in turn depends on the strength and direction of

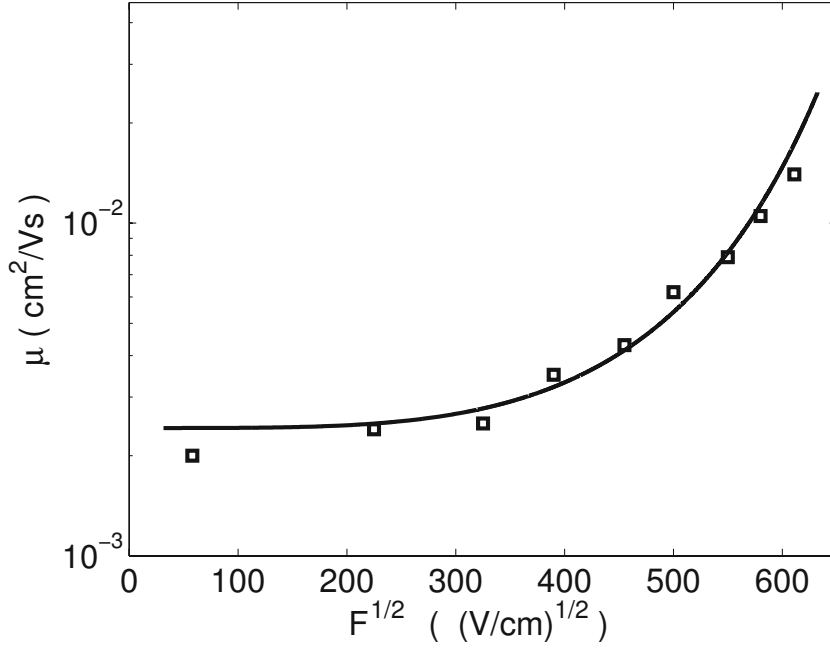


Figure 2.11: Electric field dependence of the mobility at 290K. Symbols represent Monte Carlo results [49], the line represents our work with parameter $T_0=852\text{K}$.

the electric field. Therefore, a percolation model is usually adopted, assuming site-to-site hopping currents instead of conductance [64].

However, in this case, a conductivity model for the high electric field regime can only be obtained after some approximations. According to percolation theory, the critical percolation cluster of sites would comprise a current carrying backbone with at least one site-to-site current equal to the threshold value. Since a steady-state situation would prescribe a constant current throughout the whole current carrying backbone, the charge will redistribute itself along the path, thus changing the chemical potentials of sites. Hapert omitted this rearrangement by optimization of the current with tunneling [64]. Potentially, the redistribution of charge would change the tunneling current, but this effect seems negligible compared to large spread I_{ij} . As a result, the conductivity between two sites is given by

$$\sigma_{ij} \approx \exp(-s_{ij}), \quad (2.16)$$

with

$$s_{ij} = 2\alpha R_{ij} + \ln\left(\frac{qF}{2k_B T} R_{ij}\right). \quad (2.17)$$

Combining (2.2), (2.8) and (2.17), the following expression for the percolation criterion

is obtained.

$$B_c \approx \frac{N_t}{2} \left[1 + \frac{\delta}{\Gamma(1 - T/T_0)\Gamma(1 + T/T_0)} \right] \int d\mathbf{R}_{ij}\theta(s_c - s_{ij}) \quad (2.18)$$

This gives the conductance as

$$\ln(\sigma/\sigma_0) = -2\alpha\eta - \ln\left(\frac{qF\eta}{2k_B T}\right) \quad (2.19)$$

where

$$\eta = -\frac{2k_B T}{qF} \ln \left[1 - \left(\frac{qF}{2k_B T} \right)^3 \frac{B_c}{4\pi N_t (1 + \delta/\Gamma(1 - T/T_0)\Gamma(1 + T/T_0))} \right] \quad (2.20)$$

Results and Discussion

In Fig 2.12, the conductivity is presented logarithmically as a function of $F^{1/2}$ for high electric field. In this case, a field-saturated drift velocity, i.e. $\sigma \propto F^{-1}$, is observed in accordance with the simulation work [66] and experiment [67]. At very high fields the effective disorder seen by a migrating carrier vanishes and backward transitions are excluded [9]. The temperature dependence of conductivity at the electric field of 1×10^5 V/cm is presented in Fig 2.13. An Arrhenius-like temperature dependence $\ln \sigma \propto -E_a/(k_B T)$ is also observed at low temperature.

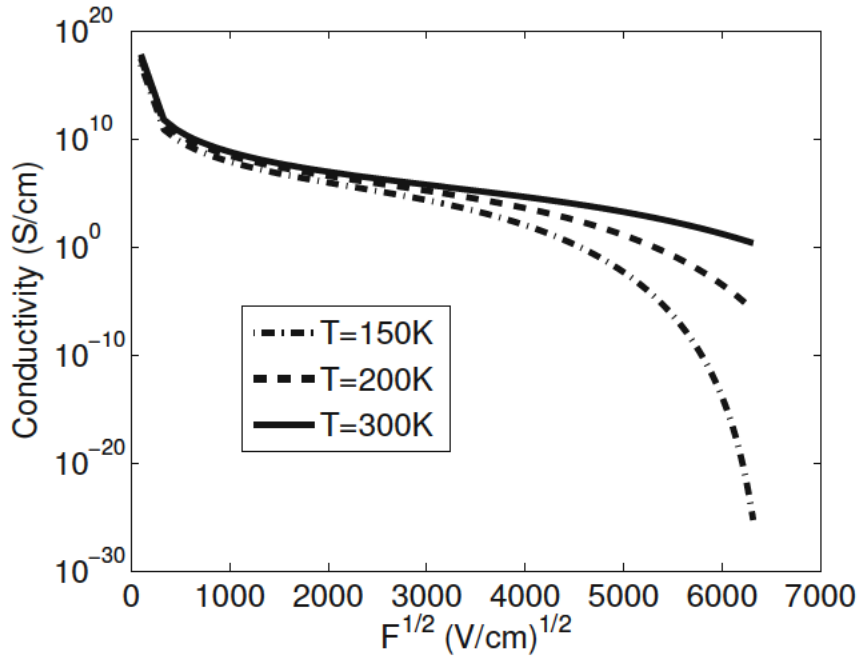


Figure 2.12: Field dependence of the conductivity at different temperatures.

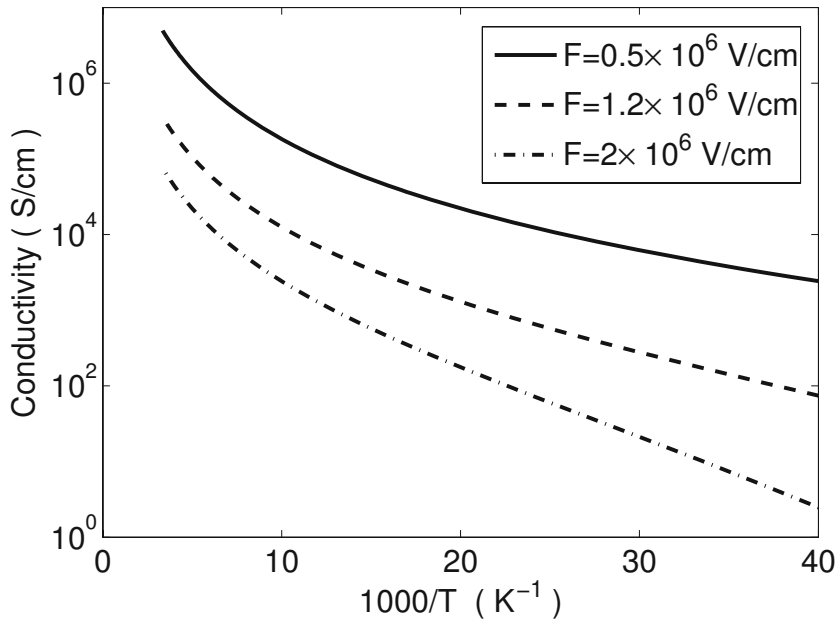


Figure 2.13: Temperature dependence of the conductivity at different electric fields.

2.4 Unified Mobility Model

Most existing models are only valid for either very low [43, 68, 69] or very high electric fields [60, 73]. Another common simplification stems from the transport energy concept [68, 69, 70], where exothermic, i.e. non-activated jumps, and jumps against the field are neglected.

The following is based on Apsley's work [19]. We will derive a formula for both the conductivity's temperature as well as its field dependence in the case of a Gaussian density of states mirroring the molecular disorder. We assume that (i) the localized states are distributed randomly in both space and energy, (ii) the states are occupied according to the Fermi-Dirac statistics, (iii) both hops upwards and hops downwards are regarded, (iv) the state energies are uncorrelated, and (v) the electric field may assume any value. Finally, the mobility's concentration dependence is discussed.

2.4.1 Theory

The amorphous structure of organic semiconductors is mirrored in localized states, which are distributed randomly in space and energy. The carrier transport between them is described as hopping, i.e. as a series of incoherent, thermally activated tunneling events.

We can define the hopping range R as

$$P_{ij} = \exp(R). \quad (2.21)$$

where P_{ij} is the Miller Abrahams rate. In the presence of an electric field F , the actual energy differences will be modified from $E_j - E_i$ to $(E_j - E_i) - qER_{ij} \cos \theta$, where θ is the angle enclosed by the jump and the field direction. Using the reduced coordinates $R_{ij}' = 2R_{ij}\alpha$ and $\epsilon = E/k_B T$, the hopping range may be re-written to

$$R = \begin{cases} (1 + \beta \cos \theta)R_{ij}' + \epsilon_j - \epsilon_i & : \epsilon_j > \epsilon_i, \\ R_{ij}' & : \epsilon_j < \epsilon_i. \end{cases} \quad (2.22)$$

where $\beta = Fq\alpha/(2k_B T)$. Since the hopping probability depends on both the spacial and the energetic difference between the hopping sites, it is natural to describe the hopping processes in a four-dimensional hopping space, which is spanned by three spacial and one energy coordinate. The hopping range R , as given by (2.22), defines a metric on this space.

In various disordered systems, a Gaussian density of states has been used to describe the hopping transport in band tails.

$$g(\epsilon) = \frac{N_t}{\sqrt{2\pi}a} \exp\left(-\left(\frac{\epsilon - \epsilon_0}{\sqrt{2}a}\right)^2\right), \quad (2.23)$$

where E_0 is the center of Gaussian function and $a = \sigma_0/k_B T$.

Let $F(E, \xi)$ be the normalized Fermi-Dirac distribution function. Then the carrier concentration can be written as

$$n(\xi) = \int_{-\infty}^{\infty} g(\epsilon) F(\epsilon, \xi) d\epsilon. \quad (2.24)$$

with ξ denoting the normalized chemical potential. The conductivity can be written as

$$\sigma(T, \beta) = -\frac{e\nu_0}{F} \int_{-\infty}^{\infty} dE'_i g(E'_i) F(E'_i) X_f \exp(-R_{nn}). \quad (2.25)$$

Here X_f is the forward hopping distance in the direction of the electric field and, R_{nn} stands for the nearest neighbor hopping range in the hopping space. To calculate the conductivity, we need to calculate R_{nn} . First, the number of unoccupied states N within a radius R in the hopping space is calculated [19].

$$N(T, \beta, R, \epsilon_i) = \int_0^\pi \int_0^R \int_{-\infty}^{K_f} g(\epsilon_j) [1 - F(\epsilon_j, \xi)] \frac{1}{8\alpha^3} 2\pi R'^2 \sin \theta d\epsilon_j dR' d\theta$$

Here $K_f = R + \epsilon_i - R'(1 + \beta \cos \theta)$. The factor $kT\alpha^3/8$ arises from the reduced coordinate system.

According to Mott, R_{nn} will be the value of the radius in the hopping space for which only one available vacant site is enclosed [72]. In other words, R_{nn} can be obtained by solving the equation

$$N(R, \epsilon_i, T, \epsilon) |_{R=R_{nn}} = 1. \quad (2.26)$$

Similarly, the expression for X_f can be calculated as [19]

$$X_f = \frac{I_1 + I_2}{I_3 + I_4}, \quad (2.27)$$

where

$$\begin{aligned} I_1 &= \int_0^\pi \sin \theta \cos \theta d\theta \int_{\epsilon_j - R_{nn}\beta \cos \theta}^{\epsilon_j + R_{nn}} g(\epsilon_i) [1 - F(\epsilon_i, \xi)] \left[\frac{R_{nn} - \epsilon_i + \epsilon_j}{1 + \beta \cos \theta} \right]^3 d\epsilon_i \\ I_2 &= \int_0^\pi \sin \theta \cos \theta d\theta \int_{-\infty}^{\epsilon_j - R_{nn}\beta \cos \theta} g(\epsilon_i) R_{nn}^3 [1 - F(\epsilon_i, \xi)] d\epsilon_i \\ I_3 &= \int_0^\pi \sin \theta d\theta \int_{\epsilon_j - R_{nn}\beta \cos \theta}^{\epsilon_j + R_{nn}} g(\epsilon_i) [1 - F(\epsilon_i, \xi)] \left[\frac{R_{nn} - \epsilon_i + \epsilon_j}{1 + \beta \cos \theta} \right]^2 d\epsilon_i \\ I_4 &= \int_0^\pi \sin \theta d\theta \int_{-\infty}^{\epsilon_j - R_{nn}\beta \cos \theta} g(\epsilon_i) [1 - F(\epsilon_i, \xi)] R_{nn}^2 d\epsilon_i \end{aligned}$$

R_{nn} depends only weakly on ϵ_j [19]. Therefore, for $\epsilon_j = 0$, we can obtain the value for R_{nn} by solving (2.26) numerically. Then the mobility for electrons at energy ϵ_i amounts to

$$\mu(\epsilon_i, T, \beta) = \frac{\nu_0}{F} X_f \exp(-R_{nn}). \quad (2.28)$$

Finally, the total conductivity for the organic semiconductor can be calculated numerically according to (2.25). The mobility can be determined from

$$\mu = \frac{\sigma}{nq}. \quad (2.29)$$

2.4.2 Results and Discussion

We investigated the mobility's temperature dependence in a three-dimensional hopping lattice. The crucial system parameters were set to the following values: $\alpha^{-1} = 0.5\text{\AA}$, $E_0 = 0$, $N_t = 1 \times 10^{21}\text{cm}^{-3}$, $F = 1 \times 10^3\text{V/cm}$ and $\xi = 30kT$. Fig 2.14 depicts the mobility as a function of the lattice temperature σ/kT . A linear dependence is observed between $\sigma/kT = 3$ and 8. Fig 2.15 displays the mobility as a function of $(\sigma/kT)^2$. The range with linear dependence of mobility on $(\sigma/kT)^2$ is not as broad as the one for the dependence of mobility on σ/kT . This can be used to test the validity of Arrhenius law $\mu \propto \exp(-E_A/k_B T)$ and the empirical model $\mu \propto \exp\left(-(\frac{2\sigma}{3})^2\right)$, where E_A is the activation energy.

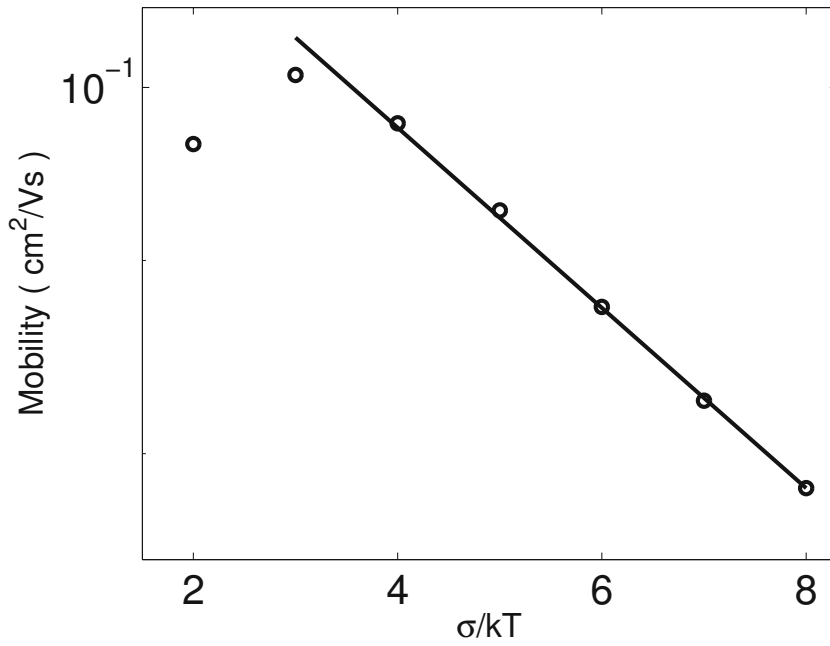


Figure 2.14: The calculated mobility (symbols) as a function of σ/kT .

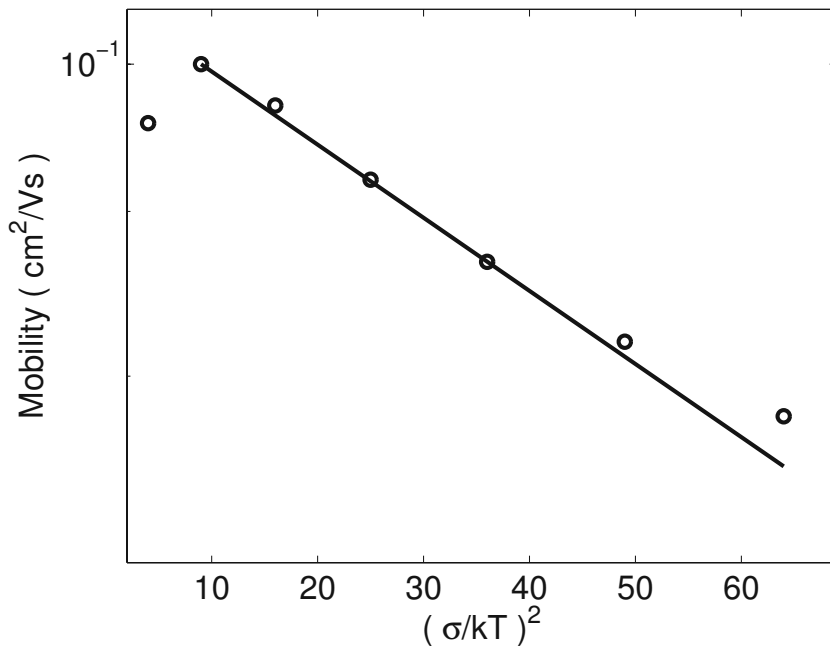


Figure 2.15: The calculated mobility (symbols) as a function of $(\sigma/kT)^2$.

These results are in accordance with the measurements reorted in [79]. As the presented model expresses, only in the regime $(\sigma/kT)^2 \leq 50$ an approximately linear relation can be observed.

The mobility versus electric field characteristics predicted by the presented model is shown in Fig 2.16. The parameters are $\alpha^{-1} = 1\text{\AA}$, $E_0 = 20kT$, $N_t = 1 \times 10^{21}\text{cm}^{-3}$ and $\sigma/kT = 4$. $\beta^{1/2} \leq 0.3$, where $\beta = Fe\alpha/2k_B T = \frac{F}{F_0}$, $F_0 \approx 1 \times 10^8\text{V/m}$, the mobility remains constant. At higher fields, it increases with the field. Therefore, the simple empirical relation between mobility and electric field of the form $\mu \propto F^{1/2}$ is not valid for all electric fields.

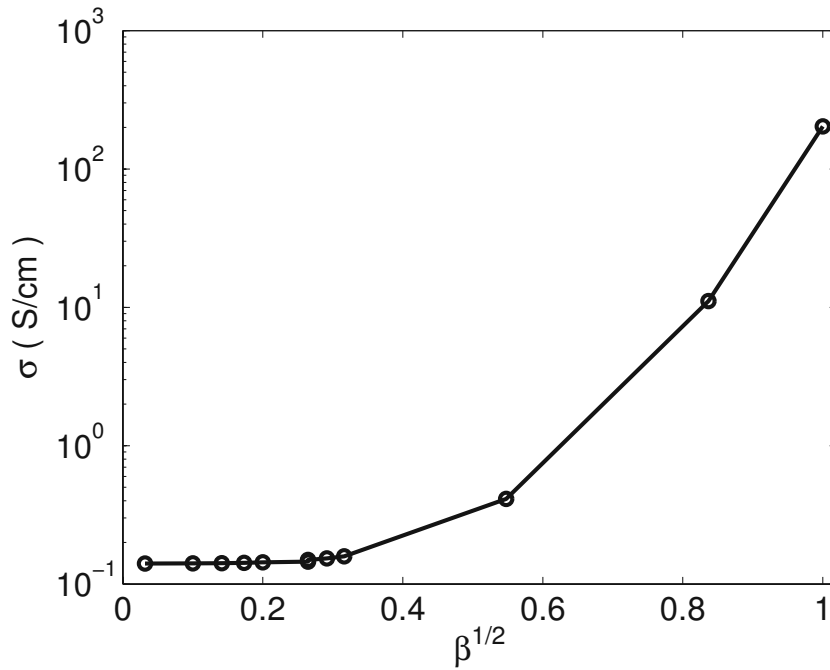


Figure 2.16: The conductivity as a function of the scaled electric field, $\beta = F/F_0$.

In addition to the temperature and electric field dependence, mobility also depends on the carrier concentration. Experiments show that for a hole-only diode and a field effect transistor fabricated from the same π -conjugated polymer, the mobility can differ up to three orders of magnitude [79]. Empirically, the mobility's dependence on the concentration N of localized states is written in the form

$$\mu \propto \exp \left[-C (N\alpha^{-3})^{-p} \right] \quad (2.30)$$

with constant C and $p = 1/3$ [59, 69, 74, 75].

With the parameter $\alpha^{-1} = 0.178\text{\AA}$, we compare the presented mobility model and this empirical formula, as shown in Fig 2.17. The agreement is quite good when we use

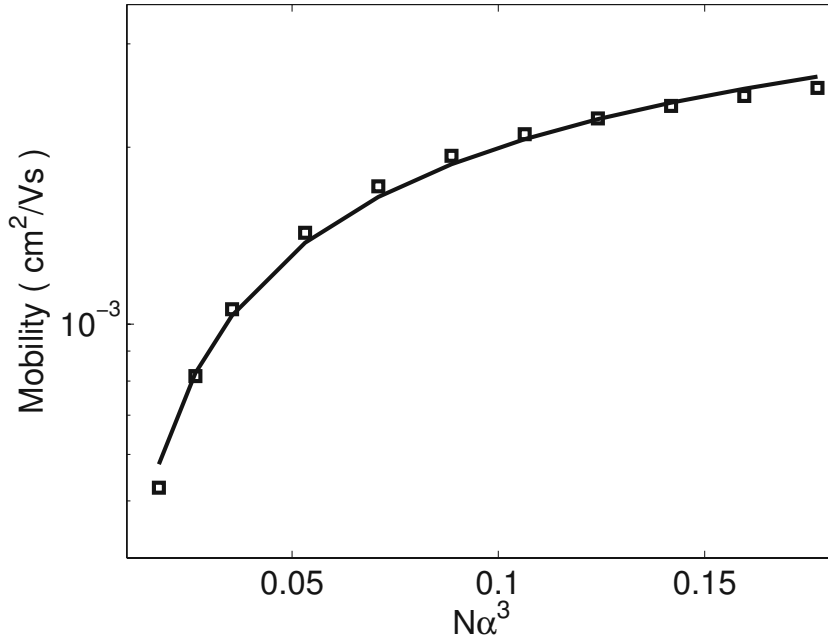


Figure 2.17: Comparison between our mobility model and analytical expression (2.30) with $p = 1/3$ and $C = 0.7$.

parameters $C = 0.75$ and $p = 1/3$. We notice that the value of C is different from $C = 2$ given in [69] and $C = 3$ given in [76]. Baranovskii [69] has stated that the parameters p and C are temperature dependent. In Fig 2.18, we also show the values of parameters p and C that provide the best fit for the solution of our model with the empirical expression (2.29). The input parameters are $\beta = 1 \times 10^{-5}$, $N_t = 1 \times 10^{21} \text{cm}^{-3}$, $E_0 = 0$ and $\alpha^{-1} = 1 \text{\AA}$. As illustrated in Fig 2.18, the parameter value of p is less than $1/3$ for temperatures low enough. The value of C is decreasing with increasing temperature, a result which coincides with [10]. Here p is not constant, since the variable range hopping (VRH) transport mechanism is based on the interplay between the spacial and energy factors in the exponent of transition probability, as given by (2.22). However, assuming nearest neighbor-hopping (NNH) regime, which does not consider the effect of energy dependent terms in (2.22) [69], leads to the values $p = 1/3$.

Next, we discuss the effect of the electric field on the parameters values p and C . The results are shown in Fig 2.19 and Fig 2.20. Input parameters are $\alpha^{-1} = 1 \text{\AA}$, $E_0 = 20 \text{kT}$, $N_t = 1 \times 10^{21} \text{cm}^{-3}$ and $\xi = 30$. From these figures we can see that the values p and C are nearly constant in the low electric field regime ($\beta \leq 1 \times 10^{-2}$).

We have shown that, as expected in the variable range hopping picture, (2.25) with $p = 1/3$ is only approximately valid for restricted ranges of temperature and electric field

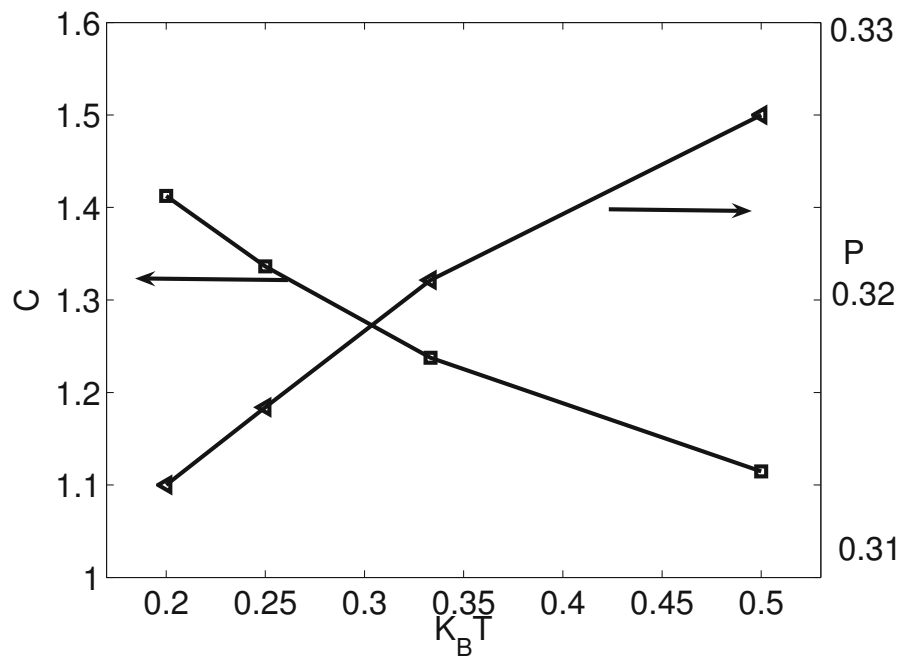


Figure 2.18: Temperature dependences of parameters C and p extracted from the analytical model.

strength. So we consider the effect of the material parameter α on the values of p and C in Fig 2.21. The input parameters are $\beta = 1 \times 10^{-5}$, $\sigma/kT = 2$ and $N_t = 1 \times 10^{21} \text{cm}^{-3}$. Remarkably, both parameter values p and C are not constant in the given range of α . With increasing α , the values of p will decrease and the ones of C will increase.

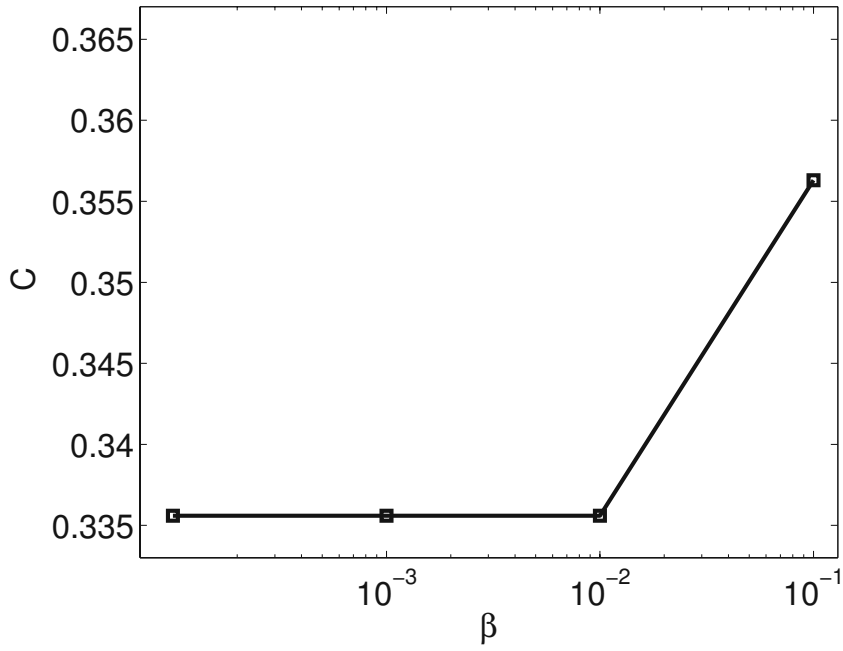


Figure 2.19: Electric field dependence of parameter C extracted from the analytical model.

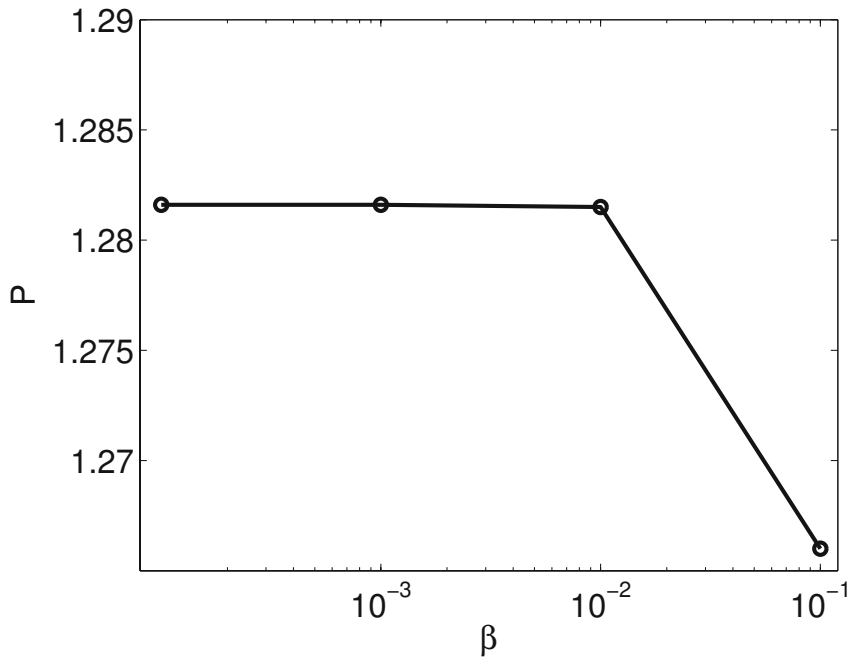


Figure 2.20: Electric field dependence of parameter p extracted from the analytical model.

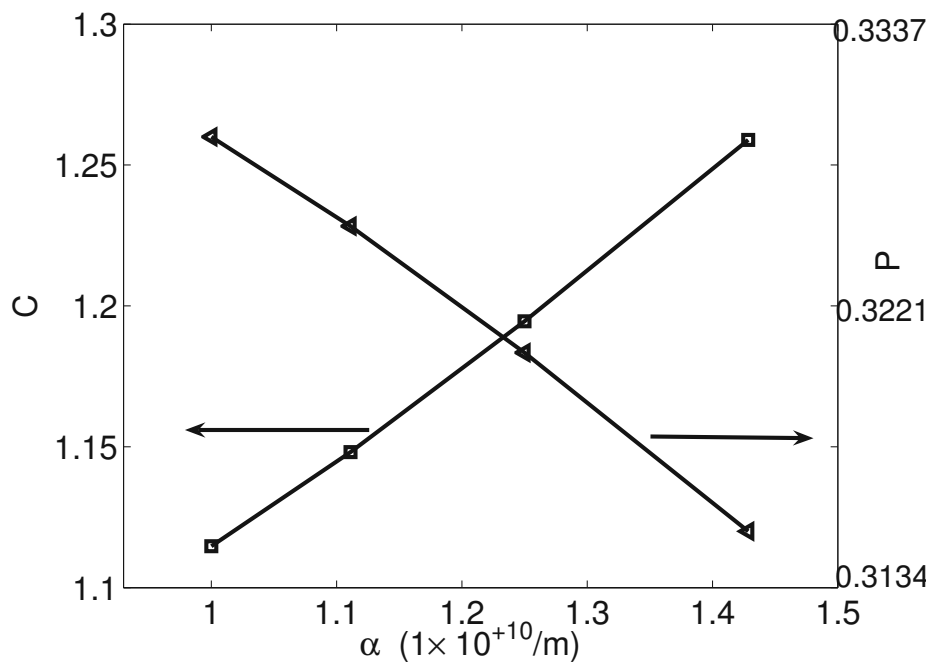


Figure 2.21: Effect of α on the values of parameters p and C extracted from the analytical model.

Chapter 3

The Effect of Fermi-Dirac Statistics on the Transport Energy

3.1 Introduction

Organic semiconductors can be considered as hopping networks and are characterized by strong disorder in both energy and space [8, 9]. This makes it very difficult to solve the problem analytically or simulate the carrier transport and recombination in such a system by starting from a one-particle master equation. Consequently, an analytical approach to this problem is normally based on a specific set of assumptions and simplifications [20, 68]. The concept of transport energy is a very useful tool for the analysis of charge hopping transport in organic semiconductors. The importance of the transport energy stems from the fact that it maximizes the probability for a carrier to hop upward. It does not depend on the initial energy of the carrier and serves as an analog of the mobility edge [10].

The transport energy concept is based on the Miller-Abrahams expression [7, 71]. This equation can be written as

$$\omega_{if} = \nu_0 \exp \left(-2\alpha R_{it} - \frac{E_t - E_i + |E_t - E_i|}{2k_B T} \right) \quad (3.1)$$

For a particular density of states $g(E)$, the transport energy can be obtained in the following way [10]. For an electron with energy E_i , the median rate of a upward hop to a neighboring localized state with energy $E_f > E_i$ is

$$\omega_{\uparrow} = \nu_0 \exp \left(-2\alpha R(E_t) - \frac{E_t - E_i}{k_B T} \right). \quad (3.2)$$

where

$$R(E_t) = \left[\frac{4\pi}{3} \int_{-\infty}^{E_t} g(E) dE \right]^{-1/3}$$

The transport energy can be calculated by maximizing the rate (3.2) with respect to the final energy E_t

$$\frac{\partial \omega_{\uparrow}(E_i, E_t)}{\partial E_t} = 0. \quad (3.3)$$

After some calculation we obtain

$$g(E_t) \left[\int_{-\infty}^{E_t} g(E) dE \right]^{-4/3} = \frac{1}{\alpha k_B T} \left(\frac{9\pi}{2} \right)^{1/3}. \quad (3.4)$$

Here we can see that the transport energy E_t does not depend on the initial energy E_i . The transport energy has been extended to an exponential DOS in [10] and later to a Gaussian DOS in [77].

3.2 Theory

In the original transport energy model [10], the downward hopping transport and the effect of degenerate statistics were neglected. An electron with energy ϵ_i , can only hop to a free localized state. In variable range hopping (VRH) theory, the numbers of empty sites enclosed by the contour R can be determined by the following equation [19].

$$N(T, \beta, R, \epsilon'_i) = \int_0^\pi \int_0^R \int_{-\infty}^{R+\epsilon'_i - R'(1+\beta \cos \theta)} g(\epsilon'_j) [1 - F(\epsilon'_j)] \frac{1}{8\alpha^3} 2\pi R'^2 \sin \theta d\epsilon'_j dR' d\theta$$

Here F is the Fermi-Dirac distribution function, and $1 - F$ is the probability that the final site is empty. The Gaussian DOS is rewritten as

$$g(\epsilon) = \frac{N_t}{\sqrt{2\pi} \cdot a} \exp \left[- \left(\frac{\epsilon - \epsilon_0}{\sqrt{2} \cdot a} \right)^2 \right], \quad (3.5)$$

where ϵ is the normalized energy $\epsilon = E/kT$, ϵ_0 is the Gaussian center, N_t is the effective DOS and a is defined as $a = \sigma_0/kT$, where σ_0 is the standard deviation of the Gaussian distribution. If we let $f(\epsilon, \xi)$ be the normalized Fermi-Dirac distribution function, then the carrier concentration can be written as

$$n(\xi) = \int_{-\infty}^{\infty} g(\epsilon) f(\epsilon, \xi) d\epsilon \quad (3.6)$$

Considering the distribution function, $R(\epsilon_t)$ will be calculated as

$$R(E_t) = \left[\frac{4\pi}{3} \int_{-\infty}^{\epsilon_t} g(E) (1 - f(\epsilon, \xi)) d\epsilon \right]^{-1/3}. \quad (3.7)$$

Substituting (3.7) into (3.3), we obtain

$$\frac{2\alpha}{3} \left(\frac{4\pi}{3}\right)^{-1/3} \left(\frac{N_t}{\sqrt{2\pi}a}\right)^{-1/3} = \eta \exp\left(\frac{1}{2} \left(\frac{\epsilon_{tr}}{a}\right)^2\right) (1 + \exp(-(\epsilon + \xi))), \quad (3.8)$$

where

$$\eta = \left[\int_{-\infty}^{\epsilon_t} \frac{\exp\left(-\frac{1}{2} \left(\frac{\epsilon}{a}\right)^2\right) d\epsilon}{1 + \exp(-(\epsilon + \xi))} \right]^{4/3}. \quad (3.9)$$

ϵ_t is the new transport energy and can be calculated by solving (3.9) numerically.

3.3 Results and Discussion

In Fig 3.1 we compare our work with Baranovskii's model for the temperature characteristics of the transport energy. The input parameters are $N_t = 1 \times 10^{22} \text{cm}^{-3}$, $E_0 = 0 \text{eV}$, $\xi = 30kT$, $\alpha^{-1} = 1 \text{\AA}$. The two models agree very well when the temperature is high enough, but differ in the low temperature range.

Calculation of transport energy versus the normalized chemical potential ξ is given for different DOS standard deviation in Fig 3.2 with parameters

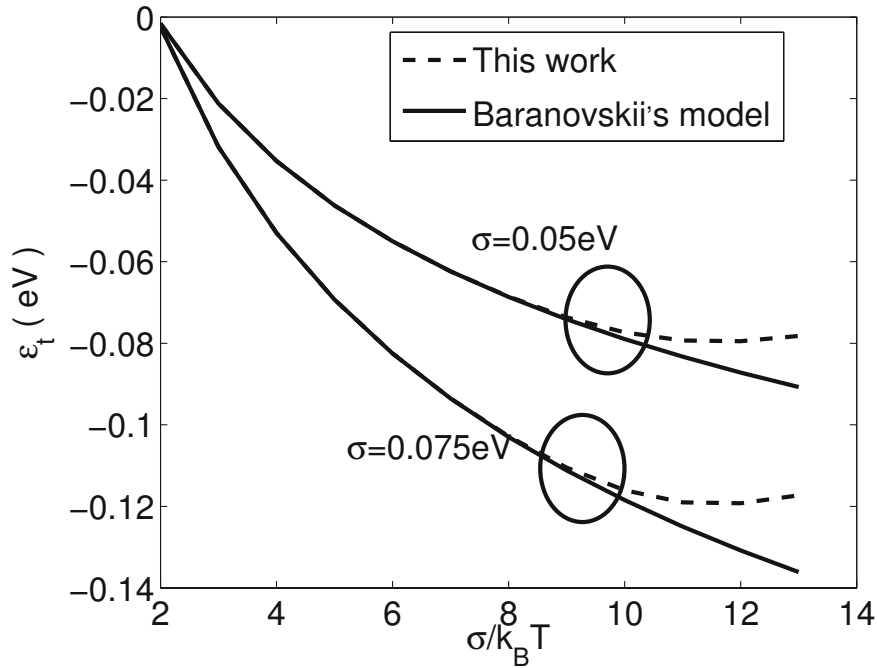


Figure 3.1: Comparison between the model (3.8) and Baranovskii's model for the temperature characteristics of E_{tr} .

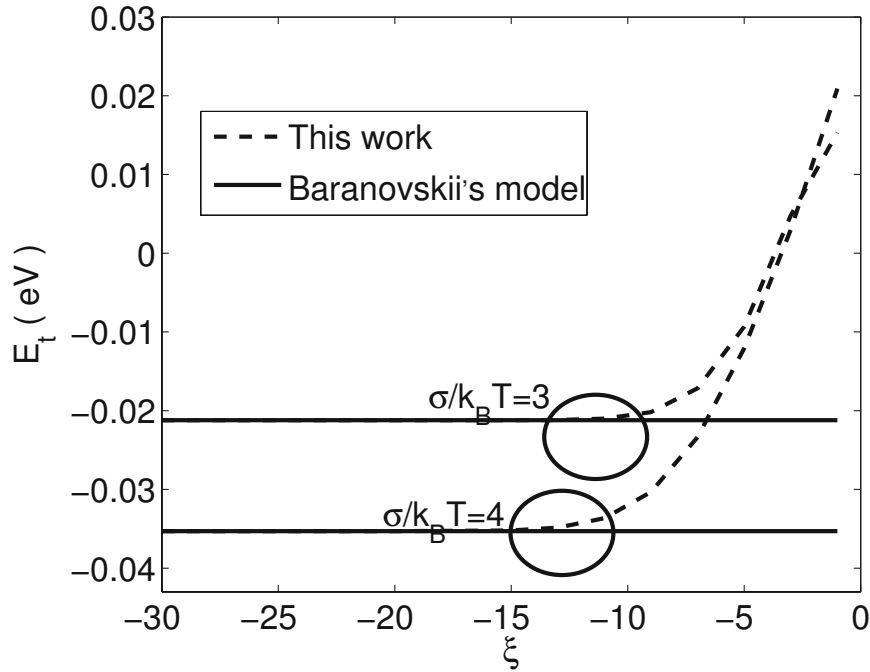


Figure 3.2: The transport energy versus the chemical potential for different standard deviations a of the DOS.

$E_0 = 0\text{eV}$, $N_t = 1 \times 10^{22}\text{cm}^{-3}$, $\alpha^{-1} = 2\text{\AA}$ and $\sigma_0 = 0.05\text{eV}$.

As expected, for a very low chemical potential level (very low carrier concentration), the two models agree very well. However, when the chemical potential goes up and thus the concentration increases, the transport energy considering Fermi statistics will increase as well, while in the Baranovskii model the transport energy is independent on the chemical potential. Baranovskii's model of the transport energy can only be used when the carrier concentration is low enough.

The dependence of the transport energy on the relative carrier concentration (n/N_t) can be seen in Fig 3.3. The transport energy increases at a relative carrier concentration of about 1×10^{-2} .

For the calculation of the hopping mobility [78], the relaxation time τ_{rel} is important, which can be calculated as

$$\tau_{rel} = \nu_0^{-1} \exp\left(2\alpha R(E_{tr}) + \frac{(E_t - E_\infty)}{k_B T}\right). \quad (3.10)$$

E_∞ is the thermal equilibrium energy of hopping carriers, defined as

$$E_\infty = -\frac{\sigma^2}{k_B T}.$$

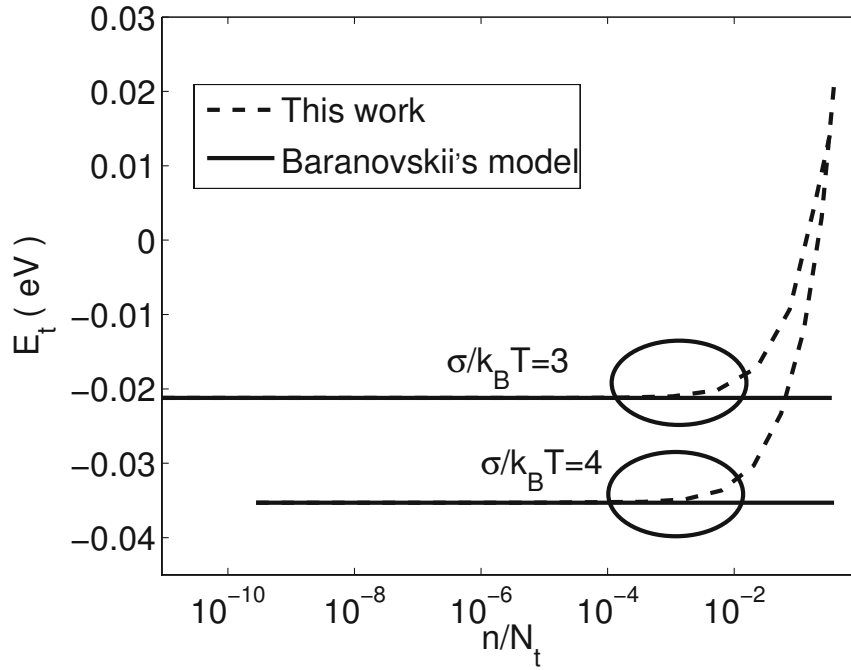


Figure 3.3: The transport energy versus the relative carrier concentration for different standard deviations a of the DOS.

We plot the relation between τ_{rel} and the carrier concentration in Fig 3.4 with parameters $N_t = 1 \times 10^{22} \text{cm}^{-3}$ and $\alpha^{-1} = 1 \text{\AA}$. We can see that the relaxation time is constant when the chemical potential is low enough, but it increases for $\xi \geq -5$ for our case.

We apply the calculated transport energy to the problem of charge mobility in organic semiconductors. Using the Einstein relation we obtain [78]

$$\mu \propto \left(\frac{q}{k_B T} \right) R (E_{tr})^2 \langle t \rangle, \quad (3.11)$$

the average hopping time is determined as

$$\langle t \rangle = \frac{\left(\int_{-\infty}^{E_{tr}} P dE \right)}{\int_{-\infty}^{E_{tr}} g(E) dE} \quad (3.12)$$

with

$$P = \nu_0 \exp \left(2\alpha R (E_{tr}) + \frac{(E_{tr} - E)}{k_B T} \right) g(E).$$

Fig 3.5 compares the temperature dependence of the carrier mobility as obtained from our model and Baranovskii's model. The input parameters are $N_t = 1 \times 10^{22} \text{cm}^{-3}$,

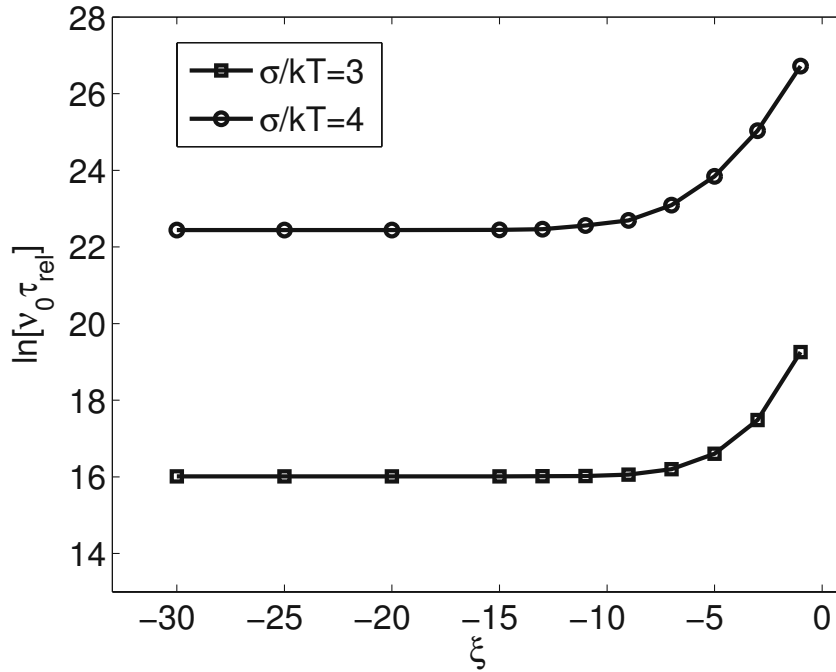
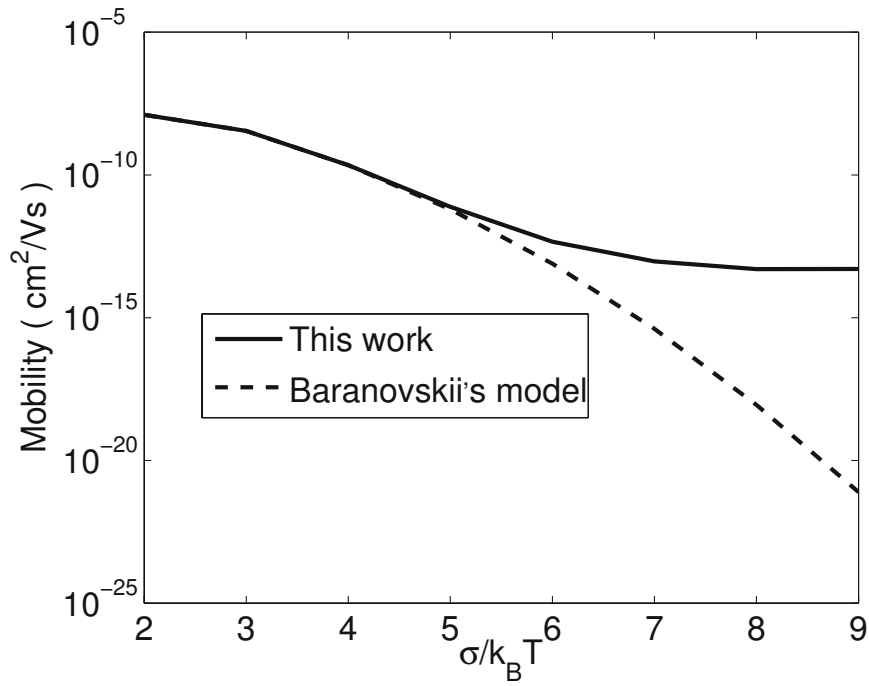


Figure 3.4: Dependence of the relaxation time on the chemical potential for different standard deviations a of the DOS .

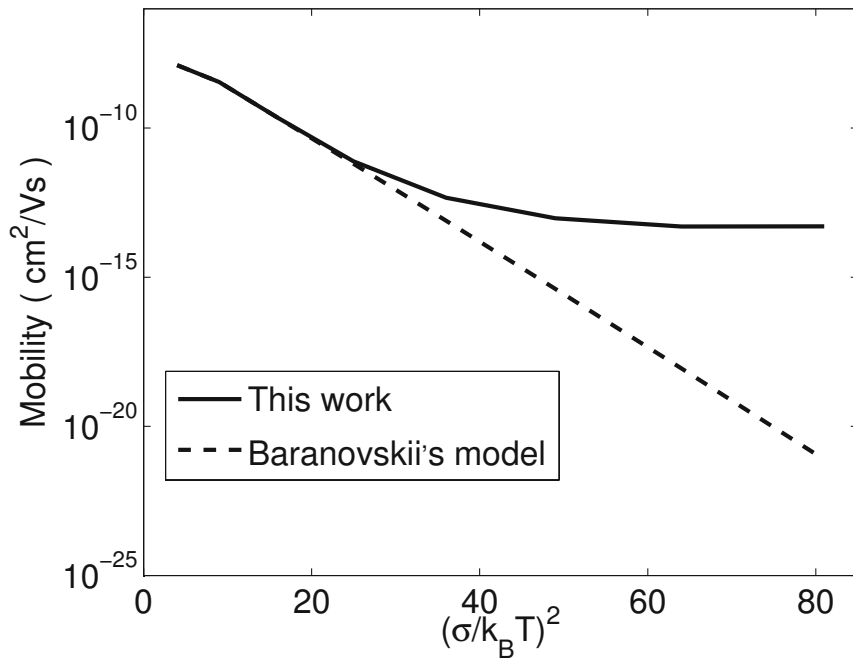
$\alpha^{-1} = 1\text{\AA}$ and $\xi = 30 k_B T$. The graph $\log \mu$ versus T^{-1} and $\log \mu$ versus T^{-2} are plotted in Fig 3.5 (a) and (b). Our model can describe a deviation from straight. In fact, at higher temperature, the mobility is controlled by jumps of carriers that occupy intrinsic sites, so that the occurrence of the traps does not change the linear relation between $\log \mu$ versus T^{-2} . At lower temperature, the traps in organic semiconductors play a more important role for charge transport [68].

In Fig 3.6 we plot the relation between the mobility and the carrier concentration. The input parameters are $N_t = 1 \times 10^{22} \text{ cm}^{-3}$, $\gamma = 1 \times 10^{15} \text{ s}^{-1}$ and $\alpha = 1\text{\AA}$.

It is illustrated that the mobility remains constant when the carrier concentration is very low. However, it will increase when the carrier concentration is above a critical value. This result coincides with experimental data given in [79] and recent work given in [80].



a



b

Figure 3.5: Temperature dependence of the carrier mobility in organic semiconductors. In (a) the data are plotted versus T^{-1} , in (b) the same data are plotted versus T^{-2} .

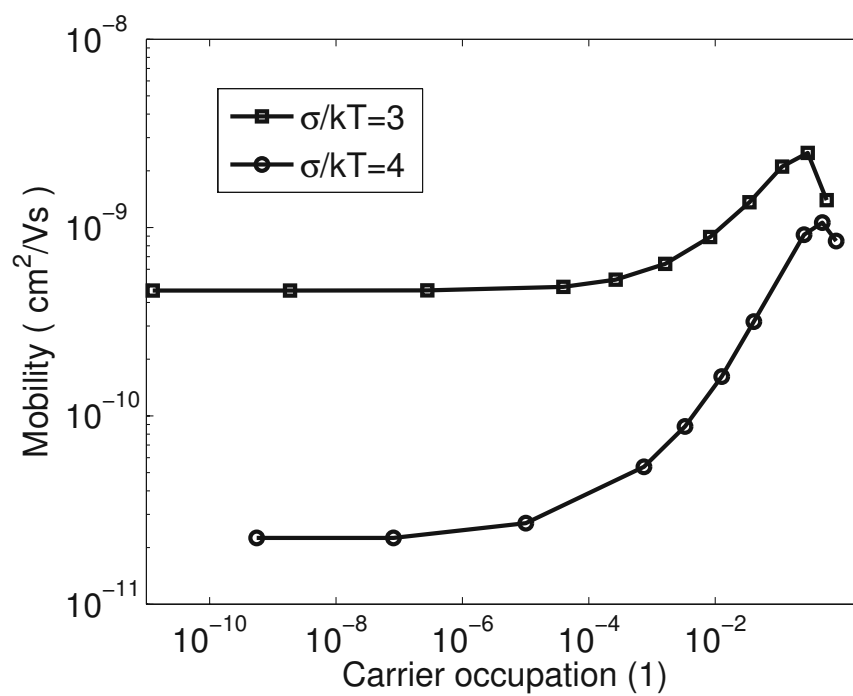


Figure 3.6: Carrier concentration dependence of the mobility in organic semiconductors.

Chapter 4

Doping and Trapping Model for Organic Semiconductors

4.1 Introduction

Despite decades of research progress, some rather ubiquitous features of the charge transport in organic semiconductors are still far from being well understood. One such example is the relation between conductivity and doping [81, 82]. The doping of organic semiconductors is just beginning to be quantitatively studied [83, 84, 85, 86, 87]. Early studies have shown that the doping of organic semiconductors (partially oxidizing or reducing them) can increase their conductivity by many orders of magnitude. There are also early studies of the effect of adding molecular dopant to thin films of organic semiconductors in an attempt to improve their photovoltaic behavior [88, 89]. Although the doping process of organic semiconductors can largely be depicted by a standard model used for crystalline inorganic semiconductors [90], a general doping model for organic semiconductors still remains a challenge. Because of the weak intermolecular forces, doping of organic semiconductors is quite difficult compared to the doping of common semiconductors. In common semiconductors, the strong covalent or covalent-ionic bonds ease doping [91]. Bending or breaking the high energy interatomic bonds at crystal defects and grain boundaries, or incorporating impurities of a valence different than the valence of the host, often produce electronic states near enough to the band edge to generate free carriers. For these reasons, it is difficult to produce truly intrinsic common semiconductors. On the other hand, organic semiconductors are van der Waals solids. Bending or breaking these low energy intermolecular bonds, or adding different molecular (PPEEB or F4-TCNQ) into the lattice, only inefficiently produce free carriers. At the same time, the mobile charge in organic semiconductors can be trapped by some

states. These charge traps are known as deep traps, and they are not well understood.

In this chapter, we present an analytical model for hopping transport in doped, disordered organic semiconductors based on the VRH and the percolation theory. This model can successfully explain the superlinear increase of conductivity with doping observed in several experimental data sets. It can also be used to describe the trapping characteristics of organic semiconductors.

4.2 Theory

For a disordered organic semiconductor system, we assume that localized states are randomly distributed in both the energy and the coordinate space, and that they form a discrete array of sites. Conduction proceeds via hopping between these sites. In the case of low electric field, the conductivity between site i and site j can be calculated as [17, 44]

$$\sigma_{ij} \approx \gamma \exp \left(-2\alpha R_{ij} - \frac{|E_i - E_F| + |E_j - E_F| + |E_i - E_j|}{2k_B T} \right) \quad (4.1)$$

where E_i and E_j are the energies at the sites i and j , respectively, E_F is the Fermi energy, R_{ij} is the distance between sites i and j , and α^{-1} is the Bohr radius of the localized wave function. The first term $2\alpha R_{ij}$ is a tunneling term, and the second one is a thermal activation term (Boltzman term).

For organic semiconductors, the manifolds of both the lowest unoccupied molecular orbitals (LUMO) and the highest occupied molecular orbitals (HOMO) are characterized by random positional and energetic disorder. Being embedded into a random medium, similarly, dopant atoms and molecules are inevitably subjected to the positional and energetic disorder, too. Since the HOMO level in most organic semiconductors is deep and the gap separating LUMO and HOMO states is wide, energies of donor and acceptor molecules are normally well below LUMO and above HOMO. So we assume a double exponential density of states

$$g(E) = \frac{N_t}{k_B T_0} \exp \left(\frac{E}{k_B T_0} \right) + \frac{N_d}{k_B T_1} \exp \left(\frac{E + E_d}{k_B T_1} \right) \quad (E \leq 0), \quad (4.2)$$

where N_t and N_d are the concentrations of the intrinsic and the dopant states, respectively, T_0 and T_1 are parameters indicating the widths of the intrinsic and the dopant distributions, respectively, and E_d is the Coulomb trap energy [92]. Vissenberg and Matters [43] pointed out that they do not expect the results to be qualitatively different for a different choice of $g(E)$, as long as $g(E)$ increases strongly with E . Therefore, we assume that transport takes place in the tail of the exponential distribution.

The equilibrium distribution of carriers $\rho(E)$ is determined by the Fermi-Dirac distribution $f(E)$ as follows

$$\rho(\epsilon) = g(E) f(E) = \frac{g(E)}{1 + \exp[(E - E_F)/k_B T]}.$$

The Fermi-energy of this system is fixed by the equation for the carrier concentration n ,

$$n = \int \frac{d\epsilon g(E)}{1 + \exp\left(\frac{E - E_F}{k_B T}\right)} = n_t + n_d \quad (4.3)$$

where

$$n_t = N_t \exp\left(\frac{\epsilon_F}{K_B T_0}\right) \Gamma(1 - T/T_0) \Gamma(1 + T/T_0)$$

$$n_d = N_d \exp\left(\frac{\epsilon_F - E_d}{K_B T_1}\right) \Gamma(1 - T/T_1) \Gamma(1 + T/T_1)$$

Here, Γ is the gamma function. According to the classical percolation theory [17], the current will flow through the bonds connecting the sites in a random Miller and Abrahams network [9]. The conductivity of this system is determined when the first infinite cluster occurs. At the onset of percolation, the critical number B_c can be written as

$$B_c = \frac{N_b}{N_s}, \quad (4.4)$$

where $B_c = 2.8$ for a three-dimensional amorphous system, N_b and N_s are, respectively, the density of bonds and the density of sites in this percolation system, which can be calculated by [43, 93, 94].

$$N_b = \int d\mathbf{R}_{ij} dE_i dE_j g(E_i) g(E_j) \theta(s_c - s_{ij}), \quad (4.5)$$

$$N_s = \int dE g(E) \theta(s_c k_B T - |E - E_F|). \quad (4.6)$$

Here \mathbf{R}_{ij} denotes the distance vector between sites i and j , θ is the unit step function, and s_c is the exponent of the conductance given by the relation [19]

$$\sigma = \sigma_0 \exp(-s_c). \quad (4.7)$$

Substituting (4.2), (4.5) and (4.6) into (4.4), we obtain the expression,

$$B_c = \frac{\kappa + p}{N_t \exp(\eta) + N_d \exp(\gamma)}, \quad (4.8)$$

where

$$\kappa = \pi N_t^2 \psi^3 \exp(2\eta) + \pi N_d^2 \xi^3 \exp(2\gamma),$$

$$p = \frac{\pi}{4} N_t N_d \exp(\eta + \gamma) (\psi^{-1} + \xi^{-1})^{-3},$$

$$\eta = \frac{E_F + k_B T s_c}{k_B T_0}, \quad \gamma = \frac{E_F - E_d + k_B T s_c}{k_B T_1},$$

$$\psi = \frac{T_0}{4\alpha T}, \quad \xi = \frac{T_1}{4\alpha T}.$$

Equation (4.8) has been obtained under the following conditions:

- the site positions are random,
- the energy barrier for the critical hop is large compared with $k_B T$,
- and the carrier concentration is very low.

The exponent s_c is obtained by a numerical solution of (4.8) and the conductivity can be calculated using (4.7).

4.3 Doping Characteristics

Fig 4.1 illustrates the temperature dependence of the carrier conductivity for different doping concentrations. Parameters are $\alpha^{-1} = 0.37 \text{ \AA}$, $E_d = 0.5 \text{ eV}$, $T_0 = 800 \text{ K}$ and $T_1 = 400 \text{ K}$. An Arrhenius-like temperature dependence

$$\log \sigma \propto -E_A/k_B T$$

can be observed clearly in Fig 4.1. In Fig 4.2, we plot $\log \sigma$ versus T^{-2} , which is observed to deviate slightly from a straight line (dashed in Fig 4.2). This is because at higher temperatures almost all the carriers occupy the intrinsic states such that the dopants do not change the trap-free hopping relation $\log \sigma \propto T^{-2}$ [95]. The doping process is quite efficient for ZnPc with dopant F4-TCNQ [63]. In Fig 4.3, we compare the measured conductivity at room temperature and the theoretical model (4.7). The agreement is quite satisfactory. The fit parameters are the same as those used in Fig 4.1, and have been chosen according to [63]. From Fig 4.1 and Fig 4.3 we can see that the conductivity increases considerably with the dopant concentration, especially in the lower temperature regime.

The superlinear dependence of conductivity on the doping concentration has been investigated extensively by several groups [81, 91, 96, 97], where the empirical formula

$$\sigma \propto N_d^\gamma$$

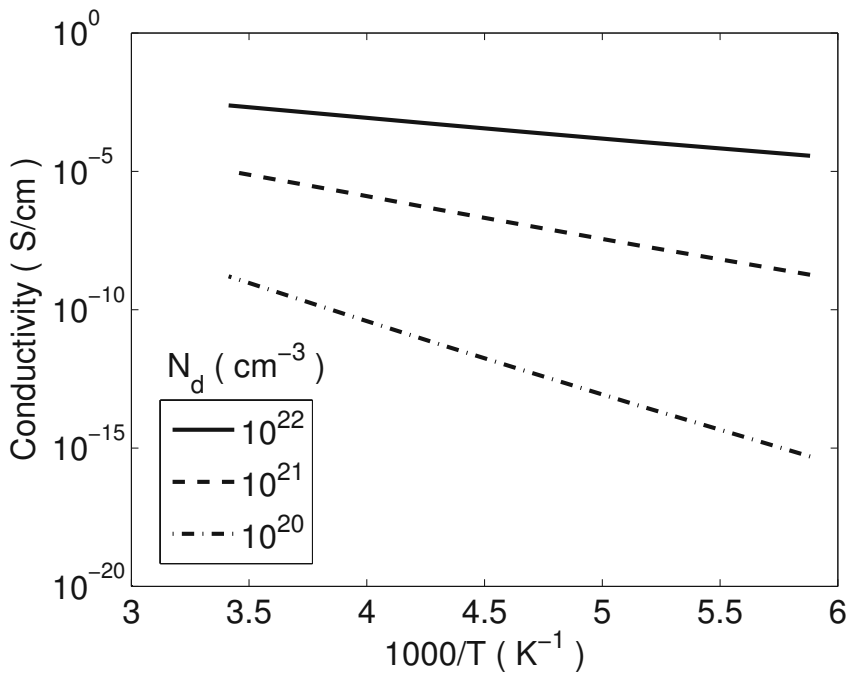


Figure 4.1: Temperature dependence of the conductivity in a disordered hopping system at different doping concentrations.

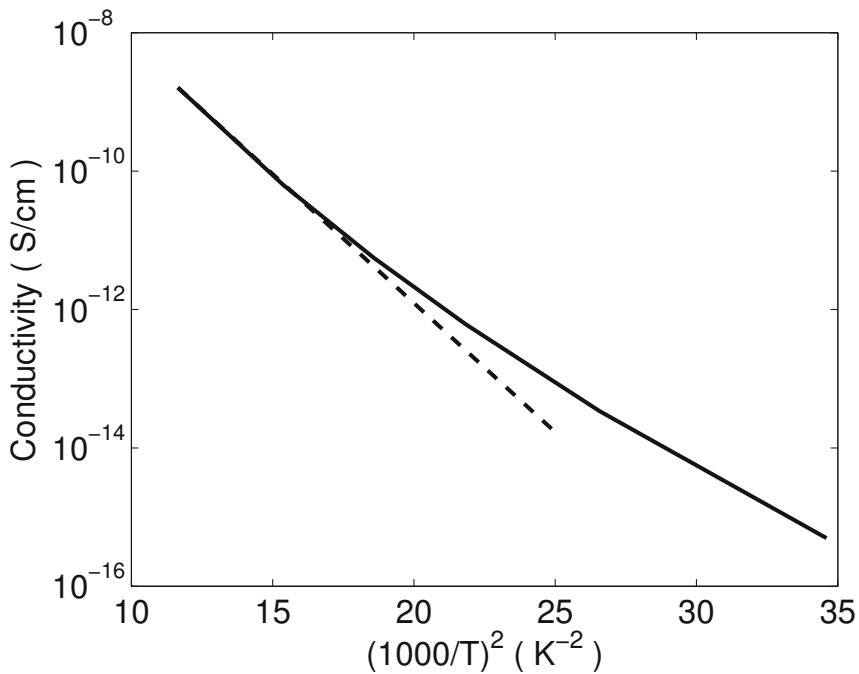


Figure 4.2: Temperature dependence of the conductivity in an organic semiconductor plotted as $\log \sigma$ versus T^{-2} . The dashed line is to guide the eye.

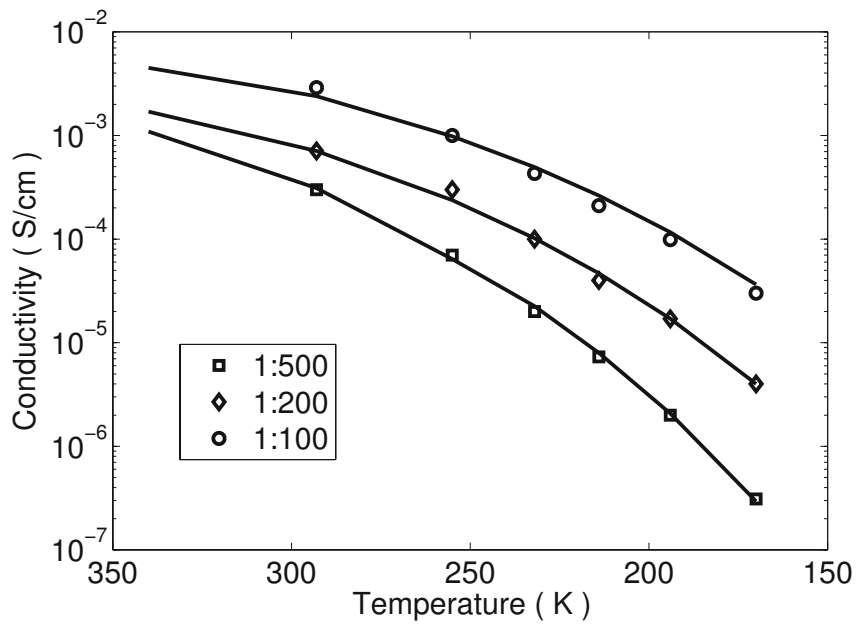


Figure 4.3: Conductivity of doped ZnPc at various doping ratios as a function of temperature. The lines represent the analytical model, experiments (symbols) are from [63].

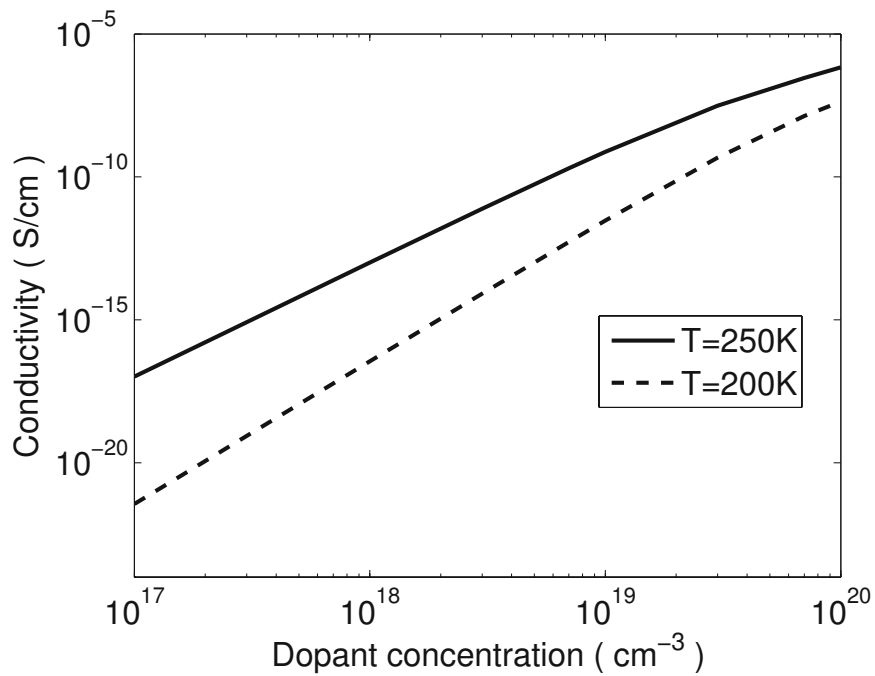


Figure 4.4: Conductivity as a function of the dopant concentration with temperature as a parameter.

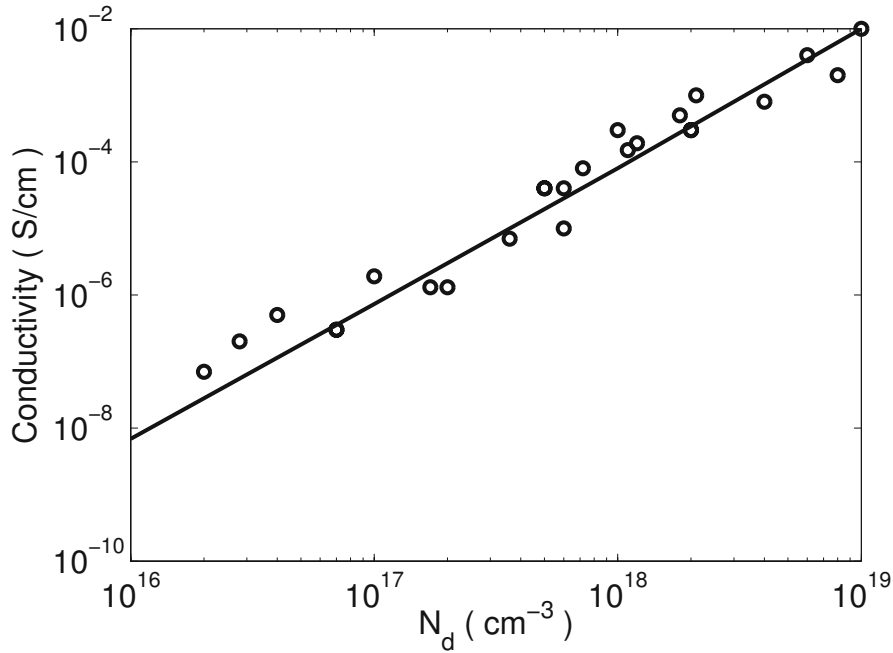


Figure 4.5: Conductivity of PPEEB films versus the dopant concentration. The line represents the analytical model. Experiments (symbols) are from [139].

is used to describe this dependence. Using our model, such superlinear increase of the conductivity upon doping can be predicted successfully. We show this in Fig 4.4, where the parameters are the same as in Fig 4.1. Our model gives $\gamma = 4.9$ for $T = 250\text{K}$, and $\gamma = 3.9$ for $T = 200\text{K}$. Note that these choices are consistent with those in [81], where the γ is chosen in the range [3,5]. In Fig 4.5, we compare the predictions of our model with the experimental data of doped PPEEB [91]. The parameters are $\alpha^{-1} = 6\text{\AA}$, $E_d = 0.6\text{eV}$, $T_0 = 1000\text{K}$ and $T_1 = 500\text{K}$. The predictions fit the experimental data very well.

In Fig 4.6 we plot the relation between the conductivity and the doping ratio, defined as

$$\frac{N_d}{N_t + N_d},$$

for different temperatures with parameters $T_0 = 1000\text{K}$, $T_1 = 500\text{K}$, $E_d = 0.5\text{eV}$ and $\sigma_0 = 1 \times 10^7\text{S/cm}$. We can see that the conductivity increases with both temperature and doping ratio. More specifically, there is a transition in the increase of the conductivity of an organic semiconductor upon doping, which is manifested by a change in the slope of the curve as shown in Fig 4.7. The conductivity increases linearly for low doping levels, and superlinearly for high doping levels. This transition has been interpreted in [92] in terms of the broadening of the transport manifold due to the enhanced disorder from

the dopant. Assuming a simple Arrhenius law

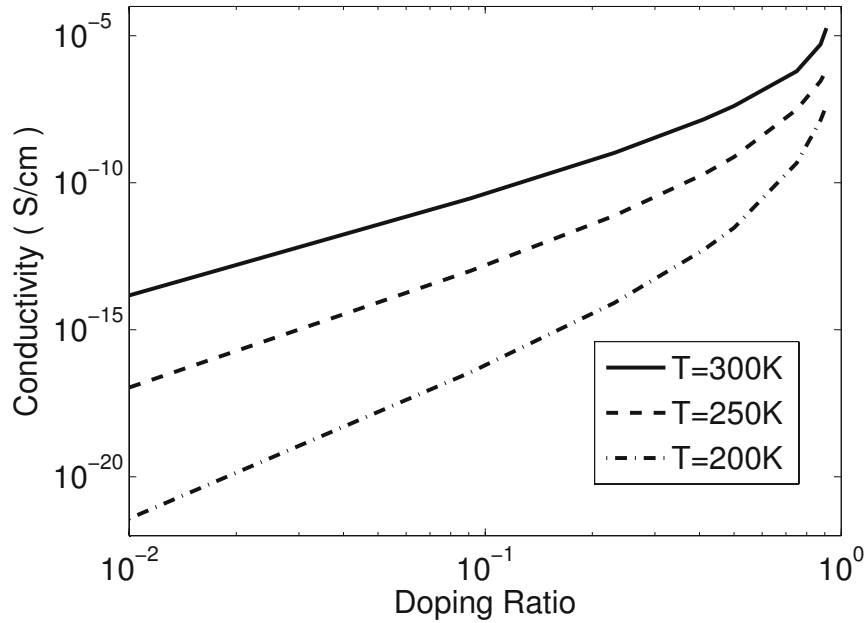


Figure 4.6: Conductivity as a function of the doping ratio with temperature as a parameter.

$$\sigma \propto \exp\left(\frac{-E_A}{k_B T}\right),$$

we can obtain the relation between activation energy E_A and doping ratio, as shown in Fig 4.8. E_A decreases with the doping ratio, indicating that less and less energy will be required for a carrier activated jump to neighboring sites when the doping ratio increases. Similar to Fig 4.7, we can also observe a transition between the two doping regimes visible as a change in the slope.

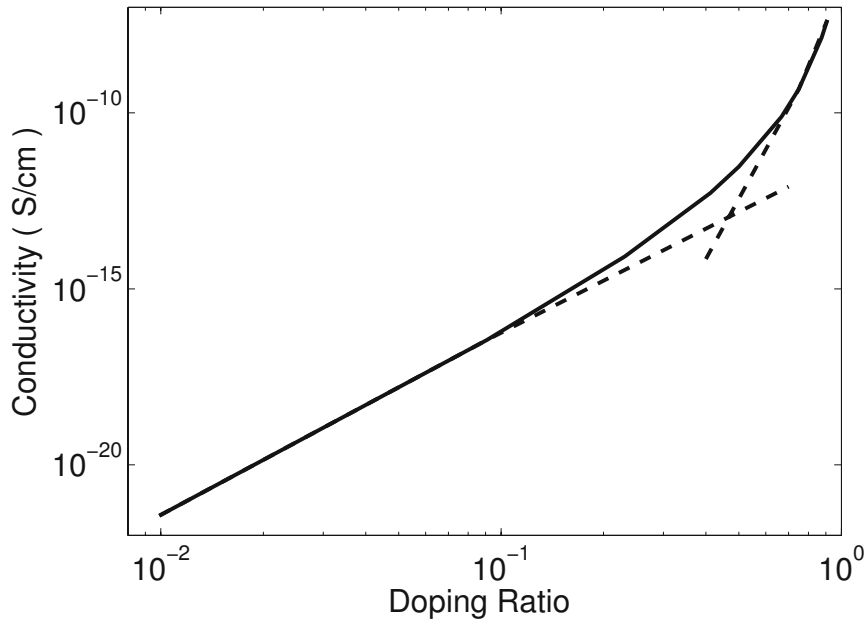


Figure 4.7: Conductivity at $T=200\text{K}$ as a function of the doping ratio. The dashed line is to guide the eye.

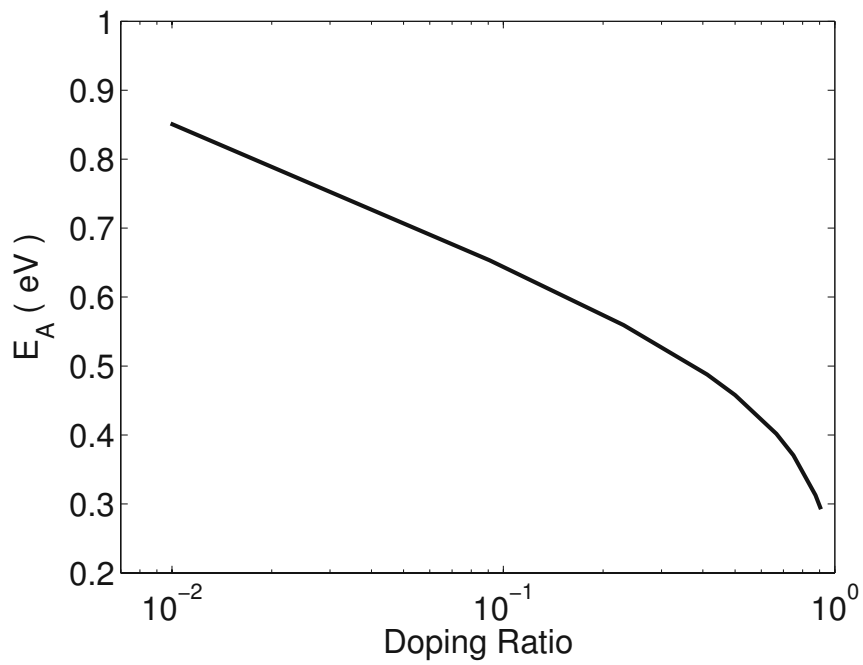


Figure 4.8: Activation energy (E_A) as a function of the doping ratio.

4.4 Trapping Characteristics

Fig 4.9 and 4.10 illustrate the temperature dependence of the carrier conductivity for different trap concentrations. The parameters are $N_t = 10^{22} \text{ cm}^{-3}$, $E_d = -0.67\text{eV}$, $T_0 = 800\text{K}$, $T_1 = 400\text{K}$, $\alpha^{-1} = 2\text{\AA}$ and $\sigma_0 = 1 \times 10^4 \text{ S/cm}$. Despite the effect of the traps, we can see an almost perfect Arrhenius-type temperature dependence in Fig 4.9, with the slope affected by the trap concentration. Increasing the latter, the activation energy decreases. In Fig 4.10, $\log \sigma$ versus T^{-2} is plotted. The deviation from a straight line occurs at higher temperature, where nearly all carriers occupy the intrinsic states, and the filled extrinsic trap states do not change the trap-free hopping relation $\log \sigma \propto T^{-2}$ [98]. However, at lower temperature, the carrier distribution will be pinned near the peak of trap DOS [68].

In Fig 4.11 we compare the analytical model with experimental data reported in [99]. Parameters are the relative trap concentration $c_t = N_d/N_t = 1 \times 10^{-2}$, $T_0 = 1200\text{K}$, $T_1 = 400\text{K}$, $E_d = -0.15\text{eV}$, $\alpha^{-1} = 1.6\text{\AA}$ and $\sigma_0 = 4.2784 \times 10^8 \text{ S/m}$. The data are for TTA with doping DAT.

The relation between conductivity and T_1 is shown in Fig 4.12. Parameters are $N_t = 1 \times 22 \text{ cm}^{-3}$, $N_d = 1 \times 19 \text{ cm}^{-3}$, $T_0 = 1200 \text{ K}$, $T = 150 \text{ K}$, $E_d = -0.5 \text{ eV}$, $\alpha^{-1} = 3\text{\AA}$ and

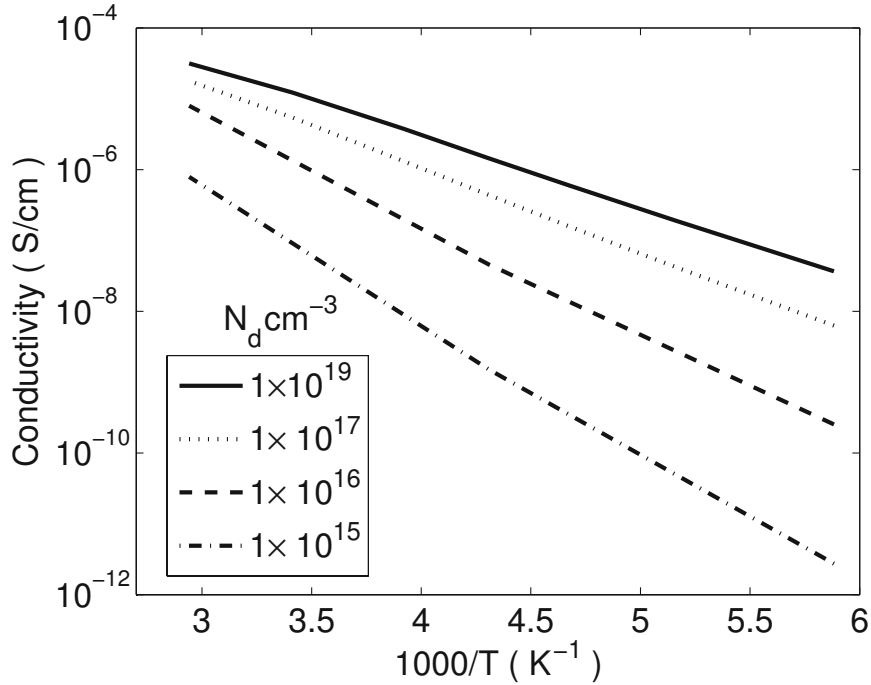


Figure 4.9: Conductivity of an organic semiconductor versus T^{-1} for different trap concentrations.

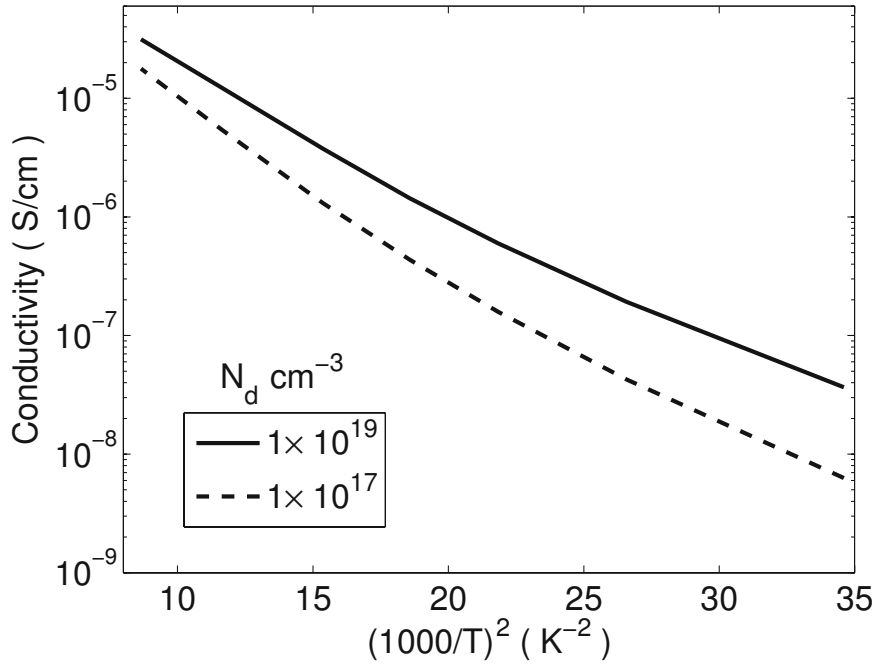


Figure 4.10: Conductivity of an organic semiconductor versus T^{-2} for different trap concentrations.

$\sigma_0 = 100$ S/m. For the exponential DOS function of the traps, the parameter T_1 is a characteristic temperature, where $k_B T_1$ represents the activation energy [100] and defines the width of the distribution [101]. Fig 4.12 confirms that the conductivity decreases with T_1 almost linearly.

The relation between conductivity and trap concentration is shown in Fig 4.13. The parameters are $N_t = 10^{22}$ cm⁻³, $\alpha^{-1} = 1.6$ Å, $T_0 = 1000$ K, $T_1 = 500$ K, $E_d = -0.2$ eV, the temperature is $T = 400$ K and $\sigma_0 = 1 \times 10^4$ S/m.

At a critical trap concentration the conductivity has a minimum. This has been verified by experiments [102] and Monte Carlo simulation [103]. The minimum is due to the onset of inter-trap transfer that alleviates thermal detrapping of carriers, which is a necessary step for charge transport [103]. We can also see that a small trap concentration has virtually no effect on the conductivity. At higher trap concentration, however, the activation energy for the conductivity decreases. The traps themselves can serve as an effective hopping transport band, so the effect of traps on the charge conductivity is qualitatively similar to that caused by a high carrier concentration. It is interesting that such transition has also been observed in thermally stimulated luminescence (TSL) measurements [104].

The relation between the conductivity and the trap energy E_t is shown in Fig 4.14.

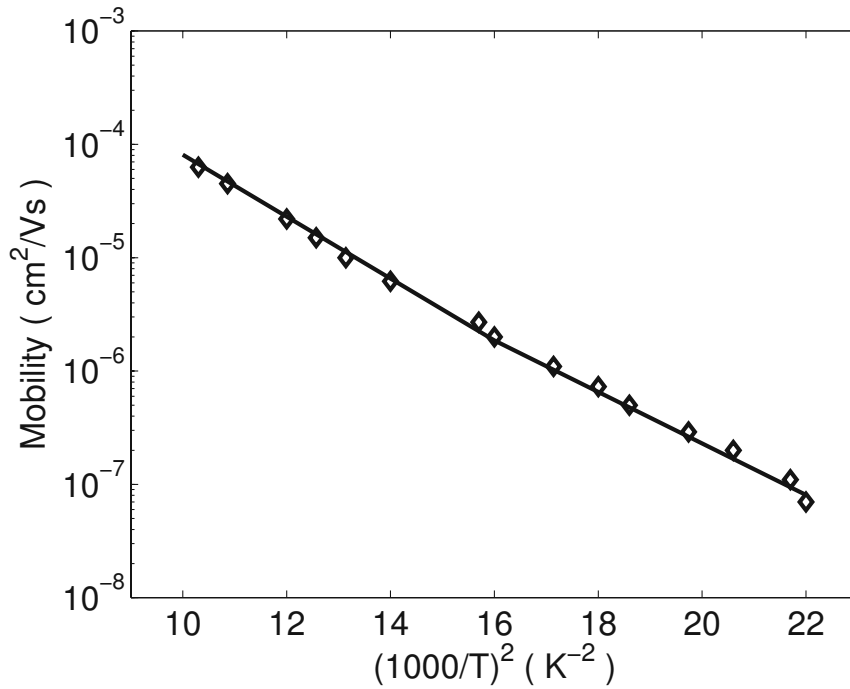


Figure 4.11: Temperature dependence of the zero-field mobility for TTA doped with DAT. Symbols represent experimental data from [99].

Parameters are $T_0 = 600\text{K}$, $T_1 = 300\text{K}$, $N_t = 1 \times 10^{22} \text{ cm}^{-3}$, $N_d = 1 \times 10^{19} \text{ cm}^{-3}$, $\alpha^{-1} = 2.5\text{\AA}$, $T = 200\text{K}$ and $\sigma_0 = 1 \times 10^4 \text{ S/m}$. From Fig 4.14 we can conclude that the conductivity increases approximately exponentially for $|E_d|$ below a certain critical value and saturates for larger $|E_d|$.

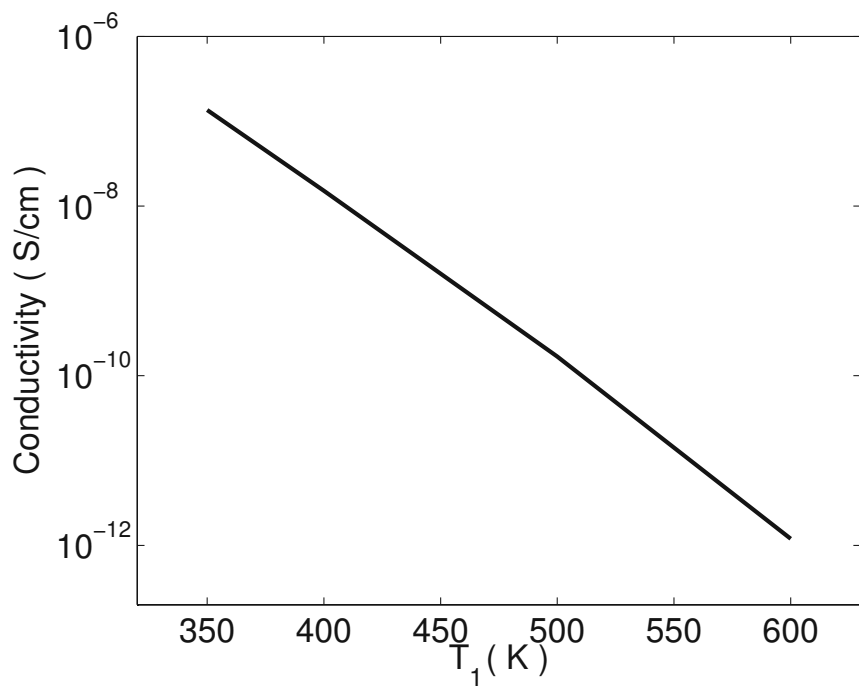


Figure 4.12: Conductivity of an organic semiconductor versus the width of the trap distribution, T_1 .

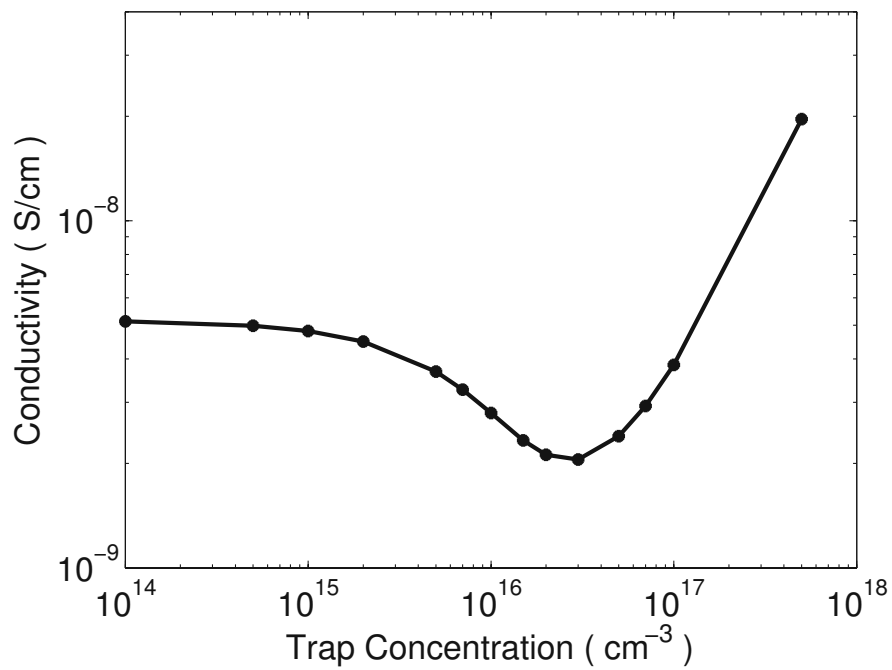


Figure 4.13: The dependence of the conductivity on the trap concentration.

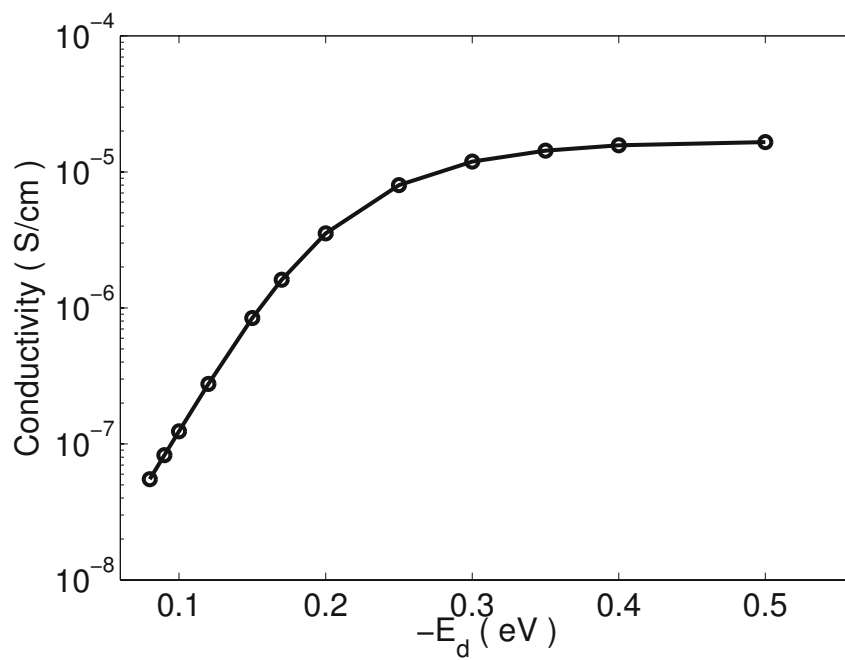


Figure 4.14: The dependence of the conductivity on the Coulombic trap energy.

Chapter 5

Charge Injection Models for Organic Light-emitting Diodes

5.1 Introduction

Over the past fifteen years, there has been a surge of interest in the development and application of organic semiconductors, such as organic light-emitting diodes (OLED) and organic field effect transistors [25, 105]. The processes of charge injection and transport play an extremely important role for OLED. Metal electrodes inject electrons and holes into opposite sides of the emissive organic layer(s), and this injection process, in most cases, governs the overall efficiency of the device. However, on the theoretical side there is still a lack of satisfactory description of the physical process underlying the charge injection in organic light-emitting diodes. One difficulty in extending our knowledge from crystalline to amorphous organic semiconductors arises because charge transport occurs no longer by free propagation in extended states, but rather by hopping in a manifold of localized states. This is reflected in the fact that there is little theoretical work that gives the electrical current at the interface in terms of experimentally obtainable parameters. Another difficulty arises from the fact that the nature of the interface in terms of composition and structure is not always understood. The sample preparation conditions, for example, have been shown to have a dramatic influence on charge injection.

The barrier height that controls hole or electron injection plays an important role in determining a measured current to be injection limited or transport limited, such as trapped charge limited transport [106, 107] or space-charge-limited (SCL) transport with a field and temperature-dependent mobility [108]. The SCL transport needs the injection barrier to be Ohmic, i.e. it must be able to supply more carriers per unit time than the sample can transport [109], which requires the injection barrier to be small

enough. The bulk-limited model predicts a dependence of the current density J on the thickness d following $J \propto 1/d^x$ ($x \leq 1$) at a constant field, where $x = 1$ in the absence of deep trap (Child's law). In the presence of an exponential distribution of traps, $x = 5$ [110].

The present work is concerned with injection-limited conduction at high electric field. The text book models to describe injection into a semiconductor are the Fowler-Nordheim (FN) model for tunneling injection and the Richardson-Schottky (RS) model for thermionic emission [111]. The FN model ignores image charge effect and invokes tunneling of electrons from a metal through a triangular barrier into unbound continuum states. It predicts a current independent of temperature.

$$J(F) = BF^2 \exp \left[-\frac{4(2m_{eff})^{1/2} \Delta^{3/2}}{3\hbar qF} \right].$$

Here Δ is the barrier height in the absence of both the external field and the image effect, F is the external field and m_{eff} is the effective mass of the carriers in the semiconductor. The RS model is based on the assumption that an electron from the metal can be injected once it has acquired a thermal energy sufficient to cross the potential maximum that results from the superposition of the external and the image charge potential. The $J(F)$ characteristic is predicted as

$$J(F) = CT^2 \exp \left[-\frac{\left(\Delta - \left(\frac{q^3 F}{4\pi \epsilon_r \epsilon_0} \right)^{1/2} \right)}{k_B T} \right],$$

where ϵ_r is the relative dielectric constant. These two models, however, are insufficient to handle disordered organic materials, where the density of states is a Gaussian distribution, with localized carriers and discrete hopping within a distribution of energy states [9]. Arkhipov presented an analytical model based on hopping theory [112] and Wolf performed detailed Monte Carlo simulations of charge injection from a metal to an organic semiconductor layer [113]. In this chapter we will present two injection models, one is based on drift-diffusion theory and the other on a master equation.

5.2 Diffusion Controlled Injection Model for OLEDs

Due to the low mobility in organic semiconductors ($\mu \ll 10^{-3} \text{cm}^2/\text{Vs}$), the diffusion transport is important for the charge injection process. Therefore, the aim of this section is to develop an analytical, diffusion-controlled charge injection model particularly suited for organic light-emitting diodes (OLED). This model is based on drift-diffusion and multiple trapping theory. The latter can be used to describe hopping transport in

organic semiconductors [114]. The presented model can explain the dependence of the injection current on the temperature, the electric field and the energy barrier height. The theoretical predictions agree well with experimental data.

5.2.1 Theory

The potential barrier $q\varphi(x)$ formed at the metal semiconductor interface is a superposition of an external electric field and a Coulomb field binding the carrier on the electrode [115, 116],

$$q\varphi(x) = \Delta - \frac{q^2}{16\pi\epsilon_0\epsilon_r x} - qFx. \quad (5.1)$$

Here, x is the distance to the metal-organic layer interface. Since the rapid variation of the potential 5.1 takes place within x_d (about 50\AA [117]) in front of the cathode, the field F can be regarded as being nearly constant.

Using the drift-diffusion theory, the hole current J can be written as

$$J = -k_B T \mu \left[\frac{q}{k_B T} p_e(x) \frac{d\varphi(x)}{dx} + \frac{dp_e(x)}{dx} \right], \quad (5.2)$$

where μ is the mobility. On taking J and μ as constant, and solving for n , we obtain

$$p_e(x) = \left[N - \frac{J}{k_B T \mu} \int_0^x \exp\left(\frac{q\varphi(x')}{k_B T}\right) dx' \right] \exp\left(-\frac{q\varphi(x)}{k_B T}\right) \quad (5.3)$$

where N is the hole concentration at $x = 0$. In multiple trapping theory [118], the total carrier concentration is given by a sum of the carrier concentrations in the extended states $p_e(x)$ and the localized states,

$$p(x) = p_e(x) + \int_0^\infty g(E, x) f(E, E_F) dE. \quad (5.4)$$

Here, $g(E)$ is the density of the localized states, $f(E, E_F)$ is the Fermi Dirac distribution, and the quasi-Fermi energy E_F can be written as [118]

$$E_F(x) = k_B T \ln \left[\frac{\nu_0 \tau_0 N_t}{p_e(x)} \right],$$

where N_t is the total concentration of localized states, τ_0 is the lifetime of carriers, and ν_0 is the attempt-to-escape frequency.

In the injection regime, very close to the contact all the traps are filled. Moreover, the carrier concentration in the extended states is much higher than that in the trapped states. At large distance from the injection contact, the main contribution to the total carrier concentration comes from the occupied localized states [112]. So we propose here

the concept of a *critical distance* x_d , where the carrier concentration in the extended states equals the carrier concentration in localized states, i.e.,

$$p_e(x_d) = \int_0^\infty g(E, x_d) f(E, E_F) dE. \quad (5.5)$$

Substituting (5.1),(5.4) and (5.5) into the Poisson equation,

$$\frac{d^2(q\varphi)}{dx^2} = -\frac{q}{\epsilon_0\epsilon} p(x), \quad (5.6)$$

then the critical distance x_d can be calculated as

$$1 = \int_0^\infty \frac{16\pi x_d^3 g(E - q\varphi(x_d))}{1 + 16\pi x_d^3 \nu_0 \tau_0 N_t \exp(-E/k_B T)} dx. \quad (5.7)$$

Solving (5.7) with a Gaussian DOS numerically, we can obtain the critical distance x_d . The free carrier concentration at x_d is calculated by (5.5). Finally, the injection current can be calculated as

$$J = k_B T \mu \frac{\left[N - p_e(x_d) \exp\left(\frac{q\varphi(x_d)}{k_B T}\right) \right]}{\int_0^{x_d} \exp\left(\frac{\varphi(x)}{k_B T}\right) dx}. \quad (5.8)$$

5.2.2 Results and Discussion

The barrier height Δ plays an important role for the injection efficiency. We calculate the relation between the injection current and the electric field for different Δ , as shown in Fig 5.1. The parameters are $N_t = 1 \times 10^{18} \text{cm}^{-3}$, $\sigma = 0.1656 \text{eV}$, $\nu_0 = 10^{11} \text{s}^{-1}$, $\tau_0 = 10^{-11} \text{s}$, $T = 300 \text{K}$ and $\mu = 1 \times 10^{-9} \text{cm}^2/\text{Vs}$. The injection current increases with the electric field, and the lower the Δ , the higher the injection current as intuitively expected. But the slope of $\log J$ versus $\log F$ is not constant. Fig 5.2 shows the temperature dependence of the injection current for $\Delta = 0.3 \text{eV}$, where the other parameters are the same as in Fig 5.1. The temperature coefficient decreases strongly with increasing electric field. The coefficient reverses sign at high electric field, which has also been observed in [115] theoretically. A comparison between the model and experimental data [112] is shown in Fig 5.3. The fitting parameters are $N_t = 1 \times 10^{17} \text{cm}^{-3}$, $\mu = 2.56 \times 10^{-11} \text{cm}^2/\text{Vs}$ for PPV-ether and $2.51 \times 10^{-9} \text{cm}^2/\text{Vs}$ for PPV-imine, respectively. The other parameters are the same as in Fig 5.1. The mobility in organic materials depends on the local electric field F as [119]

$$\mu(F) = \mu_0 \exp\left(\gamma\sqrt{F}\right). \quad (5.9)$$

Here μ_0 denotes the mobility of carriers at zero field and γ is the parameter describing the field dependence. We first substitute (5.9) into (5.2) to obtain the carrier concentration,

$$p_e(x) = \left[N - \frac{J}{k_B T \mu_0 \exp\left(\gamma\sqrt{F}\right)} \int_0^x \exp\left(\frac{q\varphi(x')}{k_B T}\right) dx' \right] \exp\left(-\frac{q\varphi(x)}{k_B T}\right). \quad (5.10)$$

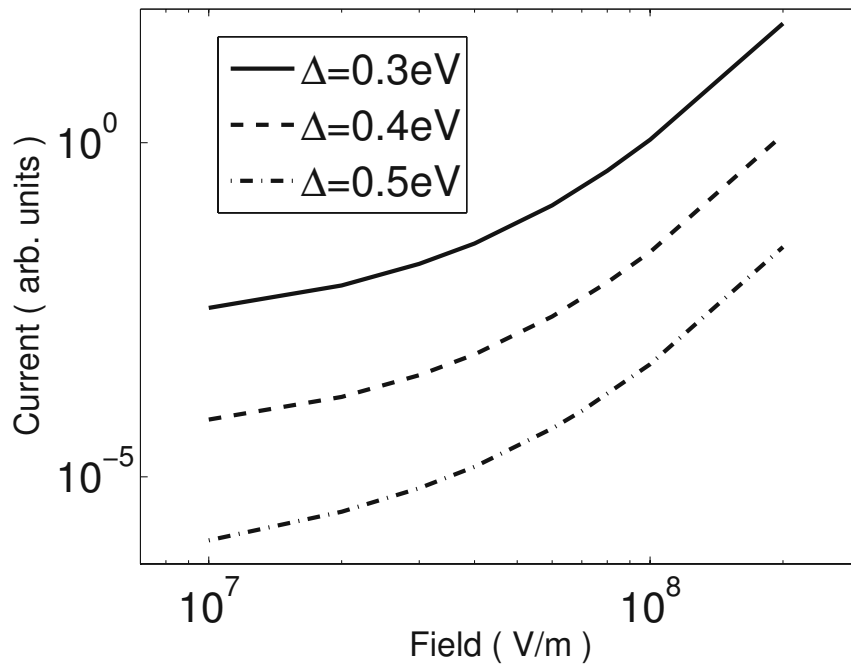


Figure 5.1: Dependence of the injection current on the barrier height.

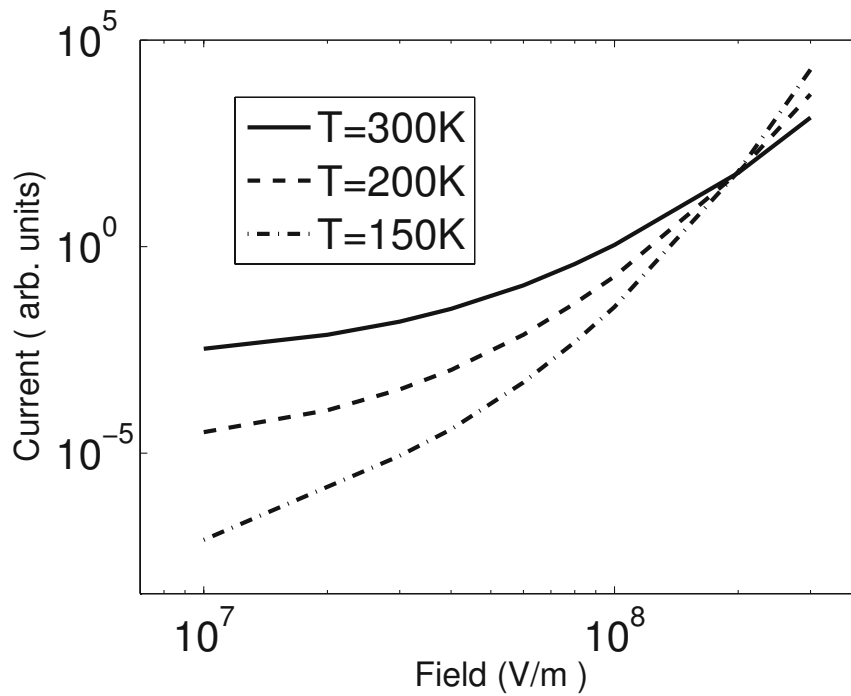


Figure 5.2: Temperature dependencies of the injection current.

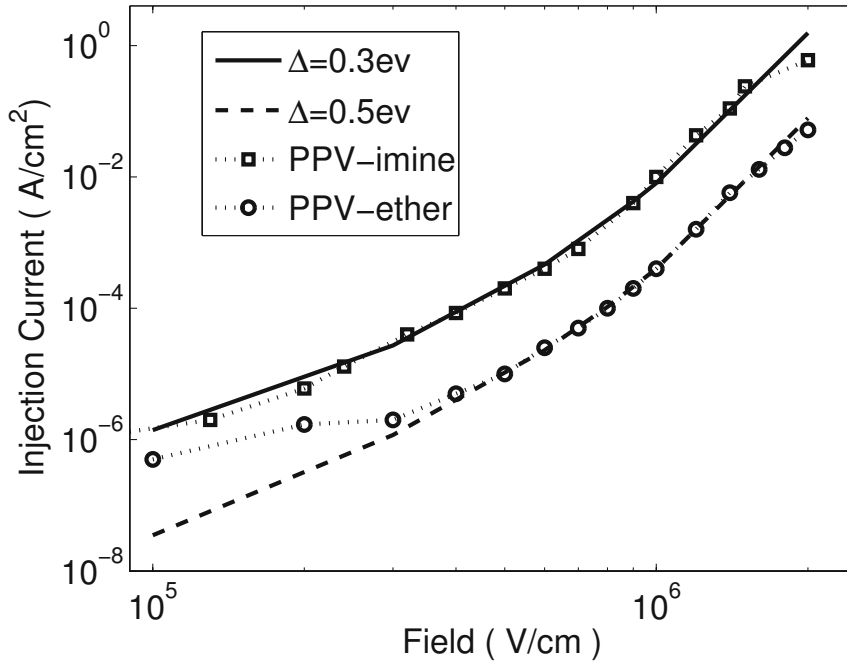


Figure 5.3: Comparison between the model and experimental data.

Then, by combining (5.7), (5.10), Gaussian DOS and (5.8), we obtain the injection current with the field-dependent mobility. Fig 5.4 illustrates the relation between injection current and electric field with field dependent mobility. Parameters are $\mu_0 = 7.3 \times 10^{-6} \text{cm}^2/\text{Vs}$, $\gamma = 1 \times 10^{-4} (\text{m/V})^{1/2}$ and $\Delta = 0.3\text{eV}$. For comparison, the injection current with constant mobility is plotted as well.

5.3 Charge Injection Model for OLED Based on Master Equation

The steady-state injection current in an OLED is the difference between the injection current from the electrode towards the organic semiconductor, I_{inj} , and the recombination current, I_{rec} , from the organic semiconductor back to the electrode. The first one is traditionally described by classical injection expressions, either FN or RS expression. In this work I_{inj} and I_{rec} enter of a master equation that describes the transport at the interface by a rate equation. This model yields the injection current as a function of electric field, temperature, energy barrier between metal and organic layer, and energetic width of the distribution of hopping sites. Good agreement with experimental data is found.

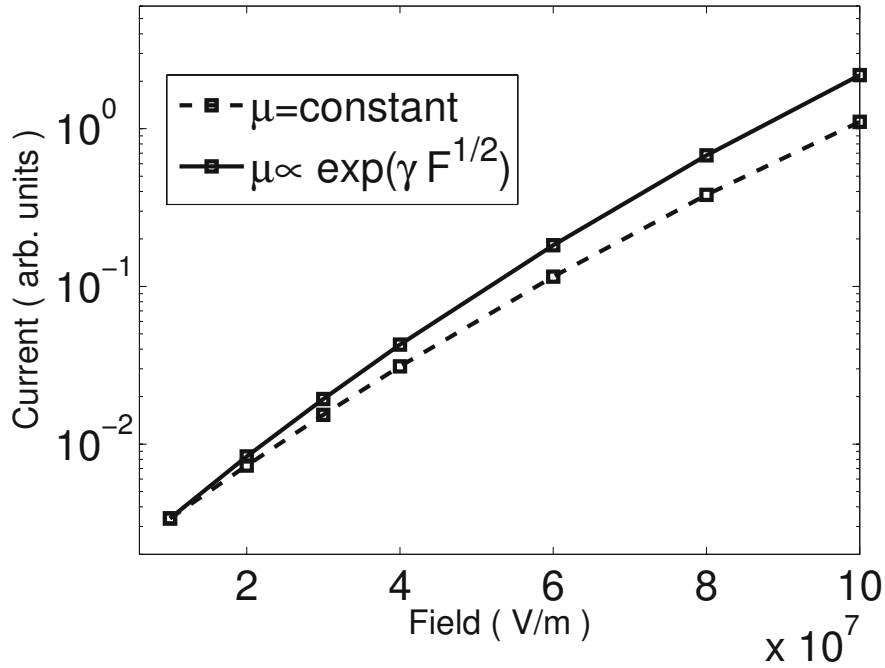


Figure 5.4: Comparison between injection currents for field dependent mobility and constant mobility.

5.3.1 Theory

The system to be considered here is an energetically and positionally random hopping system in contact with a metallic electrode. At an arbitrary distance x away from the metal-organic layer interface, located at $x = 0$, the electrostatic potential is given by the sum of the image charge potential and the applied potential described by electric field F as (5.1). Since the rapid variation of potential (5.1) takes place in front of the cathode, and space-charge effects can be ignored altogether in the calculation of the cathode characteristics [112, 117], the field F may be regarded as being nearly constant. Assuming no correlations between the occupation probabilities of different localized states, the net electron flow between two states is given as

$$I_{ij} = f_i (1 - f_j) \omega_{ij} - f_j (1 - f_i) \omega_{ji}, \quad (5.11)$$

with f_i denoting the occupation probability of site i and ω_{ij} the electron transition rate of the hopping process between the occupied state i to the empty state j . The probabilities (5.11) are then employed in a master equation for describing charge transport. With the electrochemical potential μ'_i at the position of state i the occupation probability is

described by a Fermi-Dirac distribution as

$$f_i = \frac{1}{1 + \exp\left(\frac{E'_i - \mu'_i}{k_B T}\right)}. \quad (5.12)$$

For the metal electrode we assume a fixed electron concentration P_0 and a Fermi-level of zero. All injected carriers are assumed to hop from the metal Fermi-level. Under the effect of a constant electric field F and the Coulomb field binding the carrier with its image charge on the electrode the energy and the electrochemical potential of a localized state are given by

$$\begin{aligned} E'_j &= E_j + \Delta - q\varphi(R_j, \theta), \\ \mu'_j &= \Delta - q\varphi(R_j, \theta) \\ \varphi(R_j, \theta) &= FR_j \cos \theta + \frac{q}{16\pi\epsilon R_j \cos \theta} \end{aligned}$$

where R_j denotes the distance of state j from the interface, θ the angle between F and R_j , Δ the barrier height, and E_j the energy at state j without electric field. According to Mott's formalism [44], the transition rate ω_j from the metal Fermi-level to state j reads as

$$\omega_j \propto \begin{cases} \exp\left[-2\alpha R_j - \frac{E'_j}{k_B T}\right] & : E'_j \geq 0 \\ \exp(-2\alpha R_j) & : E'_j \leq 0 \end{cases} \quad (5.13)$$

Connecting with a Gaussian DOS, the net current across the metal-organic contact can be written as

$$I = I_{\text{inj}} - I_{\text{rec}} = e\nu_0 (I_1 + I_2 - I_3 - I_4) \quad (5.14)$$

where ν_0 is the attempt-to-jump frequency and

$$\begin{aligned} I_1 &= \int_1^{+\infty} dr \int_{\beta}^{\infty} dR_j \int_{-\infty}^0 dE_j \frac{P_0(1-f_j)}{\sqrt{2\pi}\sigma} \exp\left(-2\gamma R_j - \frac{(E_j - (\Delta - e\varphi(R_j, r)))^2}{2\sigma^2}\right) \\ I_2 &= \int_1^{+\infty} dr \int_{\beta}^{\infty} dR_j \int_0^{\infty} dE_j \frac{P_0(1-f_j)}{\sqrt{2\pi}\sigma} \exp\left(-2\gamma R_j - E_j - \frac{(E_j - (\Delta - e\varphi(R_j, r)))^2}{2\sigma^2}\right) \\ I_3 &= \int_1^{+\infty} dr \int_{\beta}^{\infty} dR_j \int_0^{\infty} dE_j \frac{N_t f_j}{\sqrt{2\pi}\sigma} \exp\left(-2\gamma R_j - \frac{(E_j - (\Delta - e\varphi(R_j, r)))^2}{2\sigma^2}\right) \\ I_4 &= \int_1^{+\infty} dr \int_{\beta}^{\infty} dR_j \int_{-\infty}^0 dE_j \frac{N_t f_j}{\sqrt{2\pi}\sigma} \exp\left(E_j - 2\gamma R_j - \frac{(E_j - (\Delta - e\varphi(R_j, r)))^2}{2\sigma^2}\right) \end{aligned}$$

where $r = 1/\cos \theta$, β is the distance from the electrode to the first hopping site in the bulk and $f_j = \left(1 + \exp\left(\frac{E_j - \mu_j}{k_B T}\right)\right)^{-1}$. I_1 and I_2 describe the charge injection from the electrode downwards and upwards, respectively. I_3 and I_4 describe the backflow of charge to the electrode. The net current can be calculated by evaluating I_1 , I_2 , I_3 and I_4 numerically.

5.3.2 Results and Discussion

With the model presented we calculate the field dependence of the net, injection and backflow current. The parameters are $\Delta = 0.3\text{eV}$, $N_t = 1 \times 10^{22}\text{cm}^{-3}$, $T = 300\text{K}$, $\epsilon_r=3$, $\beta = 0.6\text{nm}$, $\gamma = 2 \times 10^8\text{cm}^{-1}$, $\sigma = 0.08\text{eV}$ and $\nu_0 = 1 \times 10^{11}\text{s}^{-1}$. Fig 5.5 shows that with electric field the injection current increases and the backflow current decreases, as intuitively expected. As a result, the net current increases with electric field quickly in the low field regime.

Fig 5.6 shows a semilogarithmic plot of the current versus $F^{1/2}$ with the same parameters as used in Fig 5.5. This presentation is appropriate for testing RS behavior as $j \propto \exp\left(\sqrt{qF/4\pi\epsilon\epsilon_0}\right)$. Since the dependence of $\log j$ versus $F^{1/2}$ is not linear, a deviation from the RS characteristics is observed.

Fig 5.7 shows the current-field characteristics for different Δ and $\nu_0 = 9 \times 10^{11}\text{s}^{-1}$, the other parameters are the same as in Fig 5.5. The injection current increases with decreasing barrier height Δ and with electric field. The comparison between calculation and experimental data of DASMB sandwiched between ITO and Al electrodes [112] is given in Fig 5.8. The parameters are $\Delta = 0.4\text{eV}$ and $T = 123\text{K}$, the other parameters are the same as in Fig 5.5. The agreements is quite good at low electric fields. The discrepancy between calculation and experimental data comes from the resistance of the ITO contact at high electric field [112].

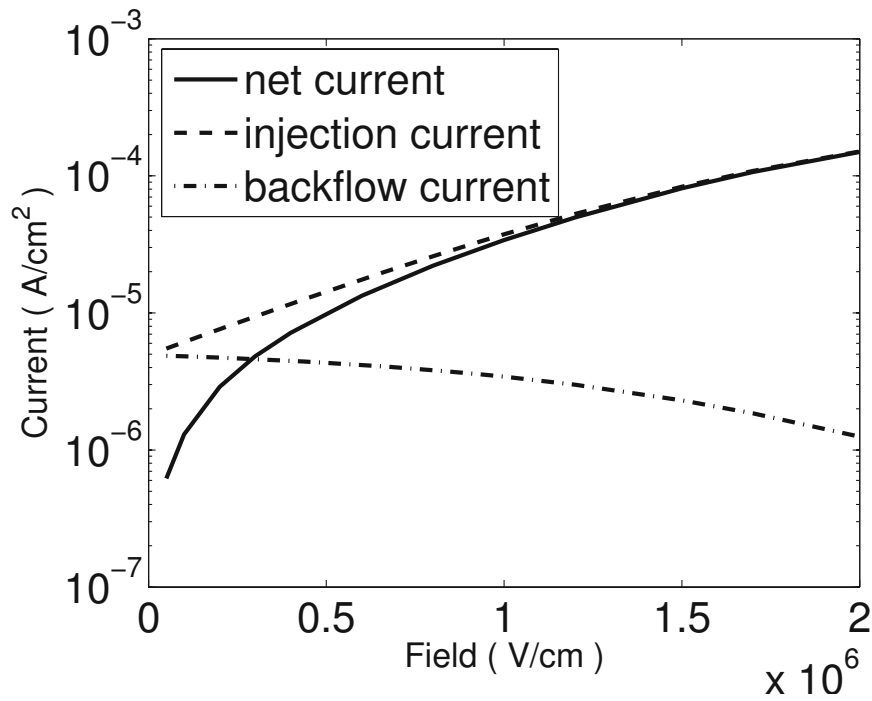


Figure 5.5: Field dependence of the net, injection, and backflow currents.

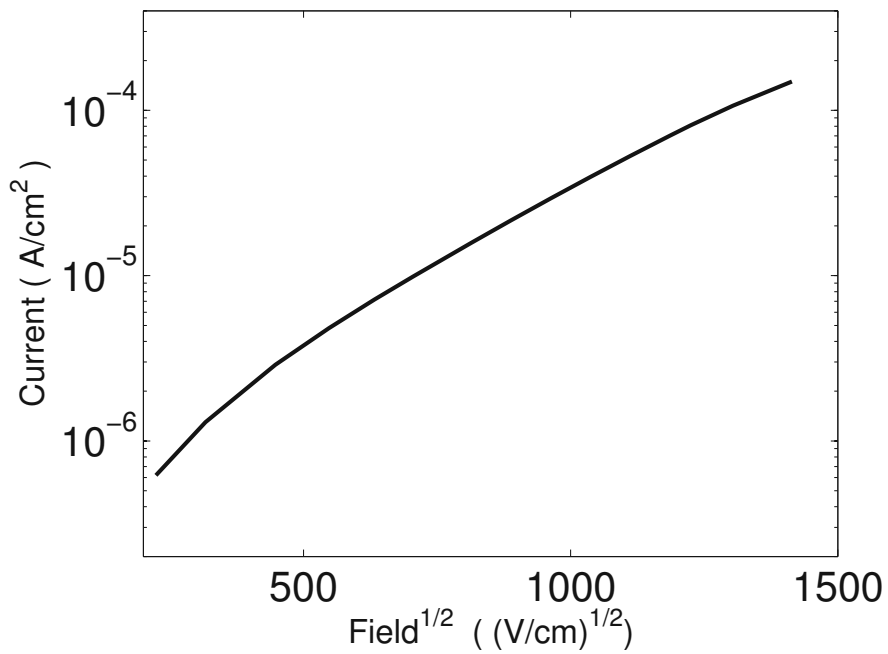


Figure 5.6: Relation between injection current and $F^{1/2}$.

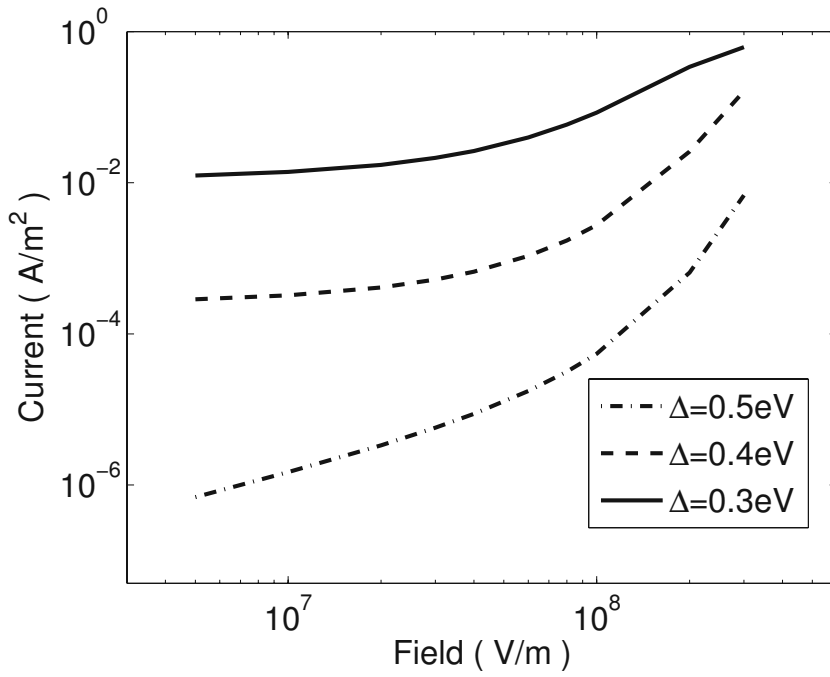


Figure 5.7: Barrier height dependence of the injection current.

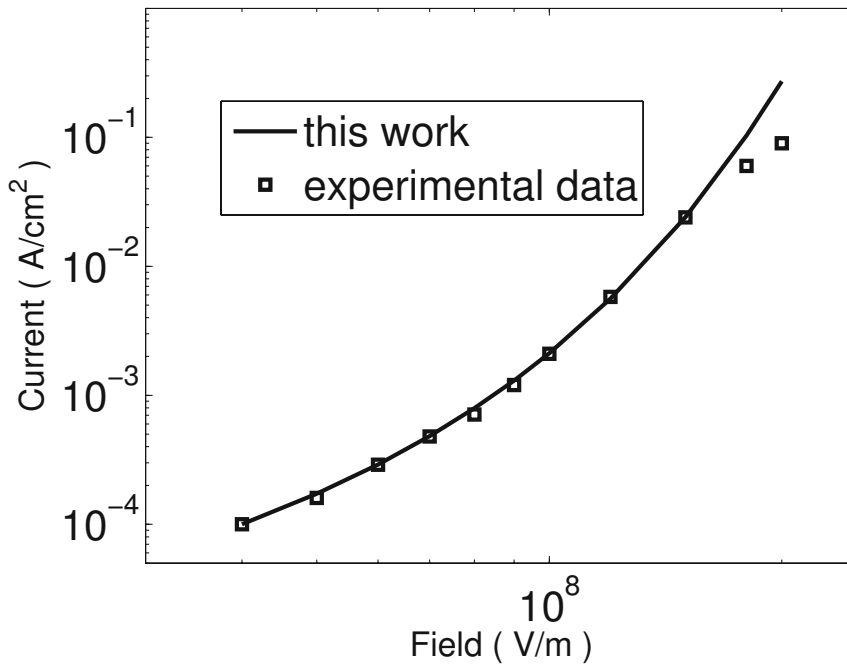


Figure 5.8: Comparison between calculation and experimental data at $T = 123K$.

Chapter 6

Space Charge Limited Current in Organic Light-emitting Diodes

6.1 Introduction

The carrier mobilities in organic semiconductors are typically low. If the injection barrier between the metal and the semiconductor is small and carriers can be efficiently injected into the device, charge transport in such devices can be described using the theory of space charge limited current (SCLC), which plays an important role in investigating the efficiency of charge injection in OLEDs and estimating parameters such as mobility and trap concentration in organic semiconductors [120, 121]. The theory of SCLC in a trap-free dielectric was formulated by Mott and Gurney [122]. Later it was extended to account for SCLC controlled by shallow traps with exponential energy distribution [123]. However, it is generally accepted that the DOS is a Gaussian distribution, and the states in the tail act as trapped states [124].

In the following, we extend Campbell's work [124] to derive a single-carrier SCLC model for organic semiconductors with a Gaussian DOS distribution. A single carrier diode can be easily fabricated by choosing metals with appropriate work functions for the contact.

6.2 Theory

The SCLC problem in dielectrics can be described by the following equations [107]

$$\frac{dF}{dx} = \frac{q}{\epsilon_r \epsilon_0} (n_f + n_t), \quad (6.1)$$

$$j = qn_f \mu F, \quad (6.2)$$

where F is the electric field intensity, ϵ_r is the relative dielectric permittivity, n_f and n_t are the concentrations of the mobile and trapped carriers, respectively, j is the current density, and μ is the drift mobility of carriers.

In this model, a Gaussian DOS function is assumed. Analysis of the optical adsorbtion spectrum and mobility for PPV indicates that the DOS can be fitted well to a Gaussian distribution with $\sigma \approx 0.1\text{eV}$. In other disordered molecular materials σ typically lies between 0.07 and 0.13eV [9].

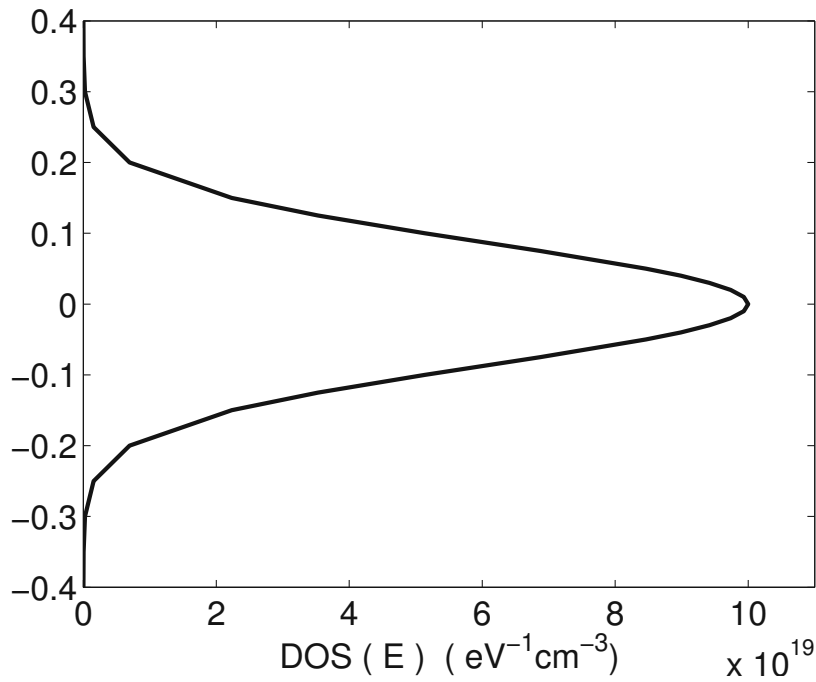


Figure 6.1: Gaussian density of states with zero mean energy. The vertical axis corresponds to energy, the horizontal axis reflects the site density. The center of the Gaussian DOS is at zero energy.

A schematic representation of the Gaussian DOS is shown in Fig 6.1. In the tail of the distribution few sites are available for hopping and their nearest neighbors are many kT away in energy, so that they serve as trap centers. Site-selective fluorescence of PPV has also shown that the sites in the tail of the distribution act as traps [125]. While the sites towards the center of DOS more neighbors are accessible and the energy between them is very close. So they provide the mobile carriers. Here we define a conduction edge [126] at about 2σ below the Gaussian center. We do not rigorously justify such edge position and it is done only for illustration purpose, though it is similar to the method applied to absorption spectrum or STM measurements [127]. So the concentrations of

mobile and trapped carriers can be calculated as

$$n_f = \int_{-2\sigma}^{\infty} g(E) f(E) dE, \quad (6.3)$$

$$n_t = \int_{-\infty}^{-2\sigma} g(E) f(E) dE, \quad (6.4)$$

with $g(E)$ being the DOS function and $f(E) = (1 + \exp[E - E_F])^{-1}$ the Fermi-Dirac distribution. Substituting (6.3) and (6.4) into (6.1) and (6.2), we obtain

$$\frac{dF}{dx} = \frac{q}{\epsilon_0 \epsilon_r} \int_{-\infty}^{\infty} g(E) f(E) dE. \quad (6.5)$$

$$F = \frac{j}{q\mu} \left(\int_{-2\sigma}^{\infty} g(E) f(E) dE \right)^{-1}. \quad (6.6)$$

Then differentiate (6.6) with respect to x to obtain the equation

$$\frac{dF}{dx} = \frac{j}{e\mu} \frac{\int_{-2\sigma}^{\infty} g(\epsilon) (1 + \exp(\epsilon - \epsilon_F))^{-2} \exp(\epsilon - \epsilon_F) d\epsilon}{\left(\int_{-2\sigma}^{\infty} g(\epsilon) (1 + \exp(\epsilon - \epsilon_F))^{-1} d\epsilon \right)^2}, \quad (6.7)$$

where $\epsilon = E/k_B T$ and $\epsilon_F = E_F/k_B T$. Substituting (6.7) into (6.5), we obtain the differential equation for quasi Fermi-energy as

$$\begin{aligned} \frac{d\epsilon_F}{dx} = & -\frac{q^2 \mu N_t^2 \exp(\epsilon_F)}{2j\pi\epsilon_0\epsilon_r\sigma_0^2} \int_{-\infty}^{\infty} \frac{\exp(-\epsilon^2/2\sigma_0^2)}{1 + \exp(\epsilon - \epsilon_F)} d\epsilon \left[\int_{-2\sigma_0}^{\infty} \frac{\exp(-\epsilon^2/2\sigma_0^2)}{1 + \exp(\epsilon - \epsilon_F)} d\epsilon \right]^2 \\ & \times \left[\int_{-2\sigma_0}^{\infty} \frac{\exp(\epsilon - \epsilon^2/2\sigma_0^2)}{[1 + \exp(\epsilon - \epsilon_F)]^2} d\epsilon \right]^{-1}. \end{aligned} \quad (6.8)$$

where $\sigma_0 = \sigma/k_B T$. Combing (6.6) and (6.8), we obtain the position-dependent electric field. the j/V characteristics can be calculated by integrating the field over the coordinate.

6.3 Results and Discussion

First we solve (6.8) numerically. The position dependence of the quasi Fermi energy is shown in Fig 6.2. The parameters are $N_t = 1 \times 10^{22} \text{cm}^{-3}$, $j = 0.4 \text{A/cm}^2$, $\mu = 1 \text{cm}^2/\text{Vs}$, $\epsilon_r = 3$, $\sigma/k_B T = 4$ and the sample thickness $L = 100 \text{nm}$. It can be seen that the quasi Fermi-energy decreases with position and increases with current density. Near the contact, the quasi Fermi energy decreases very quickly. We treat the metal electrode as site 0 with Fermi energy as $E_F = -E_m$, where E_m is the metal work function. The Ohmic contact at $x = 0$ implies that the field must drop to zero at this coordinate, so

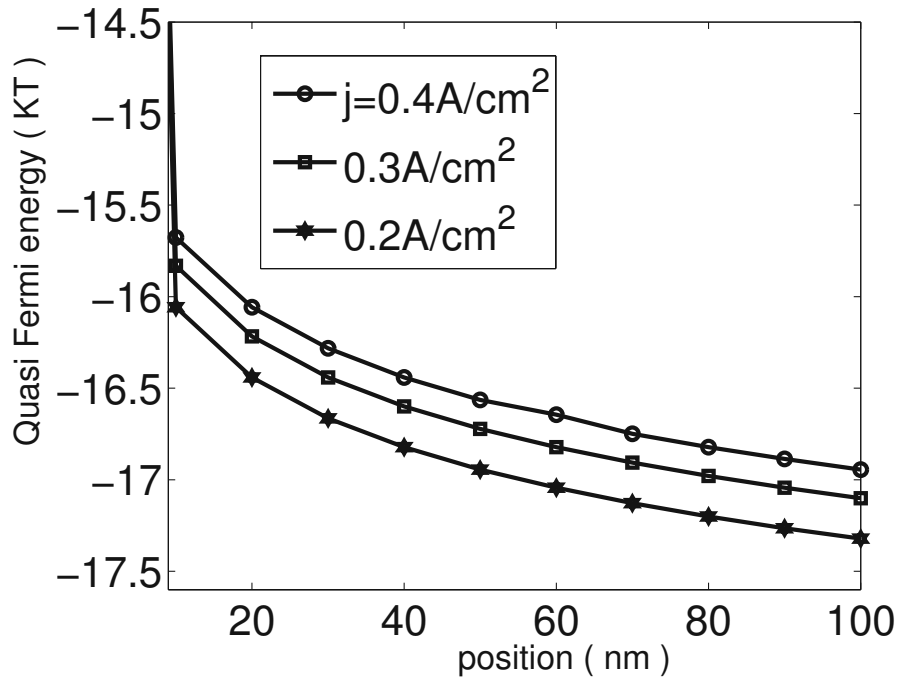


Figure 6.2: Spatial distribution of the quasi Fermi energy for different current densities.

that $F(0) = 0$. Fig 6.3 shows that the carrier concentration decreases from the contact. Fig 6.4 shows the field distribution in OLED with the same parameters as in Fig 6.2. The j/V characteristics are plotted in Fig 6.5 for different σ/kT , where the parameters are the same as Fig 6.2. As we can see, at low voltages and current densities, the current follows a $j \propto V^2$ characteristics, which may suggest either the trap-free case or the shallow-trap case. At higher voltages, the space charge is formed mainly by carriers occupying states above Fermi energy and the current increases with voltage faster than V^2 . This behavior is also predicted by a SCLC model based on an exponential DOS distribution [124], where

$$j \propto \frac{V^{m+1}}{L^{2m+1}}.$$

The parameter $m = E_t/kT$ varies between about 1 and 4, E_t is the characteristic energy of the exponential DOS and L is the layer thickness of LED.

The available models for SCLC transport assume constant mobility, and include or neglect traps. However, it was found that the mobility in organic semiconductors depends on the local electric field [119].

Integrating (6.5) yields

$$F = \frac{q}{\epsilon_0 \epsilon_r} \int_0^x \int_{-\infty}^{\infty} g(E) f(E) dE, \quad (6.9)$$

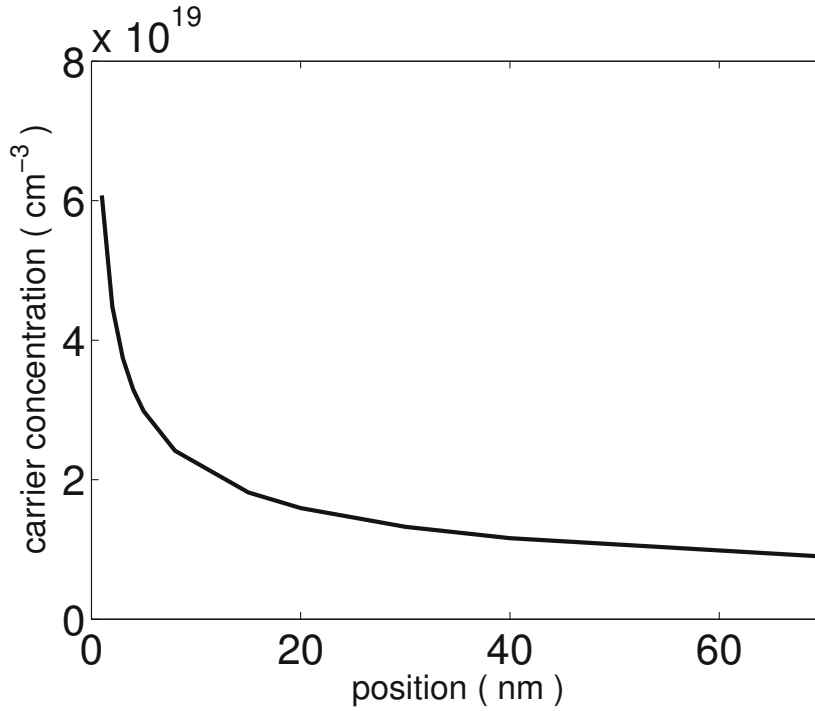


Figure 6.3: Spatial distribution of the carrier concentration near the contact for $j = 0.4\text{A}/\text{cm}^2$.

(6.6) is rewritten as

$$F\mu_0 \exp(\gamma\sqrt{F}) = \frac{j}{q} \left(\int_{-2\sigma}^{\infty} g(E) f(E) dE \right)^{-1}. \quad (6.10)$$

Substituting (6.10) into (6.9), we can obtain a new equation for quasi Fermi-energy as

$$\frac{\mu_0 q^2}{\epsilon_0 \epsilon_r j} \left(\int_0^x \int_{\infty}^{\infty} g(E) f(E) dE \right) \exp \left(\gamma \sqrt{\int_0^x \int_{\infty}^{\infty} g(E) f(E) dE} \right) = \left(\int_{-2\sigma}^{\infty} g(E) f(E) dE \right)^{-1}. \quad (6.11)$$

The quasi Fermi energy and electric field distribution can be obtained by solving (6.11) numerically. Fig 6.6 illustrates the effect of electric field dependent mobility on SCLC with $\gamma = 1 \times 10^{-3}(\text{m}/\text{V})^{1/2}$ and $\mu_0 = 1\text{cm}^2/\text{Vs}$. Other parameters are the same as in Fig 6.3. For comparison, SCLC with constant mobility and the standard SCLC model $j \propto V^2$ are also plotted as well. It should be observed that our model departs slightly from the standard one at high current densities.

For light emitting diodes, it is important to distinguish if the device is controlled by injection at the contact or by currents in the bulk of the organic layer. To determine the

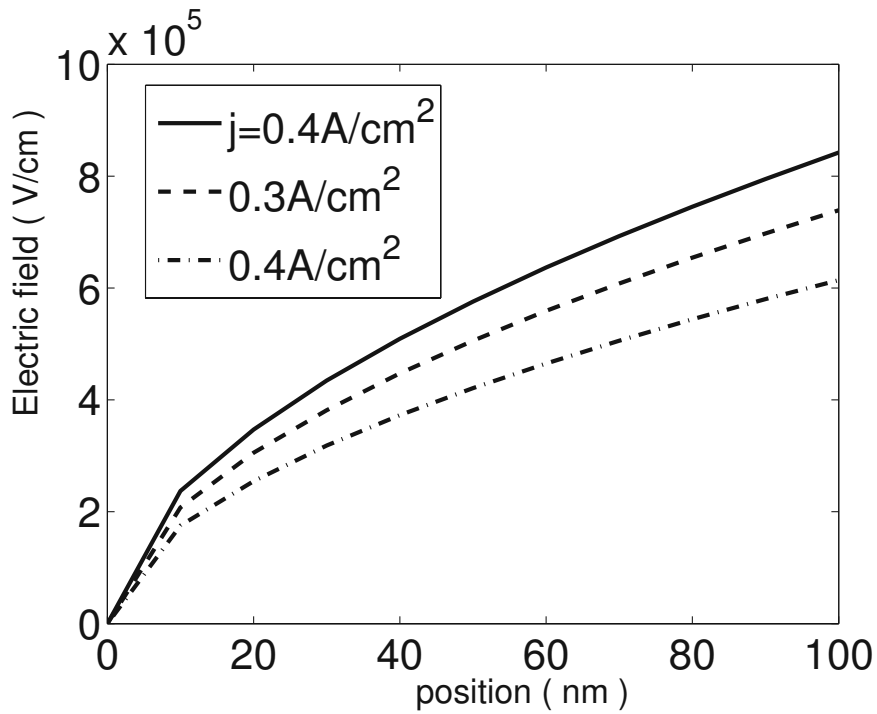


Figure 6.4: Spatial distribution of the electric field at different current densities.

dominant mechanism, an understanding of the thickness scaling is required [128, 129]. The thickness dependent SCLC in Child's law model is given as [122]

$$j = \frac{9}{8} e \epsilon_0 \epsilon_r \mu \frac{V^2}{L^3}. \quad (6.12)$$

The relation between layer thickness and SCLC in our model is shown in Fig 6.7 assuming the same parameters as in Fig 6.2. The thickness dependence of the current is also of the form $j \propto 1/L^k$ with $k = 3.2264$ for the constant mobility case and $k = 3.8$ for the field dependent mobility case. In both cases k is slightly bigger than 3 as in the standard model.

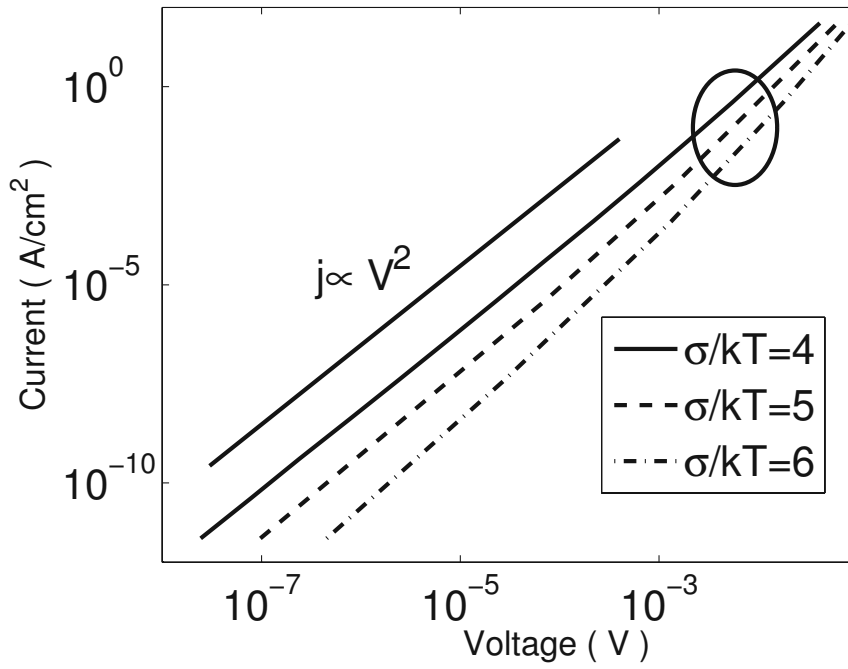


Figure 6.5: Current-voltage characteristics of a sample with Gaussian DOS distribution parametric in temperature.

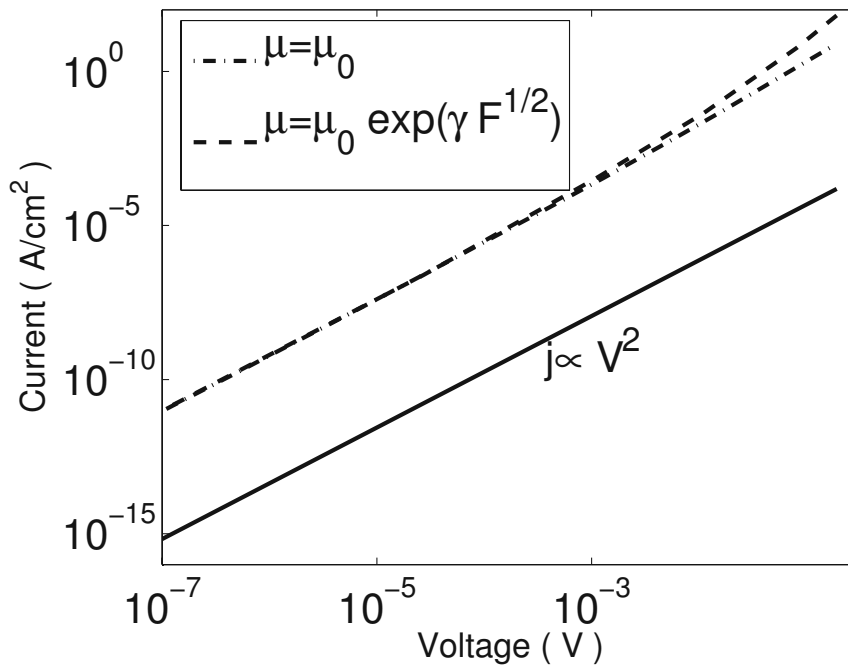


Figure 6.6: The effect of the field dependent mobility on the space charge limited current.

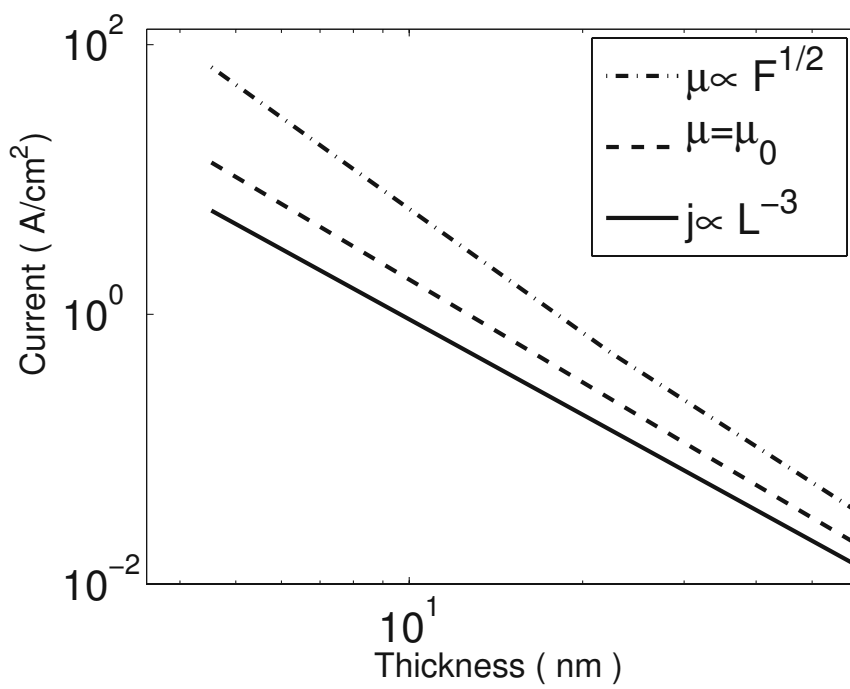


Figure 6.7: The relation between organic layer thickness and space charge limited current.

Chapter 7

Organic Semiconductor Device Models

7.1 Introduction

In recent years, organic devices including OTFT and OLED have found important application in large-area, low performance and low-cost integrated circuits. Such applications include driving devices for active matrix flat panel displays, light identification tags, sensors, etc. The key traits distinguishing devices with organic active layer from conventional FETs are their potential for low-cost and low-temperature processing, and their compatibility with flexible substrates. As organic device applications increase, a more accurate and yet simple model of device characteristics is necessary for understanding, improving, and applying these devices. Up to now, many of the numerical or analytical organic device models available in commercial devices simulators use the same expressions as used for crystalline devices. However, organic devices show several differences with respect to crystalline devices because of the low conductivity of organic semiconductors. Furthermore, OTFTs are primarily operated as accumulation field effect transistors as opposed to the usual inversion mode of crystalline MOSFETs. OTFTs are normally conducting at zero gate voltage, and the field-effect mobility usually increases with the gate voltage [130].

At the same time, different parameters such as barrier height, mobility and device length affect the current of OLEDs, so it is useful to consider organic diode structures in which single carrier type dominates the current flow in order to clarify the device operation in a relatively simple situation. Such unipolar devices can be easily fabricated by choosing the contact so that the energy barrier for one carrier type is much larger than that for the other.

7.2 Analytical Model for Organic Thin Film Transistors

In this section we derive a basic expression for the sheet conductance based on the variable range hopping (VRH) theory. This theory describes thermally activated tunneling of carriers between localized states around the Fermi level in the tail of a Gaussian distribution. It has been used to calculate the mobility of OTFTs successfully. After some simplification for the surface potential, simple and efficient analytical expressions for the transfer characteristics and output characteristics are obtained. The model does not require as input parameters the explicit definition of the threshold and saturation voltage, which are rather difficult to evaluate for this kind of device. The obtained results are in good agreement with experimental data.

7.2.1 Variable Range Hopping Transport in Organic Semiconductors

Because most organic films have an amorphous structure and disorder is dominating the charge transport, variable-range-hopping in positionally and energetically disordered systems of localized states is widely accepted as the conductivity mechanism in organic semiconductors. Different from hopping, where the charge transport is governed by the thermally activated tunneling of carriers between localized states rather than by the activation of carriers to the extended-state transport level, the concept of variable range hopping means that a carrier may either hop over a small distance with high activation energy or hop over a long distance with a low activation energy. In an organic thin film transistor with a typical structure shown in Fig 7.1, an applied gate voltage gives rise to an accumulation of carriers in the region of the organic semiconductors close to

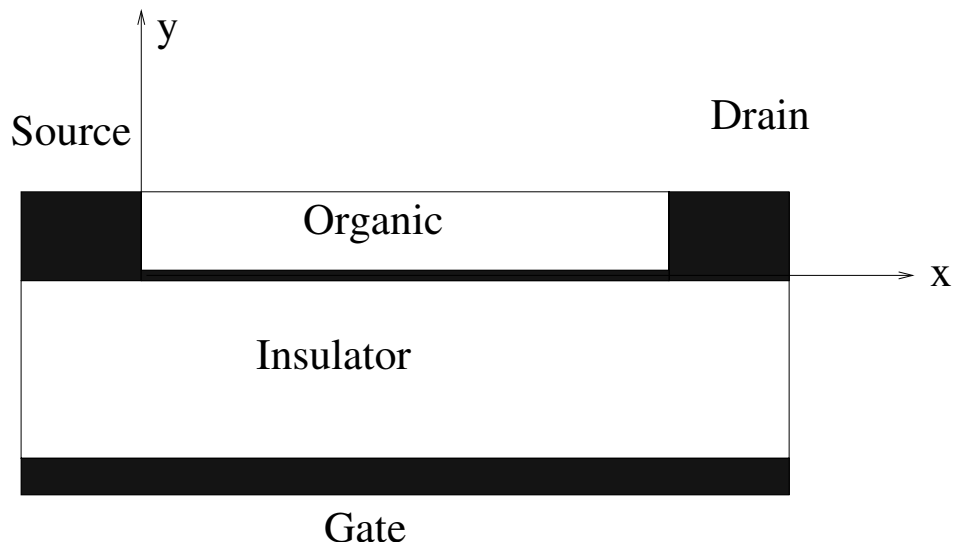


Figure 7.1: Schematic structure of an organic thin film transistor.

the insulator. As the carriers in the accumulation layer fill the low-energy states of the organic semiconductor, any additional carrier in the accumulation layer will require less activation energy to hop to a neighboring site. This results in a higher mobility with increasing gate voltage. In combination with percolation theory, Vissenberg studied the influence of temperature and the influence of the filled states on the conductivity based on the variable range hopping theory. The expression for the conductivity as a function of the temperature and carrier concentration is given by [43] where σ_0 is a prefactor, α is an effective overlap parameter, which governs the tunneling process between two localized states, and $B_c \cong 2.8$ is the critical number of bonds per site in the percolating network [131], T_0 is the effective temperature, N_t is the number of states per unit volume and δ is the fraction of the localized states occupied by a carrier. The carrier concentration δN_t can be expressed in equilibrium as

$$\rho(V) = N_t \delta(V) = N_t \delta_0 \exp\left(\frac{q\Phi}{k_B T_0}\right), \quad (7.1)$$

where Φ is the electrostatic potential, and the δ_0 is the carrier occupation far from the organic-insulator interface.

7.2.2 Sheet Conductance of the OTFT

For an amorphous TFT the drain current I_D can be expressed as

$$I_D = \frac{W}{L} \int_{V_G - V_{FB} - V_D}^{V_G - V_{FB}} G_S(V) dV, \quad (7.2)$$

where W is the channel width, L is the channel length, V_{FB} is the flat-band voltage, and G_S is the sheet conductance of the channel at $V_D = 0V$. The potential V is defined as $V = V_G - V_{FB} - V_0(y)$, where $V_0(y)$ is the potential at the edge of the space-charge layer where there is no band bending. The basic definition of the channel configuration and the variables for the OTFT investigated are illustrated in Fig 7.2.

$$\sigma(\delta, T) = \sigma_0 \left[\frac{\pi N_t \delta (T_0/T)^3}{(2\alpha)^3 B_c \Gamma(1 - T/T_0) \Gamma(1 + T/T_0)} \right]^{T_0/T}, \quad (7.3)$$

The electrostatic potential in the space charge layer at the point (x, y) in the channel is expressed as $V(x, y) = V_0(y) + \Phi(x, y)$, where the $\Phi(x, y)$ is the amount of the band bending in the channel. The conductance for an element of channel length Δy and the width W can be written as

$$G_s = \frac{W}{\Delta y} \int_0^t \sigma dx = \frac{W}{\Delta y} \frac{\sigma(\delta_0, T)}{\sigma_0} \int_0^t \exp\left(\frac{q\Phi}{k_B T}\right) dx \quad (7.4)$$

where t is the thickness of the organic layer. Changing the variable of integration yields

$$G_s = A \int_{\Phi(t(y))}^{\Phi_s(y)} \frac{\exp(q\Phi/k_B T)}{\partial\Phi/\partial x} d\Phi, \quad (7.5)$$

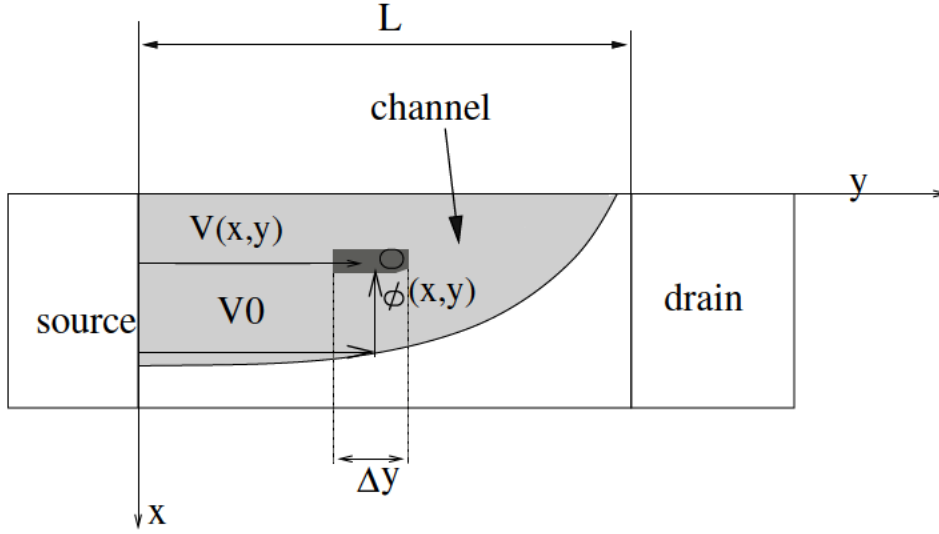


Figure 7.2: Geometric definition.

where $\Phi_s(y)$ is the surface band bending and $A = \sigma(\delta_0, T)$. With the identity

$$\Gamma(1+x)\Gamma(1-x) = \frac{\pi x}{\sin(\pi x)}$$

we obtain

$$A = \sigma_0 \left[\frac{N_t \delta_0 (T_0/T)^4 \sin(\pi T/T_0)}{B_c (2\alpha)^3} \right]^{T_0/T}$$

In order to solve (7.5) we need to get an expression for $\Phi(x)$. By solving Poisson's equation in the gradual channel approximation

$$\frac{\partial^2 \Phi(x)}{\partial x^2} = -\frac{\rho(x)}{\epsilon_0 \epsilon_s}, \quad (7.6)$$

we obtain the electric field.

$$-F_x = \frac{\partial \Phi}{\partial x} \approx \sqrt{\frac{2k_B T_0 N_t \delta_0}{\epsilon_0 \epsilon_s}} \cdot \exp \left[\frac{q\Phi(x)}{2k_B T_0} \right] \quad (7.7)$$

From (7.5) and (7.7) we obtain

$$G_s = A \int_{\Phi(t)}^{\Phi_s} \exp \left[\frac{q\Phi}{k_B} \left(\frac{1}{T} - \frac{1}{2T_0} \right) \right] d\Phi. \quad (7.8)$$

An expression for Φ_s is required. The surface charge density Q_s is related to Φ_s by

$$Q_s = -\epsilon_0 \epsilon_s F_s = \sqrt{2k_B T_0 N_t \epsilon_0 \epsilon_s \delta_0} \exp \left(\frac{q\Phi_s}{2k_B T_0} \right). \quad (7.9)$$

The surface band bending is related to the applied gate voltage by

$$V_G = V_{FB} + V_i + \Phi_s \quad (7.10)$$

where V_i is the voltage drop across the insulator,

$$V_i = \frac{Q_s}{C_i} \quad (7.11)$$

where $C_i = \epsilon_i/d_i$ is the insulator capacitance per unit area. From the equations above, an expression for Φ_s is obtained

$$V_G - V_{FB} - \Phi_s = \gamma \exp\left(\frac{q\Phi_s}{2k_B T_0}\right) \quad (7.12)$$

For an accumulation mode OTFT, the surface potential is negative, $\Phi_s \leq 0$, corresponding to $V_G \leq 0$.

$$V_G = V_{FB} + \Phi_s - \frac{\sqrt{2k_B T_0 \delta_0 N_t \epsilon_0 \epsilon_s}}{C_i} \exp\left(-\frac{q\Phi_s}{2k_B T_0}\right). \quad (7.13)$$

In order to reduce computation time, an explicit yet accurate relation between surface potential and gate voltage is preferable. In (7.13) we can get Φ_s using a numerical approach. However, in the accumulation mode, it holds $\exp(-\Phi_s) \gg \Phi_s$, so that an approximate expression of surface potential can be obtained as

$$\Phi_s = -\frac{2k_B T_0}{q} \ln \left[\frac{(V_{FB} - V_G) C_i}{\sqrt{2k_B T_0 \delta_0 N_t \epsilon_0 \epsilon_s}} \right]. \quad (7.14)$$

A comparison between numerical calculation and approximate calculation is shown in Fig 7.3 and Fig 7.4. As can be seen, the agreement is very satisfactory. Parameters are from [132, 133].

With the simplified surface potential and (7.8) we can get the simplified sheet conductance as

$$G_s = \beta \left[\left(\frac{V_G - V_{FB}}{\varrho} \right)^{2T_0/T-1} - 1 \right] \quad (7.15)$$

For a thick organic semiconductor layer, $\Phi(t) = 0$ and the coefficient β is

$$\beta = \sigma_0 \sqrt{\frac{2\epsilon_0 \epsilon_s K_B T_0}{\delta_0 N_t}} \frac{k_B T}{q(T - 2T_0)}$$

$$\varrho = \frac{(2\alpha)^3 B_c 2k_B T_0 \epsilon_0 \epsilon_s}{C_i^2 (T_0/T)^3 \sin(\pi T/T_0)}$$

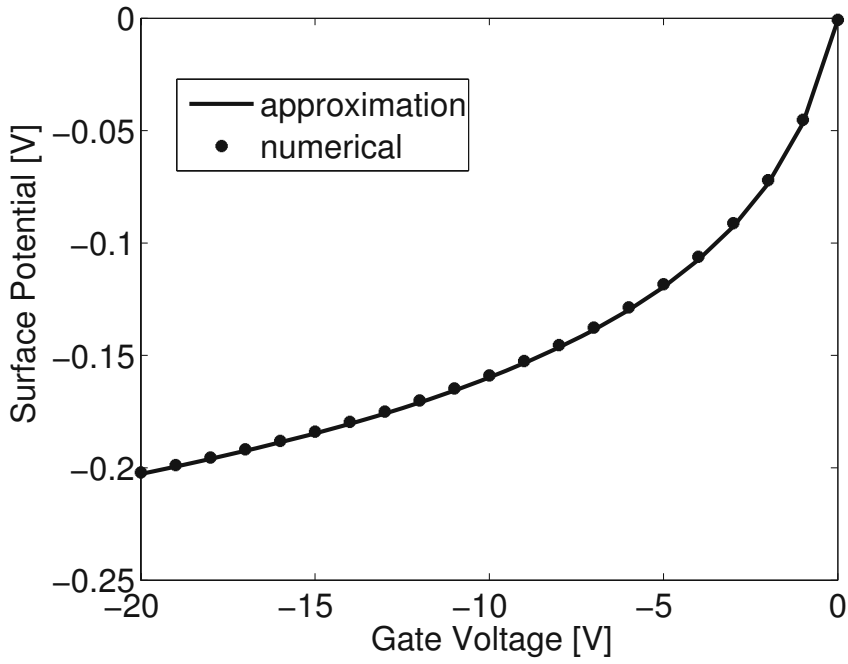


Figure 7.3: The electrostatic surface potential as a function of gate voltage obtained by the implicit relation (7.13) and the approximation (7.14) (solid line).

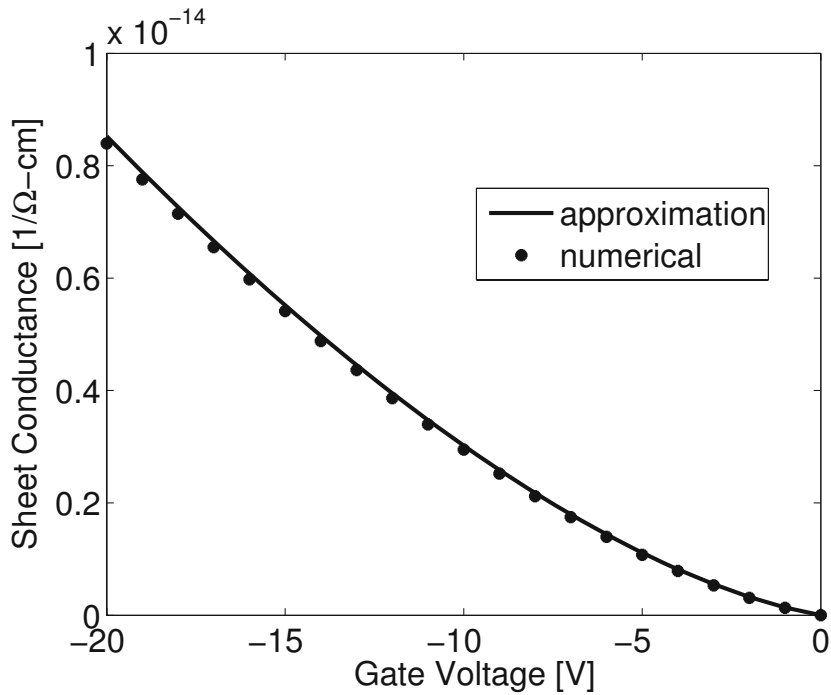


Figure 7.4: Sheet conductance from numerical calculation (symbols) and the approximation.

7.2.3 Drain Current

The drain current can be calculated by substituting the expression for G_s into (7.2). We obtain

$$I_D = \beta \frac{W}{L} \left[\left(\frac{V_G - V_{FB}}{\varrho} \right)^{2T_0/T} - \left(\frac{V_G - V_{FB} - V_D}{\varrho} \right)^{2T_0/T} \right] \quad (7.16)$$

in the triode region ($V_{GS} - V_{FB} \geq V_{DS}$) and

$$I_D = \beta \frac{W}{L} \left(\frac{V_{GS} - V_{FB}}{\varrho} \right)^{2T_0/T} \quad (7.17)$$

in saturation ($V_{GS} - V_{FB} \leq V_{DS}$).

7.2.4 Results and Discussion

This model has been confirmed by comparisons between experimental data and simulation results. Input parameters are taken from [132]: $W = 20,000\mu m$, $L = 10\mu m$, $\epsilon_s = 3$, $C_i = 17F/(\mu m)^2$, $\sigma_0 = 3.5S/m$, $\alpha^{-1} = 3.1\text{\AA}$, $T_0 = 385K$.

In Fig 7.5 and Fig 7.6 the transfer characteristics of a pentacene OTFT are given for $V_{FB} = 1V$ at different drain voltage and different temperature. Both figures show a good agreement between the analytical model and experimental data. Here we also model the transfer characteristics of a PTV OTFT, where some parameters are different from those for pentacence: $T_0 = 382K$, $\sigma_0 = 5.6S/m$, $\alpha^{-1} = 1.5\text{\AA}$, as shown in Fig 7.7. The modeled output characteristics of the pentacene OTFT is shown in Fig 7.8.

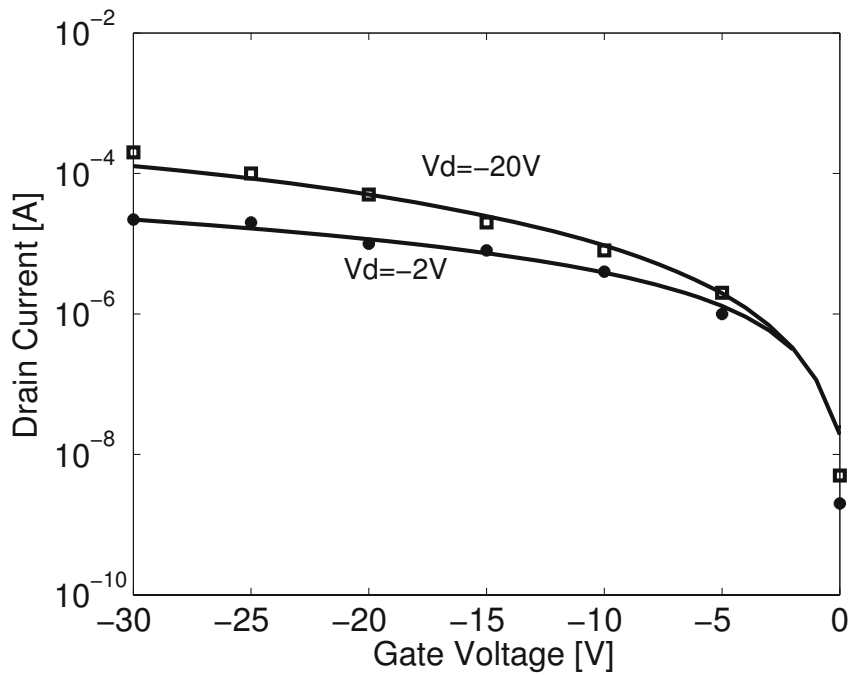


Figure 7.5: Measured (symbols) and calculated transfer characteristics of a pentacene OTFT at room temperature.

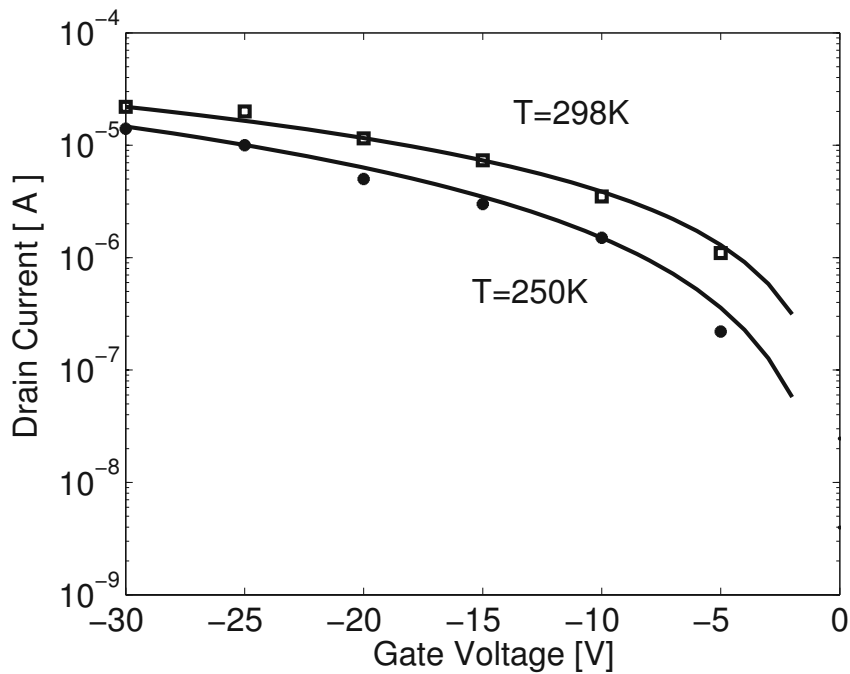


Figure 7.6: Measured (symbols) and calculated transfer characteristics of a pentacene OTFT at different temperatures at $V_D = -2V$.

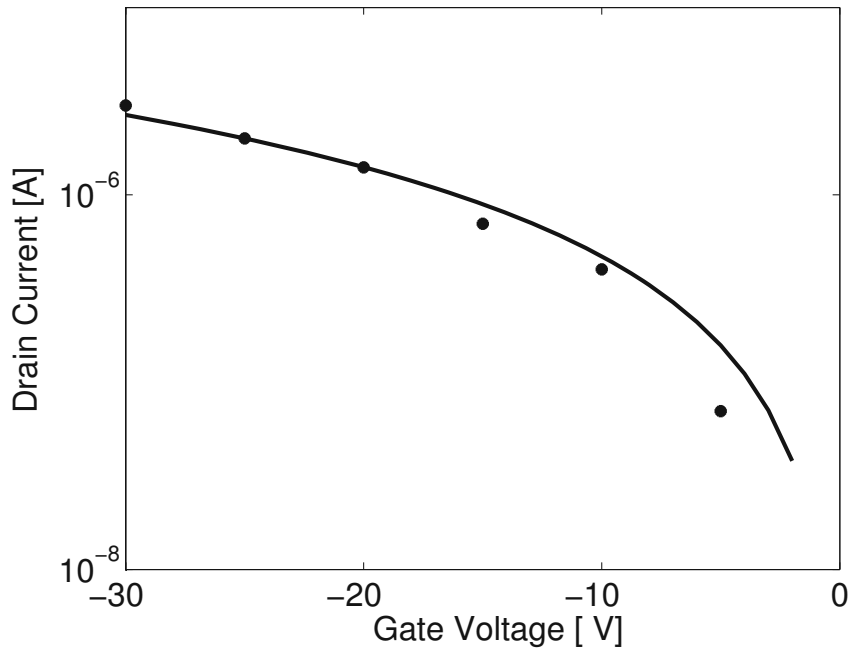


Figure 7.7: Measured (symbols) and calculated transfer characteristics of a PTV OTFT at room temperature at $V_D = -2V$.

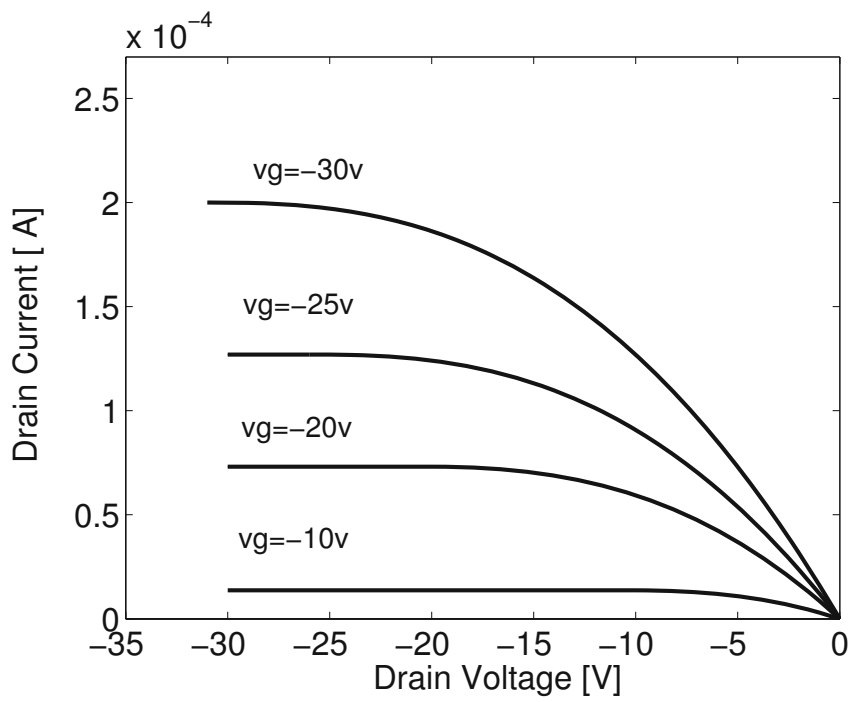


Figure 7.8: Modeled output characteristics of a pentacene OTFT.

7.3 Device Model for Unipolar OLEDs

In this section we present a unified device model for unipolar OLEDs which includes charge injection, transport, and space charge effects in the organic material.

7.3.1 Theory

In order to analyze the interplay between charge injection and bulk conductivity one must use specific models for both injection and charge transport in bulk. Here we treat the charge injection as diffusion controlled and the transport within multiple trapping theory as presented in Chapter 5. By multiplying $\exp\left(-\frac{e\varphi(x)}{k_B T}\right)$ in both sides of (5.2) and integrating x from 0 to x_d , we obtain

$$\frac{-J}{qD_n} \int_0^{x_d} \exp\left(-\frac{q\varphi(x)}{k_B T}\right) dx = f(x_d) - f(0), \quad (7.18)$$

where D_n is the diffusion coefficient and

$$f(x) = n_e(x) \exp\left(-\frac{q\varphi(x)}{k_B T}\right).$$

In the transport regime of the device, the potential expression (5.1) does not hold true anymore, instead, the potential must be calculated from the Poisson equation

$$\frac{d^2 q\varphi}{dx^2} = -\frac{dF}{dx} = -\frac{q}{\epsilon_0 \epsilon} p(x). \quad (7.19)$$

In the bulk regime, (5.2) is rewritten as

$$p_e(x) = \left[p_e(x_d) - \frac{J}{qD_n} \int_0^\infty dx \exp\left(\frac{q\varphi(x)}{k_B T}\right) \right] \times \exp\left(-\frac{p\varphi(x)}{k_B T}\right). \quad (7.20)$$

In order to calculate the J/V characteristics of OLEDs, one must solve (7.19) together with (5.4) and (7.20) self-consistently. The injection boundary conditions are $\varphi(0) = \varphi(x_d)$, $J = J_{inj}(F_0)$ and $F(0) = F_0$.

7.3.2 Results and Discussion

With the device model presented above we calculate the device characteristics of one carrier type at different barrier height Δ , as shown in Fig 7.9. The input parameters are $T = 300K$, $\sigma_0 = 0.08\text{eV}$, $N_t = 1 \times 10^{16}\text{cm}^{-3}$, $\nu_0 = 10^{11}\text{s}^{-1}$, $\tau_0 = 10^{-11}\text{s}$, $\mu = 1 \times 10^{-4}\text{cm}^2/\text{Vs}$ and the device length is 100nm . The comparison between our work and

experimental data of hole only ITO/NPB/Al [135] is plotted in Fig 7.10 with $\Delta = 0.1\text{eV}$, $\mu = 2.9 \times 10^{-1}\text{cm}^2/\text{Vs}$ and device length 65nm . The other parameters are the same as in Fig 7.9. The current is neither the pure injected limited current nor SCLC [135].

A single carrier OLED model including charge injection and transport is presented here. This model is based on a Gaussian DOS and multiple trapping theory. It can explain barrier height dependence of current/voltage characteristics and agrees with experimental data [135].

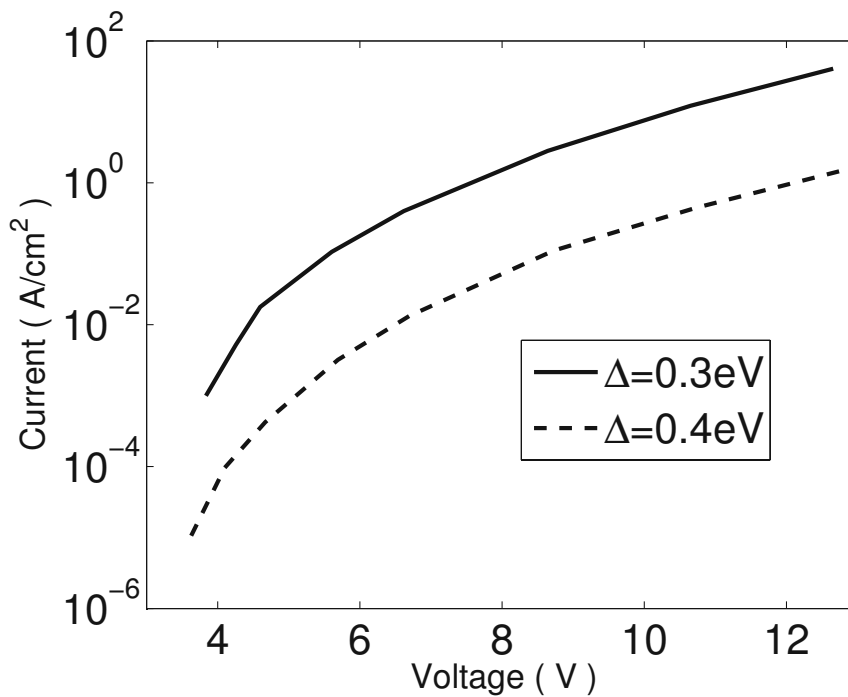


Figure 7.9: Barrier height dependence of current/voltage characteristics for unipolar OLED.

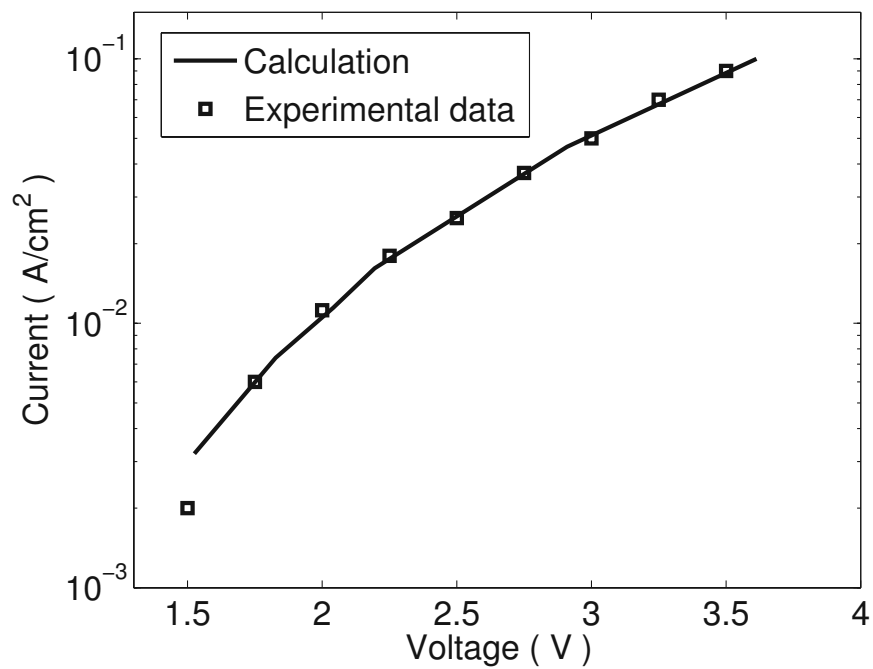


Figure 7.10: Comparison between the model and experimental data for unipolar OLED.

Chapter 8

Conclusion

In this thesis, we investigated a series of open problems related to charge injection and transport in organic semiconductor devices such as OLEDs and OTFTs. This is a relatively new area and even more work is needed to improve our understanding of the nature of charge transport in these devices.

8.1 Current Progress

Our first contribution was the formulation of a charge transport mobility model, which is one of the most important parameters in organic semiconductors. Using three different analytical models, we separately explain the mobility's dependence on carrier concentration, electric field and temperature. We showed that the density of states function is an important factor for the carrier concentration dependence of the mobility and the exponential DOS function is not entirely reliable for the low carrier concentration regime. Furthermore, a physical model was developed to explain the Poole-Frenkel behavior of the electric field dependent mobility.

In order to deal with the effect of Fermi-Dirac statistics on the transport energy, we extended Baranovskii's transport energy model. This model shows that the Fermi-Dirac statistics plays an important role in transport energy when the temperature is low and carrier concentration is higher.

Then, we developed analytical models to describe the doping and trap characteristics of organic semiconductors. This model can successfully explain the superlinear increase of conductivity upon trap concentration and the relation between trap concentration and conductivity.

Despite of the successful application of the Fowler-Nordheim and Richardson-Schottky injection models to some experimental data of organic devices, it is very important to

discuss the role of diffusion transport and backflow current in the charge injection process for organic devices. For this goal, we have presented two different injection models for organic light-emitting diodes, one is based on multiple trapping theory and the other on a master equation.

In the next step we investigated the SCLC in organic devices within the frame work of variable range hopping transport. It was shown that the SCLC controlled by a Gaussian density of states distribution obeyed the $j \propto V^2$ relation remarkably similar to SCLC controlled by shallow traps in the low current density regime when the mobility was constant, while field-dependent mobility would change this relation slightly in the high current regime.

Up to now, many of the numerical or analytical organic device models available in commercial device simulators use the same expressions as used for the crystalline devices. However, organic devices present several differences with respect to crystalline devices. In the final part of this thesis, we presented two analytical models that describe the DC characteristics of organic thin film transistors and organic light-emitting diodes. Both models are based on hopping transport theory and good agreement between calculation and experimental data was found.

8.2 Future Work

Using the advances as the foundation for further study, we finally consider some possibilities for future work. Of course, there is initial work on device models [136, 137, 138], which, however, did not take into account the disorder in organic semiconductors or the hopping transport effect on device characteristics. So the first extension would implement the mobility models and injection models into device simulators.

Another extension would be to consider the role of the limiting effect of the space charge on the injection current. This can be incorporated into our injection model, either diffusion model or master equation model through solving the Poisson equation.

Further, it may be important to consider the effect of Coulomb forces on the doping and trapping model. It has been pointed out that doping in organic semiconductors produces a random distribution of dopant ions [139], which electrostatically interact with carriers localized in intrinsic hopping sites. This interaction further increases the energy disorder and broadens the deep tail of the DOS distribution.

Finally, an improvement of Arkhipov's transport [140] energy model may be developed. This model should consider the effect of both downward and upward hops on transport. It can be used to explain the electric field dependence of the mobility in organic semiconductors.

The framework provided by this thesis can be a starting point for these, and possibly other, further investigations. By continuing to successively remove some of the more restrictive assumptions of our work, significant progress may continue towards a better understanding of these organic semiconductors materials and devices.

List of Figures

1.1	Two examples of use of OLEDs in commercial products. The image on the left shows a new Philips shave introduced to the market in 2002. The image on the right shows the OLED TV produced by Sony recently. Images were taken from [6].	2
1.2	Charge transport mechanism in solids. The left image describes the band transport. In a perfect crystal, depicted as a straight line, free carriers are delocalized. There are always lattice vibrations that disrupt the crystal symmetry. Carriers are scattered at these phonons, which limit the carriers mobility. The image on the right describes hopping transport. If a carrier is localized due to defects, disorder or selflocalization, the lattice vibrations are essential for a carrier to move from one site to another. The figure is from [8].	3
1.3	Left: device layout of a typical organic light-emitting diode (OLED). It consists of a glass substrate with an indium-tin-oxide (ITO) coating functioning as anode, a spin-coated layer of an organic semiconductor as the active layer, and an evaporated metal cathode. Right: working principle of an OLED. Four important processes are shown: (1) Charge injection (2) Transport (3) Exciton formation (4) Photon emission. The last two steps form the recombination process.	11
1.4	Left: A schematic view of a bottom contact OFET. The source electrode is grounded, while the drain and the gate are biased negatively. In this mode, holes are injected from the source and collected at the drain. Right: a top contact OFET with the electrodes patterned on top of the organic semiconductor.	12
2.1	Comparison between the analytical model (2.9) and empirical model $\mu \approx \exp\left(- (C\sigma/k_B T)^2\right)$ for different temperature.	18
2.2	The mobility as a function of $(T_\sigma/T)^{1/3}$ for different α	19

2.3	Fermi-energy as a function of the carrier occupation probability. The symbols represent Fermi-Dirac and the solid lines Boltzmann represent statistics. Panel (a) shows the case of carrier occupation between 10^{-40} and 1. Panel (b) shows the case of carrier occupation bigger than 10^{-10} .	20
2.4	The calculated mobility versus carrier occupation at different temperature.	21
2.5	Comparison between calculation and typical experimental results [41].	21
2.6	Plot of $\log \sigma$ versus $T^{-1/4}$ at the electric field $100V/cm$.	24
2.7	Conductivity and mobility versus temperature for ZnPc as obtained from the model (2.14) and (2.15) in comparison with experimental data (symbols).	24
2.8	Logarithm of the mobility versus T^{-1} . The electric field is $10^5V/cm$, $\sigma_0 = 1.1 \times 10^9 S/cm$, $T_0 = 340K$, $\alpha^{-1} = 0.5 \text{ \AA}$	25
2.9	The same data as in Fig 2.8 plotted versus T^{-2} .	25
2.10	Plot of $\log \sigma$ versus $F^{1/2}$ at $T = 204 K$.	26
2.11	Electric field dependence of the mobility at 290K. Symbols represent Monte Carlo results [49], the line represents our work with parameter $T_0=852K$.	27
2.12	Field dependence of the conductivity at different temperatures.	28
2.13	Temperature dependence of the conductivity at different electric fields.	29
2.14	The calculated mobility (symbols) as a function of σ/kT .	32
2.15	The calculated mobility (symbols) as a function of $(\sigma/kT)^2$.	32
2.16	The conductivity as a function of the scaled electric field, $\beta = F/F_0$.	33
2.17	Comparison between our mobility model and analytical expression (2.30) with $p = 1/3$ and $C = 0.7$.	34
2.18	Temperature dependences of parameters C and p extracted from the analytical model.	35
2.19	Electric field dependence of parameter C extracted from the analytical model.	36
2.20	Electric field dependence of parameter p extracted from the analytical model.	36
2.21	Effect of α on the values of parameters p and C extracted from the analytical model.	37

3.1	Comparison between the model (3.8) and Baranovskii's model for the temperature characteristics of E_{tr}	40
3.2	The transport energy versus the chemical potential for different standard deviations a of the DOS.	41
3.3	The transport energy versus the relative carrier concentration for different standard deviations a of the DOS.	42
3.4	Dependence of the relaxation time on the chemical potential for different standard deviations a of the DOS	43
3.5	Temperature dependence of the carrier mobility in organic semiconductors. In (a) the data are plotted versus T^{-1} , in (b) the same data are plotted versus T^{-2}	44
3.6	Carrier concentration dependence of the mobility in organic semiconductors.	45
4.1	Temperature dependence of the conductivity in a disordered hopping system at different doping concentrations.	50
4.2	Temperature dependence of the conductivity in an organic semiconductor plotted as $\log \sigma$ versus T^{-2} . The dashed line is to guide the eye.	50
4.3	Conductivity of doped ZnPc at various doping ratios as a function of temperature. The lines represent the analytical model, experiments (symbols) are from [63].	51
4.4	Conductivity as a function of the dopant concentration with temperature as a parameter.	51
4.5	Conductivity of PPEEB films versus the dopant concentration. The line represents the analytical model. Experiments (symbols) are from [139]. . .	52
4.6	Conductivity as a function of the doping ratio with temperature as a parameter.	53
4.7	Conductivity at $T=200\text{K}$ as a function of the doping ratio. The dashed line is to guide the eye.	54
4.8	Activation energy (E_A) as a function of the doping ratio.	54
4.9	Conductivity of an organic semiconductor versus T^{-1} for different trap concentrations.	55
4.10	Conductivity of an organic semiconductor versus T^{-2} for different trap concentrations.	56

4.11	Temperature dependence of the zero-field mobility for TTA doped with DAT. Symbols represent experimental data from [99].	57
4.12	Conductivity of an organic semiconductor versus the width of the trap distribution, T_1	58
4.13	The dependence of the conductivity on the trap concentration.	58
4.14	The dependence of the conductivity on the Coulombic trap energy.	59
5.1	Dependence of the injection current on the barrier height.	64
5.2	Temperature dependencies of the injection current.	64
5.3	Comparison between the model and experimental data.	65
5.4	Comparison between injection currents for field dependent mobility and constant mobility.	66
5.5	Field dependence of the net, injection, and backflow currents.	69
5.6	Relation between injection current and $F^{1/2}$	69
5.7	Barrier height dependence of the injection current.	70
5.8	Comparison between calculation and experimental data at $T = 123K$. . .	70
6.1	Gaussian density of states with zero mean energy. The vertical axis corresponds to energy, the horizontal axis reflects the site density. The center of the Gaussian DOS is at zero energy.	72
6.2	Spatial distribution of the quasi Fermi energy for different current densities.	74
6.3	Spatial distribution of the carrier concentration near the contact for $j = 0.4A/cm^2$	75
6.4	Spatial distribution of the electric field at different current densities.	76
6.5	Current-voltage characteristics of a sample with Gaussian DOS distribution parametric in temperature.	77
6.6	The effect of the field dependent mobility on the space charge limited current.	77
6.7	The relation between organic layer thickness and space charge limited current.	78
7.1	Schematic structure of an organic thin film transistor.	80
7.2	Geometric definition.	82

7.3	The electrostatic surface potential as a function of gate voltage obtained by the implicit relation (7.13) and the approximation (7.14) (solid line). . .	84
7.4	Sheet conductance from numerical calculation (symbols) and the approximation.	84
7.5	Measured (symbols) and calculated transfer characteristics of a pentacene OTFT at room temperature.	86
7.6	Measured (symbols) and calculated transfer characteristics of a pentacene OTFT at different temperatures at $V_D = -2V$	86
7.7	Measured (symbols) and calculated transfer characteristics of a PTV OTFT at room temperature at $V_D = -2V$	87
7.8	Modeled output characteristics of a pentacene OTFT.	87
7.9	Barrier height dependence of current/voltage characteristics for unipolar OLED.	89
7.10	Comparison between the model and experimental data for unipolar OLED.	90

Bibliography

- [1] C. K. Chiang, C. R. Fincher, J. Y. W. Parker, A. J. Heeger, H. Shirakawa, E. J. Louis, S. C. GAU, and A. G. MacDiarmid, "Electrical Conductivity in Doped Polyacetylene," *Phys. Rev. Lett.*, vol. 39, no. 17, pp. 1098–1101, 1977.
- [2] J. M. Shaw and P. F. Seidler, "Organic electronics: Introduction," *IBM J. Res. Dev.*, vol. 45, no. 1, pp. 3–10, 2001.
- [3] J. C. Scott and G. G. Malliaras, *In conjugated polymers*. Germany: Wiley-VCH, 1999.
- [4] J. M. Nunzi, "Organic photovoltaic materials and devices," *C. R. Phys.*, vol. 3, no. 4, pp. 523–542, 2002.
- [5] B. A. Gregg, "Excitonic Solar Cells," *J. Phys. Chem. B.*, vol. 107, no. 20, pp. 4688–4698, 2002.
- [6] C. Deboer, "Organic LED Display," *www.audioholics.com*.
- [7] A. Miller and E. Abrahams, "Impurity Conduction at Low Concentrations," *Phys. Rev.*, vol. 120, no. 3, pp. 745–755, 1960.
- [8] M. Pope, *Electronic processes in organic crystals and polymers*. UK: Oxford University Press, 1999.
- [9] H. Bassler, "Charge transport in disordered organic photoconductors," *Phys. Stat. Sol.(b)*, vol. 175, pp. 15–55, 1993.
- [10] S. D. Baranovskii, P. Thoms, and G. J. Adriaenssens, "The Concept of Transport Energy and its Application to Steady-State Photoconductivity in Amorphous Silicon," *J. Non-Cryst. Solids*, vol. 190, no. 3, pp. 283–287, 1995.
- [11] G. Horowitz, R. Hajlaoui, and P. Delannoy, "Temperature Dependence of the Field-Effect Mobility of Sexithiophene. Determination of the Density of Traps," *J. Phys. III*, vol. 5, pp. 355–371, 1995.

- [12] J. Noolandi, "Multiple-trapping model of anomalous transit-time dispersion in a-Si," *Phys. Rev. B*, vol. 16, no. 10, pp. 4466–4473, 1977.
- [13] M. Sahimi, *Application of percolation theory*. UK: Taylor Francis, 1994.
- [14] Y. N. Garstein, E. M. Conwell, "High-field hopping mobility in disordered molecular solids: A Monte Carlo study of off-diagonal disorder effects," *J. Chem. Phys.*, vol. 100, pp. 9175–9180, 1994.
- [15] B. Hartenstein, H. Bassler, "Charge transport in molecularly doped polymers at low dopant concentrations: simulation and experiment," *Chem. Phys.*, vol. 191, pp. 321–332, 1995.
- [16] N. F. Mott and E. A. Davis, *Electronics processes in noncrystalline materials*. UK: Clarendon, 1971.
- [17] V. Ambegaokar, B. I. Halperin, and J. S. Langer, "Hopping Conductivity in Disordered Systems," *Phys. Rev. B*, vol. 4, no. 8, pp. 2612–2620, 1971.
- [18] V. I. Arkipov, P. Heremans, E. V. Emelianova, G. J. Adriaenssens, and H. Bassler, "Weak-field carrier hopping in disordered organic semiconductors: the effects of deep traps and partly filled density-of-states distribution," *J. Phys: Condens Matter*, vol. 14, no. 42, pp. 9899–9913, 2002.
- [19] N. Apsley and H. P. Hughes, "Temperature- and field-dependence of hopping conduction in disordered systems. II," *J. Phys: Condens Matter*, vol. 31, no. 6, pp. 1327–1339, 1975.
- [20] H. Scher and E. W. Montroll, "Anomalous transit-time dispersion in amorphous solids " *Phys. Rev. B*, vol. 12, no. 6, pp. 2455–2477, 1975.
- [21] E. B. McLean, J. G. A. Ausman, J. H. E. Boesch, and J. M. McGarrity, "Application of stochastic hopping transport to hole conduction in amorphous SiO₂ " *J. Appl. Phys.*, vol. 47, no. 4, pp. 1529–1532, 1976.
- [22] R. C. Hughes, "Time-resolved hole transport in a-SiO₂" *Phys. Rev. B*, vol. 15, no. 4, pp. 2012–2020, 1977.
- [23] H. Scher and M. Lax, "Stochastic Transport in a Disordered Solid. I. Theory," *Phys. Rev. B*, vol. 7, no. 10, pp. 4491–4502, 1973.
- [24] J. H. E. Boesch, F. B. McLean, J. M. McGarrity, and J. G. A. Ausman, "Hole transport and charge relaxation in irradiated SiO₂ MOS capacitors," *IEEE. Nucl. Sci.*, NS. 22, pp. 2163–2167, 1975.

- [25] J. H. Burroughes, A. B. D. Bradley, R. Friend, P. Burn, and A. Holmers, "Light-emitting diode based on conjugated polymers," *Nature*, vol. 347, no. 19, pp. 539–543, 1990.
- [26] A. Dodabalapur, "Organic light emitting diodes," *Solid State Commun.*, vol. 102, no. 2, pp. 259–267, 1997.
- [27] X. Zhang and S. A. Jenekhe, "Electroluminescence of multicomponent conjugated polymers. 1. Roles of polymer/polymer interfaces in emission enhancement and voltage-tunable multicolor emission in semiconductor polymer/polymer heterojunctions," *Macromolecules*, vol. 33, p. 2069–2082, 2000.
- [28] F. Garnier, "Thin-film transistors based on organic conjugated semiconductors," *Chem. Phys.*, vol. 227, pp. 253–262, 2000.
- [29] H. E. Katz and Z. Bao, "The Physical Chemistry of Organic Field-Effect Transistors," *Phys. Chem. B*, vol. 104, no. 4, pp. 671–678, 2000.
- [30] G. Horowitz, "Organic thin film transistors: from theory to real devices," *J. Mater. Res.*, vol. 19, p. 1946–1962, 2004.
- [31] N. S. Sariftci and A. J. Heeger, *Organic conductive molecules and polymers*. USA: Wiley, 1997.
- [32] G. Wang, J. Swensen, D. Moses, and A. J. Heeger, "Increased mobility from regioregular poly(3-hexylthiophene) field-effect transistors," *J. Appl. Phys.*, vol. 93, no. 10, pp. 6137–6141, 2003.
- [33] H. Sirringhaus, P. J. Brown, R. H. Friend, M. M. Nielsen, K. Bechgaard, B. M. W. Landveld-Voss, A. J. H. Spiering, R. A. J. Janssen, E. W. Meijer, P. Herwig, and D. M. de Leeuw, "Two-dimensional charge transport in self-organized, high-mobility conjugated polymers," *Nature*, vol. 401, pp. 685–689, 1999.
- [34] R. A. Street, A. Salleo, and M. L. Chabinyc, "Bipolaron mechanism for bias-stress effects in polymer transistors," *Phys. Rev. B*, vol. 68, no. 8, pp. 085316–083323, 2003.
- [35] J. Veres, S. D. Ogier, S. W. Leeming, D. C. Cupertino, and S.M. Khaffaf, "Low-k Insulators as the Choice of Dielectrics in Organic Field-Effect Transistors," *Adv. Funct. Mat.*, vol. 13, no. 3, pp. 199–204, 2003.
- [36] T. Yasuda, K. Fujita, H. Nakashima, and T. Tsutsui, "Organic Field-Effect Transistors with Gate Dielectric Films of Poly-p-Xylylene Derivatives Prepared by Chemical Vapor Deposition," *Jap. J. Appl. Phys.*, vol. 42, no. 1, pp. 6614–6618, 2003.

- [37] A. Salleo, M. L. Chabinyo, M. S. Yang, and R. A. Street, “Polymer thin-film transistors with chemically modified dielectric interfaces,” *Appl. Phys. Lett.*, vol. 81, no. 2, pp. 4383–4385, 2002.
- [38] H. Sirringhaus, N. Tessler, and R. H. Friend, “Integrated Optoelectronic Devices Based on Conjugated Polymers,” *Science*, vol. 280, no. 5730, pp. 1741–1744, 1998.
- [39] R. J. Kline, M. D. McGehee, E. N. Kadnikova, J. Liu, and J. J. Frechet, “Controlling the Field-Effect Mobility of Regioregular Polythiophene by Changing the Molecular Weight,” *Adv. Mat.*, vol. 15, no. 18, pp. 1519–1522, 2003.
- [40] H. Sirringhaus, R. J. Wilson, and R. H. Friend, “Mobility enhancement in conjugated polymer field-effect transistors through chain alignment in a liquid-crystalline phase,” *Appl. Phys. Lett.*, vol. 77, no. 3, pp. 406–408, 2000.
- [41] C. Tanase, E. J. Meijer, P. W. M. Blom, and D. M. de Leeuw, “Unification of the Hole Transport in Polymeric Field-Effect Transistors and Light-Emitting Diodes,” *Phys. Rev. Lett.*, vol. 91, no. 21, pp. 216601–216604, 2003.
- [42] S. D. Baranovskii, O. Rubel, and P. Thomas, “Theoretical description of hopping transport in disordered materials,” *Thin Solid Films*, vol. 487, no. 1, pp. 2–7, 2005.
- [43] M. C. J. M. Vissenberg and M. Matters, “Theory of the field-effect mobility in amorphous organic transistors,” *Phys.Rev.B*, vol. 57, no. 20, pp. 12964–12967, 1998.
- [44] N. F. Mott, “On the transport to metallic conduction in semiconductors,” *Can. J. Phys.*, vol. 34, no. 12, pp. 1356–1368, 1956.
- [45] I. P. Zvyagin and A. V. Plyukhin, “Low temperature relaxation in disordered organic semiconductors,” *Mos.Univ.Phys.Bull.*, vol. 45, pp. 84–88, 1990.
- [46] P. N. Butcher, *Linear and Nonlinear Electron Transport in Solids*. USA: Plenum press, 1976.
- [47] R. M. Corless, G. H. Gonner, and D. E. G. Hare, “On the Lambert W function,” *Adv.Comput.Math.*, vol. 5, no. 1, pp. 329–359, 1996.
- [48] P. M. Borsenberger, E. H. Magin, M. V. der Auweraer, and F. C. de Schryver, “The role of disorder on charge transport in molecularly doped polymers and related materials,” *Phys. Status Solidi B*, vol. 175, p. 9–47, 1993.
- [49] A. B. Walker, A. Kambili, and S. J. Martin, “Modelling temperature-dependent current voltage characteristics of an MEH-PPV organic light emitting device,” *J. Phys: Condens. Matter*, vol. 14–9876, pp. 9825–9876, 2002.

- [50] C. Godet, “Analytic derivation of the effective temperature for field-dependent hopping conductivity,” *Phil.Mag.Lett.*, vol. 83, pp. 691–698, 2003.
- [51] G. Schonherr, H. Bassler, and M. Silver, “Dispersive hopping transport via sites having a Gaussian distribution of energies,” *Phil.Mag.B*, vol. 44, no. 1, p. 47–61, 1981.
- [52] H. Bassler, *Hopping and related phenomena: Advances in disordered semiconductors*. Singapore: World Scientific, 1990.
- [53] B. Movaghar, M. Grunewald, H. Bassler, and D. Wurtz, “Diffusion and relaxation of energy in disordered organic and inorganic materials,” *Phys.Rev.B*, vol. 33, no. 8, pp. 5545–5554, 1986.
- [54] S. Boutiche, “Variable Range Hopping Conductivity: Case of the non-constant density of states,” <http://hal.ccsd.cnrs.fr/docs/00/03/00/41/PDF/>, pp. 1–10, 2001.
- [55] K. Horiuchi, S. Uchinobu, S. Hashii, A. Hashimoto, T. Kato, T. Sasaki, N. Aoki, and Y. Ochiai, “Variable range hopping in a C60 field-effect transistor,” *Appl.Phys.Lett.*, vol. 85, no. 11, pp. 1987–1989, 2004.
- [56] G. Paasch, P. H. Nguyen, and S. L. Drechsler, “Equilibrium theory of space charge layers in conjugated polymers I. Non-degenerate limit,” *Syn.Metals*, vol. 97, no. 3, pp. 255–265, 1998.
- [57] Y. Preezant, Y. Roichman, and N. Tessler, “Amorphous organic devices degenerate semiconductors,” *J.Phys.: Condens.Matter*, vol. 14, pp. 9913–9924, 2002.
- [58] C. Tanase, P. W. M. Blom, D. M. de Leeuw, and D. Leeuw, “Charge carrier density dependence of the hole mobility in poly(p-phenylene vinylene),” *Phys.stat.sol.(a)*, vol. 201, no. 6, pp. 1236–1245, 2004.
- [59] W. D. Gill, “Drift mobilities in amorphous charge-transfer complexes of trinitrofluorenone and poly-n-vinylcarbazole,” *J. Appl. Phys.*, vol. 43, no. 12, vol. 43, pp. 5033–5040, 1972.
- [60] M. Pollak and I. Riess, “Magnetic properties of the flux line lattice in paramagnetic superconductors,” *J. Phys. C*, vol. 9, pp. 2239–2352, 1976.
- [61] H. Bottger and V. V. Bryskin, *Hopping Conduction in Solids*. Germany: Akademie Verlag, 1985.
- [62] L. Li, G. Meller, and H. Kosina, “Temperature and electric field dependent mobility model in organic semiconductors,” *3rd European Conference on Organic Electronics and Related Phenomena, Book of Abstracts*, pp. 112–113, 2005.

- [63] B. Maennig, M. Pfeiffer, A. Nollau, X. Zhou, and K. Leo, "Controlled p-type doping of polycrystalline and amorphous organic layers: Self-consistent description of conductivity and field-effect mobility by a microscopic percolation model," *Phys. Rev. B*, vol. 64, no. 19, pp. 1952081–1952089, 2001.
- [64] J. van Hapert, *Hopping conduction and chemical structure: A study on silicon suboxides*. PhD thesis, University Utrecht, Netherlands, 2002.
- [65] E. H. Magin and P. M. Borsenberger, "Electron transport in N,N-bis(2-phenethyl)-perylene-3,4,9,10-bis(dicarboximide)," *J. Appl. Phys.*, vol. 73, no. 2, pp. 787–791, 1993.
- [66] B. Hartenstein, H. Bassler, P. G. Debrunner, and K. J. Schulten, "Charge transport in molecularly doped polymers at low dopant concentrations: Simulation and experiment," *Chem. Phys.*, vol. 191, pp. 321–332, 1995.
- [67] R. H. Young and N. G. Rule, "Electronic hopping velocities that decrease as the electric field strength increases," *Phys. Rev. Lett.*, vol. 72, no. 3, pp. 388–391, 1994.
- [68] V. I. Arkipov, J. Reynaer, P. Heremans, and H. Bassler, "The effect of deep traps on carrier hopping in disordered organic materials," *Synthetic Metals*, vol. 138, pp. 209–212, 2002.
- [69] O. Rubel, S. D. Baranovskii, and P. Thomas, "Concentration dependence of the hopping mobility in disordered organic solids," *Phys. Rev. B*, vol. 69, pp. 0142061–0142065, 2004.
- [70] P. M. Boesenberger and H. Bassler, "Dispersive and nondispersive charge transport in a molecularly doped polymer with superimposed energetic and positional disorder," *Phys. Rev. B*, vol. 47, pp. 4289–4295, 1993.
- [71] N. F. Mott, "Conduction in non-crystalline materials. III. Localized states in a pseudogap and near extremities of conduction and valence bands," *Phil. Mag.*, vol. 19, no. 160, pp. 835–852, 1969.
- [72] N. F. Mott and E. A. Davis, *Electronic Processes in Non-crystalline Solids*, UK: Oxford University Press, 1971.
- [73] D. Bourbie and N. Ikrelief, "High-field electrical conductivity in disordered systems," *Phil. Mag. Lett.*, vol. 82, no. 11, pp. 641–649, 2002.
- [74] C. J. A. Nemeth-Buchin, V. Arkipov, and H. Bassler, "Scaling properties of transport parameters in molecularly doped polymers," *Phil. Mag. Lett.*, vol. 74, no. 4, pp. 295–302, 1996.

- [75] M. Abkowitz, M. Stolka, and M. Morgan, “Behavior of the drift mobility in the glass transition region of some hole-transporting amorphous organic films,” *J. Appl. Phys.*, vol. 52, no. 5, pp. 3453–3457, 1981.
- [76] B. I. Shklovskii, *Electronic properties of doped semiconductors*. Heidelberg: Springer, 1984.
- [77] S. D. Baranovskii, T. Faber, and P. Thoms, “The applicability of the transport-energy concept to various disordered materials,” *J. Phys: Condensed Matter*, vol. 9, pp. 2699–2706, 1997.
- [78] S. D. Baranovskii, T. Faber, and P. Thoms, “Charge-carrier transport in disordered organic solids,” *Phys. Rev. B*, vol. 62, pp. 7934–7938, 2000.
- [79] C. Tanase, P. W. M. Blom, and D. Leeuw, “Local charge carrier mobility in disordered organic field-effect transistors,” *Organic Electronics*, vol. 4, pp. 33–37, 2003.
- [80] R. Coehoorn, W. F. Pasveer, P. A. Bobbert, and M. A. J. Michels, “Charge-carrier transport in disordered organic solids,” *Phys.Rev. B*, vol. 62, pp. 7934–7938, 2000.
- [81] C. P. Jarrett, R. H. Friend, A. R. Brown, and D. M. de Leeuw, “Field effect measurements in doped conjugated polymer films: Assessment of charge carrier mobilities,” *J. Appl. Phys.*, vol. 77, pp. 6289–6294, 1995.
- [82] G. Ganzorig and M. Fujihira, “Improved drive voltages of organic electroluminescent devices with an efficient p-type aromatic diamine hole-injection layer,” *Appl. Phys. Lett.*, vol. 77, pp. 4211–4213, 2000.
- [83] J. Blochwitz, M. Preiffer, T. Fritz, and K. Leo, “Low voltage organic light emitting diodes featuring doped phthalocyanine as hole transport material,” *Appl. Phys. Lett.*, vol. 73, pp. 729–731, 1998.
- [84] M. Preiffer, A. Beyer, A. Nollau, T. Fritz, K. Leo, D. Schlettwein, S. Hiller, D. Wörhle, “Controlled p-doping of pigment layers by cosublimation: Basic mechanisms and implications for their use in organic photovoltaic cells,” *Sol. Energy. Mat. Sol. Cell*, vol. 63, pp. 83–99, 2000.
- [85] B. A. Gregg, and R. A. Cormier, “Doping molecular semiconductors: n-Type doping of a liquid crystal perylene diimide,” *J. Am. Chem. Soc.*, vol. 123, pp. 7959–7960, 2001.
- [86] X. Zhou, M. Pfeifer, J. Blochwitz, A. Werner, A. Nollau, T. Fritz, and K. Leo, “Very-low-operating-voltage organic light-emitting diodes using a p-doped amorphous hole injection layer,” *Appl. Phys. Lett.*, vol. 78, pp. 410–412, 2001.

- [87] M. Preiffer, A. Beyer, T. Fritz, and K. Leo, "Controlled doping of phthalocyanine layers by cosublimation with acceptor molecules: A systematic Seebeck and conductivity study," *Appl. Phys. Lett.*, vol. 73, pp. 3202–3204, 1998 .
- [88] P. Leempoel, M. C. Acuna, F. F. Fan, and A. J. Bard, "Semiconductor electrodes. 43. The effect of light intensity and iodine doping on the stabilization of n-silicon by phthalocyanine films," *J. Phys. Chem.*, vol. 86, pp. 1396–1400, 1982.
- [89] D. R. Kearns, G. Tollin, and M. Calvin, "Electrical Properties of Organic Solids. II. Effects of Added Electron Acceptor on Metal-Free Phthalocyanine," *J. Chem. Phys.*, vol. 32, pp. 1020–1025, 1960.
- [90] A. Nollau, M. Pfreiffer, T. Fritz, and K. Leo, "Controlled n-type doping of a molecular organic semiconductor: Naphthalenetetracarboxylic dianhydride (NTCDA) doped with bis(ethylenedithio)-tetrathiafulvalene (BEDT-TTF)," *J. Appl. Phys.*, vol. 87, pp. 4340–4333 , 2000.
- [91] B. A. Gregg, S. G. Chen, and H. M. Branz, "On the superlinear increase in conductivity with dopant concentration in excitonic semiconductors," *Appl. Phys. Lett.*, vol. 84, pp. 1707–1709, 2004.
- [92] Y. Shen, K. Diest, M. H. Wong, B. R. Hsieh, D. H. Dunlap, and G. G. Malliaras, "Charge transport in doped organic semiconductors," *Phys. Rev. B*, vol. 68, pp. 0812041–0812044, 2005.
- [93] P. N. Butcher, *Linear and Nonlinear Electron Transport in Solids*, USA: Plenum press, 1976.
- [94] N. F. Mott, "Conduction in glasses containing transition metal ions," *J. Non-Cryst. Solids*, vol. 1, pp. 1–17, 1968.
- [95] M. Pope and C. E. Swenberg, "Electronic Processes in Organic Solids," *Ann. Rev. Phys. Chem.*, vol. 35, pp. 613–655, 1984.
- [96] D. M. de Leeuw, "Stable solutions of doped thiophene oligomers," *Synthetic Metals*, vol. 57, pp. 3597–3602, 1993.
- [97] M. Maitrot and B. Boudjema, J. J. Andre, and J. Simon, "Molecular material-based junctions: Formation of a Schottky contact with metallophthalocyanine thin films doped by the cosublimation method," *J. Appl. Phys.*, vol. 60, pp. 2396–2400, 1986.
- [98] V. I. Arkhipov, *International symposium on electrical insulating materials 1995*, vol. 1, pp. 271–274, 1995.
- [99] P. M. Borsenberger, W. T. Gruenbaum, U. Wolf, and H. Bassler, "Hole trapping in tri-p-tolylamine-doped poly(styrene)," *Chem. Phys.*, vol. 234, pp. 277–284, 1998.

- [100] Z. Chinguvare and V. Dyakonov, "Trap-limited hole mobility in semiconducting poly(3-hexylthiophene)," *Phys. Rev. B.*, vol. 70, pp. 2352071–2352078, 2004.
- [101] J. A. Anta, J. Nelson, and N. Quirke, "Charge transport model for disordered materials: Application to sensitized TiO₂ ," *Phys. Rev. B*, vol. 65, pp. 1253241–12532410, 2004.
- [102] D. M. Pai, J. F. Yanus, and M. Stolka, "Trap-controlled hopping transport," *J. Phys. Chem.*, vol. 88, pp. 4714–4717, 1984.
- [103] U. Wolf, H. Bassler, P. M. Borsenberger, and W. T. Gruenbaum, "Hole trapping in molecularly doped polymers," *Chem. Phys.*, vol. 222, pp. 259–267, 1997.
- [104] I. I. Fishchuk and H. Bassler, "Nondispersive charge-carrier transport in disordered organic materials containing traps ," *Phys. Rev. B*, vol. 66, pp. 2052081–20520812, 2002.
- [105] J. R. Sheat, H. Antoniadis, M. Hueschen, W. Leonard, J. Miller, R. Moon, D. Roitman, and A. Stocking, "Organic electroluminescent devices," *Science*, vol. 16, pp. 884–888, 1996.
- [106] P. E. Burrows, Z. Shen, V. Bulovic, d. M. McCarty, S. R. Forrest, J. A. Cronin, and M. E Thompson, "Relationship between electroluminescence and current transport in organic heterojunction light-emitting devices," *J. Appl. Phys.*, vol. 79, pp. 7991–8006, 1996.
- [107] M. A. Lampert and P. Park, *Current Injection in Solids*, USA: Academic Press, 1970.
- [108] P. W. M. Blom, M. J. M. de Jong, and M. G. V. Munster, "Electric-field and temperature dependence of the hole mobility in poly(p-phenylene vinylene) ," *Phys. Rev. B*, vol. 55, no. 2, pp. 656–659, 1997.
- [109] M. A. Abkowitz and D. Pai, "Comparison of the drift mobility measured under transient and steady-state conditions in a prototypical hopping system," *Phil. Mag. B*, vol. 53, no. 3, pp. 193–216, 1986.
- [110] P. W. M. Blom, M. J. M. de Jong and J. J. M. Velggar, "Electron and hole transport in poly(p-phenylene vinylene) devices," *Appl. Phys. Lett.*, vol. 68, no. 23, pp. 3308–3310, 1996.
- [111] C. Weissmantel and C. Hamann, *Grundlagen der Festkörperphysik*, Germany: Deutscher Verlag der Wissenschaften, 1981.

- [112] V. I. Arkhipov, E. V. Emelianova, Y. H. Tak, and H. Bassler, “Charge injection into light-emitting diodes: Theory and experiment,” *J. Appl. Phys.*, vol. 84, no. 2, pp. 848–856, 1998.
- [113] U. Wolf, V. I. Arkhipov, and H. Bassler, “Current injection from a metal to a disordered hopping system. I. Monte Carlo simulation,” *Phys.Rev.B*, vol. 59, no. 11, pp. 7507–7513, 1999.
- [114] M. Pope and C. E. Swenberg, *Electronic Processes in Noncrystalline Materials*, UK: Oxford University Press, 1979.
- [115] V. I. Arkhipov, U. Wolf, and H. Bassler, “Current injection from a metal to a disordered hopping system. II. Comparison between analytic theory and simulation,” *Phys. Rev. B*, vol. 59, no. 11, pp. 7514–7520, 1999.
- [116] S. M. Sze, *Physics of semiconductor devices*, USA: Wiley, 1981.
- [117] P. R. Emtage and J. J. ODwyer, “Richardson-Schottky Effect in Insulators,” *Phys. Rev. Lett.*, vol. 16, no. 9, pp. 356–358, 1966.
- [118] V. I. Arkhipov, and P. Heremans, E. V. Emelianova, and G. J. Adriaenssens, “Space-charge-limited currents in materials with Gaussian energy distributions of localized states,” *Appl. Phys. Lett.*, vol. 79, no. 25, pp. 4154–4156, 2001.
- [119] D. M. Pai, “Transient Photoconductivity in Poly(N-vinylcarbazole),” *J.Phys. Chem.*, vol. 52, no. 5, pp. 2285–2291, 1970.
- [120] C. W. Tang and S. A. VanSlyke, “Organic electroluminescent diodes,” *Appl. Phys. Lett.*, vol. 51, no. 12, pp. 913–915, 1987.
- [121] O. D. Jurchescu, J. Baas, and T. T. M. Palstra, “Effect of impurities on the mobility of single crystal pentacene,” *Appl. Phys. Lett.*, vol. 84, no. 16, pp. 3061–3063, 2004.
- [122] N. F. Mott and R. W. Gurney, *Electron Processes in Ionic Crystals*, UK: Oxford University Press, 1948.
- [123] N. F. Mott, and E. A. Davis, *Electron Processes in Noncrystalline Materials*, UK: Oxford University Press, 1979.
- [124] A. J. Campbell, D. D. C. Bradley, and D. G. Lidzey, “Space-charge limited conduction with traps in poly(phenylene vinylene) light emitting diodes,” *J. Appl. Phys.*, vol. 82, no. 12, pp. 6326–6342, 1997.

- [125] S. Heun, R. F. Mahr, A. Greiner, U. Lemmer, H. Bassler, D. A. Halliday, D. D. Bradley, P. L. Burn, and A. B. Holmes, “Conformational effects in poly(p-phenylene vinylene) revealed by low-temperature site-selective fluorescence,” *J. Phys.: Condensed Matter*, vol. 5, pp. 247–260, 1993.
- [126] F. Neumann, Y. A. Genenko, and H. von Seggern, “The Einstein relation in systems with trap-controlled transport,” *J. Appl. Phys.*, vol. 99, pp. 0137041–0137044, 2006.
- [127] S. F. Alvarado, L. Muller, P. F. Seidler, and W. Riess, “STM-excited electroluminescence and spectroscopy on organic materials for display applications,” *IBM J. Res. Dev.*, vol. 45, pp. 89–92, 2001.
- [128] W. Brutting, S. Berleb, and A. G. Muckl, “Space-charge limited conduction with a field and temperature dependent mobility in Alq light-emitting devices,” *Synth. Met.*, vol. 122, pp. 99–104, 2001.
- [129] D. Natali, and M. Sampietro, “Field-dependent mobility from space-charge-limited current voltage curves,” *J. Appl. Phys.*, vol. 92, pp. 5310–5318, 2002.
- [130] A. Brown, C. Jarrett, D. de Leeuw, and M. Matters, “Field-effect transistors made from solution-processed organic semiconductors,” *Synthetic Metals*, vol. 88, no. 1, pp. 37–55, 1997.
- [131] G. Pike and C. Seager, “Percolation and conductivity: A computer study. I,” *Phys. Rev. B*, vol. 10, no. 4, pp. 1421–1434, 1974.
- [132] E. Meijer, C. Tanase, P. Blom, E. Veenendaal, B. Huisman, D. de Leeuw, and T. Klapwijk, “Switch-on voltage in disordered organic field-effect transistors,” *Appl. Phys. Lett.*, vol. 80, no. 20, pp. 3838–3840, 2002.
- [133] E. Calvetti, L. Colalongo, and Z. Kovacs-Vajna, “Organic thin film transistors: a DC/dynamic analytical model,” *Synthetic Metals*, vol. 49, pp. 567–577, 2005.
- [134] J. Scherbel, P. H. Nguyen, G. Paasch, W. Brutting, and M. Schwoerer, “Temperature dependent broadband impedance spectroscopy on poly-(p-phenylene-vinylene) light-emitting diodes,” *J. Appl. Phys.*, vol. 83, pp. 5045–5055, 1998.
- [135] W. Brutting, S. Berleb, A. G. Muckl, “Device physics of organic light-emitting diodes based on molecular materials,” *Organic Electronics*, vol. 2, pp. 1–36, 2001.
- [136] S. Scheinert, G. Paasch, and T. Doll, “Subthreshold characteristics of field effect transistors based on poly(3-dodecylthiophene) and an organic insulator,” *J. Appl. Phys.*, vol. 92, pp. 330–337, 2002.

- [137] G. Paasch, A. Nesterov, and S. Scheinert, “Simulation of organic light emitting diodes: influence of charges localized near the electrodes,” *Syn. Metals.*, vol. 139, pp. 425–432, 2003.
- [138] B. K. Crone, P. S. Davis, I. H. Campbell, and D. L. Smith, “Device physics of single layer organic light-emitting diodes,” *J. Appl. Phys.*, vol. 86, pp. 5767–5774, 1999.
- [139] B. A. Gregg, Si. G. Chen, and R. A. Cormier, “Coulomb Forces and Doping in Organic Semiconductors,” *Chem. Mater.*, vol. 16, pp. 4586–4599, 2004.
- [140] V. I. Akhipov, E. V. Emelianova, P. Heremans, and G. J. Adriaenssens *J. Adv. Mater.*, vol. 4, pp. 425 (2002)

Own Publications

- [1] L. Li, G. Meller, and H. Kosina, “Diffusion-controlled charge injection model for organic light-emitting diodes,” *Applied Physics Letters*, vol. 91, pp. 1721111–1721113, 2007.
- [2] L. Li, G. Meller, and H. Kosina, “Analytical conductivity model for doped organic semiconductors,” *Journal of Applied Physics*, vol. 101, pp. 0337161–0337164, 2007.
- [3] L. Li, G. Meller, and H. Kosina, “Carrier concentration dependence of the mobility in organic semiconductors,” *Synthetic Metals*, vol. 157, pp. 243–246, 2007.
- [4] L. Li, G. Meller, and H. Kosina, “Influence of traps on charge transport in organic semiconductors,” *Solid State Electronics*, vol. 51, pp. 445–448, 2007.
- [5] L. Li, G. Meller, and H. Kosina, “Temperature and field-dependence of hopping conduction in organic semiconductors,” *Microelectronics Journal*, vol. 38, pp. 47–51, 2007.
- [6] L. Li, G. Meller, and H. Kosina, “Percolation current in organic semiconductors,” *Journal of Computational Electronics*, vol. 6, pp. 357–361, 2007.
- [7] G. Meller, L. Li, and H. Kosina, “Simulation of carrier injection and propagation in molecularly disordered systems,” *Optical and Quantum Electrons*, vol. 38, pp. 993–1004, 2006.
- [8] L. Li, G. Meller, and H. Kosina, “Charge injection model in organic light-emitting diodes based on a master equation,” in *International Conference on Simulation of Semiconductor Processes and Devices 2007*, pp. 377–380, 2007.
- [9] L. Li, G. Meller, and H. Kosina, “Charge injection model in organic light-emitting diodes,” in *International Conference on Organic Electronics*, p. 32, 2007.
- [10] L. Li, G. Meller, and H. Kosina, “Field-dependent effective transport energy in organic semiconductors,” in *The 3rd Meeting on Molecular Electronics*, pp. t2–pc18, 2006.

- [11] L. Li, G. Meller, and H. Kosina, “Doping dependent conductivity in organic semiconductors,” in *International Conference on Simulation of Semiconductor Processes and Devices 2006*, pp. 204–207, 2006.
- [12] L. Li, G. Meller, and H. Kosina, “Percolation current in organic semiconductors,” in *11th International Workshop on Computational Electronics Book of Abstracts*, pp. 161–162, 2006.
- [13] L. Li, G. Meller, and H. Kosina, “An analytical model for organic thin film transistors,” in *Proceeding of the 2005 IEEE conference on Electron Devices and Solid-State Circuits*, pp. 571–574, 2005.
- [14] L. Li, G. Meller, and H. Kosina, “Temperature and field-dependence of hopping conduction in organic semiconductors,” in *3rd European Conference on Organic Electronics and Related Phenomena Book of Abstracts*, pp. 112–113, 2005.
- [15] L. Li, G. Meller, and H. Kosina, “Micro and macroscopic modeling of charge flows in molecularly disordered organic semiconductors,” in *SISPAD 2007 Companion Workshop Organic Electronics*, 2007.
- [16] G. Meller, L. Li, and H. Kosina, “Dynamic Monte Carlo simulation of an amorphous organic devices,” in *International Conference on Simulation of Semiconductor Processes and Devices 2007*, pp. 373–376, 2007.
- [17] G. Meller, L. Li, and H. Kosina, “Simulation of carrier injection and propagation in molecularly disordered systems,” in *Proceedings of the 6th International Conference on Numerical Simulation of Optoelectronics Devices*, pp. 1–2, 2006.
- [18] G. Meller, L. Li, and H. Kosina, “Kinetic Monte Carlo simulation of molecularly doped organic semiconductors,” in *Second Meeting on Molecular Electronics*, p. 107, 2005.
- [19] G. Meller, L. Li, and H. Kosina, “Monte Carlo simulation of molecularly doped organic semiconductors,” in *3rd European Conference on Organic Electronics and Related Phenomena Book of Abstracts*, pp. 44–45, 2005.

	Author	Co-Author	Total
Journals	6	1	7
Conferences	8	4	12
Total	14	5	19

Table 8.1: Publication Statistics.

Curriculum Vitae

Ling Li

September 27th, 1976

Born in Sichuan, China.

1997-2001

Bachelor Degree of Microelectronics and Solid State Electronics at the University of Electronics Science and Technology of China, Chengdu, China.

2001-2004

Master of Science of Microelectronics at the Institute of Microelectronics, Chinese Academy of Science. Subject: Microelectronics Process Simulation and Nano-fabrication.

2005-2007

Ph.D candidate at the Institute for Microelectronics, TU-Wien under the supervision of Prof. Hans Kosina.